António César Rodrigues Águia

Study and Development of Paints for the Photocatalytic oxidation of NOx

Dissertation presented for obtaining the degree of
Doctor of Philosophy in Chemical and Biological Engineering
by
University of Porto

Supervisors:

Adélio Miguel Magalhães Mendes

Luís Miguel Palma Madeira

LEPAE – Laboratory for Process, Environmental and Energy Engineering

Chemical Engineering Department, Faculty of Engineering - University of Porto

March 2011

Acknowledgements

I am grateful to the Portuguese Foundation for Science and Technology (FCT) for the PhD grant (SFRH/BD/23263/2005) and financial support under the framework of the project POCI/EQU/60366/2004, QREN project NOxOUT (ref. 5365) and CRUP (Integrated Action, ref. E-28/08). I am also grateful to the companies for supplying the commercial photocatalytic TiO_2 samples.

Thankful words are also directed to LEPAE, DEQ and FEUP for providing the necessary conditions to carry out my work.

I must express my gratitude to Professor Adélio Mendes; your help was far beyond the one that a supervisor could give…thank you Professor! I would also like to express my gratitude to Professor Miguel Madeira for the helpful discussions and all the good sense given to me during this journey.

I am very grateful to Professor Hermenegildo Garcia, Francesc Llabres and Esther Dominguez (Instituto de Tecnología Química CSIC-UPV, Universidad Politécnica de Valencia) who received me like a true member of their Institute, and helped me even in the most difficult moments. Thank you also to Abdessamad, Clara and Maria who made Valência become my second home. A special thanks to João: you should have given me a ticket to see Valência football team, but anyway.

To my parents…whenever there is a wish, there is a will! This was also your wish.

……to the women who most inspired my life until this moment…with her smile, kindness, and love…I wonder you could live this moment with me….this thesis is for you, avó!

And the last but not the least…to Catarina, who make the sunshine, even when the rain seems to do not stop.

To my grandmother…

Preface

The present work was carried out at the Laboratory for Process, Environmental and Energy Engineering (LEPAE), in the Chemical Engineering Department of the Faculty of Engineering – University of Porto (FEUP), between 2006 and 2010, under the framework of the project POCI/EQU/60366/2004 (funded by the Fundação para a Ciência e Tecnologia) and under the grant SFRH/BD/23263/2005. The thesis starts with an introductory chapter (chapter 1) and ends with the overall conclusions and perspectives for future work (chapter 7). It contains 4 scientific articles (chapters 2, 3, 4 and 6) published, accepted or submitted for publication. Chapter 5 was published in the proceedings of an international conference.

Contents

FIGURE CAPTIONS xiii

TABLE CAPTIONS xvii

NOMENCLATURE xix

ABSTRACT xxvii

SUMÁRIO xxix

SOMMAIRE xxxi

RESUMEN xxxiii

PART I - *NOX AND PHOTOCATALYSIS* 1

CHAPTER 1 – INTRODUCTION 3

1.1 NOX: A PRIORITY POLLUTANT 3

1.2 FROM PHOTOELECTROCHEMISTRY TO PHOTOCATALYSIS OF NOX 9

1.3 PHOTOCATALYTIC OXIDATION OF NOX 16

1.3.1 LAB TESTS ON PURE PHOTOCATALYTIC TiO_2 16

1.3.2 PHOTOCATALYTIC CONSTRUCTION MATERIALS 17

1.4 MOTIVATION AND OUTLINE 22

REFERENCES 23

PART II – *COMMERCIALLY AVAILABLE TIO_2* 29

CHAPTER 2 – PHOTOCATALYTIC OXIDATION OF NO – SCREENING OF COMMERCIAL TiO_2 31

ABSTRACT 31

2.1 INTRODUCTION 32

2.2 EXPERIMENTAL 33

2.2.1 PHOTOCATALYTIC FILMS 33

2.2.2 EXPERIMENTAL SETUP 35

2.2.3 UV LAMP SYSTEM 38

2.3 RESULTS AND DISCUSSION 39

2.3.1 PHOTOCATALYTIC TESTS 39

2.3.1.1 Effect of the activation step on the photoactivity *41*
2.3.1.2 Repeatability and effect of photo-TiO_2 load *43*
2.3.1.3 Steady state photoactivity of the powder pressed and paint films *46*
2.3.2 Diffuse reflectance and SEM analyses 49
2.4 Conclusions 51
References 55

PART III – *THE PAINT MATRIX* 59
Chapter 3 – Influence of Paint Components on P25 Photoactivity – Powder and organic paint components 61
Abstract 61
3.1 Introduction 61
3.2 Experimental 63
3.2.1 Photocatalytic films 63
3.2.2 Experimental setup 65
3.3 Results and discussion 68
3.3.1 UV/Vis diffuse reflectance 68
3.3.2 Photoactivity of powder pressed (PP) films 70
3.3.3 Photoactivity of pseudo-paint (PsP) films 74
3.4 Conclusions 78
References 79

Chapter 4 - Influence of Paint Components on P25 Photoactivity – Wet effect and paint matrix degradation 81
Abstract 81
4.1 Introduction 83
4.2 Experimental 85
4.2.1 Photocatalytic films 85
4.2.2 Photocatalytic tests 89
4.2.3 Physicochemical characterization 91
4.3 Results and discussion 91
4.3.1 Photoactivity of powder pressed (PP) films 91
4.3.2 Photoactivity of pseudo-paint (PsP) films 97

4.4 Conclusions 103
References 105

PART IV – *THE PHOTOCATALYST* 107
Chapter 5 – Supported Photocatalytic TiO_2 Produced by Ion Exchange 109
Abstract 109
5.1 Introduction 110
5.2 Experimental 110
5.2.1 Supported photocatalysts, synthesis and characterization 110
5.2.2 Photocatalytic films 111
5.2.3 Experimental setup and photocatalytic tests 111
5.3 Results and discussion 112
5.3.1 Physicochemical characterization 112
5.3.2 Photocatalytic tests 114
5.4 Conclusions 116
References 117

Chapter 6 - Supported Photocatalytic TiO_2 Produced by Impregnation 119
Abstract 119
6.1 Introduction 120
6.2 Experimental 122
6.2.1 Supported photocatalyst synthesis 122
6.2.2 Physicochemical characterization 122
6.2.3 Photocatalytic tests 123
6.3 Results and discussion 125
6.3.1 Physicochemical characterization 125
6.3.2 Photocatalytic tests 123
6.4 Conclusions 138
References 138

PART V – *CONCLUSIONS AND FUTURE WORK* 143
Chapter 7 - Conclusions and future work 145
7.1 Main Conclusions 145

7.2 FUTURE WORK 147
7.3 A POSSIBLE ROADMAP 149
REFERENCES 150

APPENDIX 151
APPENDIX A – EXPERIMENTAL SETUP – ADDITIONAL AND BRIEF OVERVIEW 153

Figure captions

Figure 1.1 – Thermodynamic equilibrium concentration of NO (●, ■) and NO_2 (◆, ▲) starting from NO + NO_2 = 300 ppm in air (●,◆) and in oxygen depleted air (■, ▲) (adapted from [3]).

Figure 1.2 – Sketch of major reactions involving airborne NOx (rectangles represent anthropogenic primary gas emissions; bold lines represent reaction with direct involvement of NOx; NMHC – non-methane hydrocarbon; VOC – volatile organic compound) – adapted from [5, 6].

Figure 1.3 – Typical smog episodes: a) London, late of XIX century, photo and portrait by Monet; b) Beijing nowadays.

Figure 1.4 – NOx emission by source in the USA by 2005 (top) [9] and EU-27 by 2008 (bottom) [10].

Figure 1.5 – NO and NO_2 concentrations in June and December from 1995 to 2007 at Lisbon (adapted from [15]).

Figure 1.6 – Redox position bands of various semiconductors and their bandgaps (adapted from [18]).

Figure 1.7 – Simplified sketch of photocatalytic phenomena over TiO_2 and relation with redox potentials and flat band energy positions.

Figure 1.8 – Detail image of TiO_2 (adapted from [46]).

Figure 1.9 – Schematic models for O_2 and H_2O coadsorption on TiO_2 surface (adapted from [46]).

Figure 1.10 – TiO_2 anatase valence and conduction band reduction potential dependence on pH and reduction potential of some possible photocataytic reactions of NO, water and oxygen - reagents and products (adapted from [50 - 53]).

Figure 1.11 – Poison effect on photocatalytic paint films.

Figure 1.12 – Estimated number of patents on TiO_2 photocatalysis per year for air (filled diamond) and water treatment (empty triangles) and self-cleaning surfaces (empty circles) (adapted from [77]).

Figure 2.1 – Sketch of the experimental setup used for the photocatalytic tests (arrows represent the gas flow direction).

Figure 2.2 – Schematic representation of the photoreactor (top view).

Figure 2.3 – Irradiance as a function of the position inside the photoreactor and respective uncertainty (maximum 5% considered); irradiance obtained with eq.(1) (full circles) and the corresponding interpolation curve (continuous line).

Figure 2.4 – NO conversion (full symbols) and selectivity (empty symbols) histories as a function of the activation protocol for paint films incorporating ANX type PA.

Figure 2.5 – NO conversion (full symbols) and selectivity (empty symbols) histories in two consecutive runs, with 24 hours resting period, with a photocatalytic paint film incorporating *UVLP7500*.

Figure 2.6 – NO conversion (full symbols) and selectivity (empty symbols) for (a) powder-pressed films of P25 (Runs #1-3) and (b) photocatalytic paint films of P25 (Runs # 6-8), as described in Table 2.

Figure 2.7 – Steady state NO conversion (full circles) and selectivity (empty circles) for all tested powder pressed (X axis) and paint (Y axis) films.

Figure 2.8 – Yield (product of NO conversion and selectivity) obtained at steady state for all tested powder pressed (X axis) and paint (Y axis) films.

Figure 2.9 – Diffuse reflectance (DR) powder pressed films and incident UV lamp spectrum (a) and absorbed spectral radiant power for the same powder pressed films (b).

Figure 2.10 – NO conversion and selectivity as a function of the total absorbed radiant power by the powder pressed films between 315 nm and 390 nm.

Figure 2.11 – SEM images of the photo-TiO_2 in powder (left images) and paint (right images) films – 100 000x mag.

Figure 3.1 – Sketch of the experimental setup used for the photocatalytic tests (arrows represent the gas flow direction).

Figure 3.2 – Diffuse reflectance (DR) of pure powder films of P25, $CaCO_3$, $BaSO_4$, pigmentary TiO_2 and films tested in the photoreactor (Table 1); it was used an aluminum support for powder deposition except for $CaCO_3$ – B (black support - Leneta test charts) and $CaCO_3$ – W (white support - Leneta test charts).

Figure 3.3 – Conversion (full symbols) and selectivity (empty symbols) histories on 3 different powder pressed films of pure P25 (experiment PP0).

Figure 3.4 – Steady state conversion and selectivity on PP0 films with different loads and areas of P25: *14.8(6x5)* – 14.8 $mg \cdot cm^{-2}$ and 6 x 5 cm^2 (length x width); *13.5(10x5)* – 13.5 $mg \cdot cm^{-2}$ and 10 x 5 cm^2 and *23.7(10x5)* – 23.7 $mg \cdot cm^{-2}$ and 10 x 5 cm^2.

Figure 3.5 – Conversion (full symbols) and selectivity (empty symbols) history for experiments PP1, PP2 and PP3.

Figure 3.6 – Conversion (full symbols) and selectivity (empty symbols) history for experiments PP3, PP4 and PP5.

Figure 3.7 – Conversion (full symbols) and selectivity (empty symbols) history of experiments PsP6, PsP7 and PsP8.

Figure 3.8 – Conversion (full symbols) and selectivity (empty symbols) history of experiment PsP9, employing fresh and 6 months in-can pseudo-paint.

Figure 3.9 – Conversion (full symbols) and selectivity (empty symbols) history of experiment PsP10, using pseudo-paints produced from two different batches.

Figure 3.10 – Conversion (full symbols) and selectivity (empty symbols) history of experiment RP11, after harsher activation.
Figure 4.1 – Schematic representation of the production procedure of the photocatalytic films.
Figure 4.2 – Schematic representation of the photocatalytic reactor.
Figure 4.3 – NO conversion (full symbols) and selectivity (empty symbols) histories obtained with powder films PP0 and wPP0.
Figure 4.4 - High-resolution XPS spectra at O 1s region for powders of fresh P25 and P25 after mechanical mixture and sonication.
Figure 4.5 – Diffuse reflectance (DR) spectra of powder pressed films PP0 and wPP0.
Figure 4.6 - NO conversion (full symbols) and selectivity (empty symbols) histories obtained with PP# (circles) and wPP# (triangles) films of P25 mixed with: a) silicates; b) $CaCO_3$; c) pigmentary TiO_2 and d) all powder components (silicates, $CaCO_3$ and pigmentary TiO_2).
Figure 4.7 - Conversion (top graph) and selectivity (bottom graph) histories on films PsP1, PsP2 and RP (the later with hasher activation).
Figure 4.8 – TG analysis of PsP1, PsP2, BP and RP films without (0 h) and with (24 h or 150 h) standard activation (mass variations were calculated based on 100 % mass at 120 ºC).
Figure 4.9 – Diffuse refectance (DR) spectra of P25, pigmentary TiO_2, wPP4 and RP films (star points - lamp spectrum).
Figure 4.10 – DTG curves of (a) fresh samples of PsP1, PsP2, BP and RP films and (b) RP fresh and aged films for 24 h and 150 h.
Figure 5.1 – X-ray diffraction patterns (top) and nitrogen adsorption isotherms performed at 77 K (bottom) for the supported photocatalysts into zeolite Y.
Figure 5.2 – Transformed Kubelka–Munk function vs. energy of the excitation source.
Figure 5.3 – NO conversion and ionic selectivity at steady state for all tested films of Table 2.
Figure 6.1 – Schematic representation of the photocatalytic reactor.
Figure 6.2 – XRD patterns of supports and respective composite materials (P25 used for reference).
Figure 6.3 – SEM images of βCP811 (left side images) and TiO_2@βCP811 (right side images).
Figure 6.4 – SEM images of CBV100 (left side images) and TiO_2@CBV100 (right side images).
Figure 6.5 – SEM images of CBV500 (left side images) and TiO_2@CBV500 (right side images).
Figure 6.6 – Diffuse reflectance (DR) spectra of zeolite in pure form and with TiO_2.
Figure 6.7– Infrared results to CBV500 zeolite and respective photocatalytic material TiO_2@CBV500.
Figure 6.8 – Transformed Kubelka–Munk function vs. energy of the excitation source.
Figure 6.9 – History of NO conversion (a) and selectivity (b) for P25, CBV500 and CBV100.
Figure 6.10 – NO adsorption isotherm on composite photocatalysts TiO_2@CBV100 and TiO_2@CBV500 at 25 °C.

Figure 6.11 – NO conversion for photocatalytic paint containing 9 wt.% of P25 (open symbols) and 9 wt.% of TiO_2@CBV100 (ca. 0.3 wt.% of TiO_2).
Figure 7.1 – A view of the photocatalytic technological solutions and its major areas of knowledge.
Figure 7.2 – An approach for chronological technological applications of photocatalytic paints.
Figure A.1 – General overview of one of the setups used.
Figure A.2 – Detail of the thermostatic cabinet.
Figure A.3 – Detail of the photocatalytic reactor.

Table Captions

Table 1.1 – Lifetime, acidity, PM_{10} mass factors and ozone formation potential for NOx and other priority pollutants [11].

Table 2.1 – Properties of the photo-TiO_2 used (data provided by the manufacturers).

Table 2.2 – Steady state NO conversion and selectivity of powder pressed and photocatalytic paint films of P25 and VLP7101 photo-TiO_2 – study of repeatability and load effect.

Table 2.3 – Photo-TiO_2 loads of the powder pressed and paint films shown in Figure 7.

Table 2.4 – Particle diameter and shape of the photo-TiO_2, obtained by SEM.

Table 3.1 – Mass fraction (with two decimal places) of paint components in the film used in each experiment, load of P25 and content of powders and organic components (dry basis).

Table 4.1 –Base and reference paint formulations (wt.% are given for the specific case of reference paint).

Table 4.2 – Mass fraction (with two decimal places) of powder paint components and load of P25 for films prepared via the powder pressed route.

Table 4.3 – Mass fraction (with two decimal places) of all components in the paint films used in each experiment, load of P25 and content of powders and organic components (dry basis).

Table 4.4 – Crystalline phase fraction, density, particle diameter and crystallographic net parameters of fresh P25 and P25 after mechanical mixture and sonication, obtained by XRD.

Table 4.5 - Results of curve fitting of high-resolution XPS spectra at O1s region of fresh P25 and P25 after mechanical mixture and sonication (percentage of Ti-O vs. O-H bonds obtained by peak deconvolution).

Table 4.6 – TG mass losses at 900 °C of fresh and aged samples for 24 h and 150 h and relative mass loss due to photodegradation during UV aging.

Table 5.1 – Results of elemental analysis performed by ICP, and BET surface areas obtained by nitrogen adsorption isotherms performed at 77 K.

Table 5.2 – Photocatalytic materials and estimated TiO_2's mass in each experiment.

Table 6.1 – Pristine and composite zeolite surface area (S_{BET}), pore volume (V_p) and average pore size ($\square_P$) of the prepared samples.

Table 6.2 – EDS analyses, corresponding to the zones indicated in Figures 3, 4 and 5.

Table 6.3 – Photocatalyst bandgap, bandgap shift related to P25 and corresponding wavelength for absorption threshold.

Table 6.4 – Mass of composite photocatalyst and P25 used, corresponding TiO_2 mass and load (mass normalized by the film area; 6 x 5 cm^2).

Table 6.5 – Fraction of UV light absorption by each photocatalytic material.

Table 6.6 – Mass of composite photocatalyst and P25 in dry paint film, corresponding TiO_2 mass and load.

Nomenclature

Abbreviations, symbols and chemicals	Definition	Units
AgCl	Silver Chloride	
AirK	Synthetic air	
AMT100	A commercial grade of photocatalytic titanium dioxide	
ANX type PA	A commercial grade of photocatalytic titanium dioxide	
$BaSO_4$	Barium sulfate	
BP	Base paint	
$CaCO_3$	Calcium carbonate	
$Ca(NO_3)_2$	Calcium nitrate	
CB	Conduction band	
CFCs	Chlorofluorocarbons	
CNO^{in}	Inlet gas phase concentration of NO	ppm
CNO^{out}	Outlet gas phase concentration of NO	ppm
CNO_2^{in}	Inlet gas phase concentration of NO_2	ppm
CNO_2^{out}	Outlet gas phase concentration of NO_2	ppm
CO	Carbon monoxide	
CPVC	Critical Pigment Volume Concentration	
DAQ	Data acquisition	
DR	Diffuse reflectance	
DTG	Differential thermogravimetric/thermogravimetry	
e^-	Electron	

Abbreviations, symbols and chemicals	Definition	Units
E (or $E_{A+/A}$ or $E_{B/B-}$)	Reduction potential	V
EDS	Energy-dispersive x-ray spectroscopy	
e^-/h^+	Electron-hole pair	
Eb	Binding energy	eV
EEA	European Environment Agency	
EPA	USA Environmental Protection Agency	
EU-27	European Union at 27 member states	
F(R)	Kubelka-Munk function	
FS	Full scale	
fwhm	Full width at half of peak maximum	
H^+	Proton (derived from hydrogen atom)	
h^+	Positive charge (hole)	
HNO_3	Nitric acid	
HNO_2	Nitrous acid	
HOMO	Highest occupied molecular orbital	
$HO_2^{\bullet}$	Hydroperoxy radicals	
H_2O	Water	
H_2O_{ads}	Adsorbed water (on TiO_2 surface)	
H_2O_2	Hydrogen peroxide	
hν	Photonic energy	eV or J
H_2	Hydrogen molecule	
ICP	Induced Coupled Plasma	

Abbreviations, symbols and chemicals	Definition	Units
IPCC	International Panel for Climate Change	
IR	Infrared	
ISO	International Standard Organization	
$< I_{film} >$	Average irradiance reaching the photocatalytic film	$W \cdot m^{-2}$
$< I(z_i)_{read} >$	Irradiance per axial position in reactor chamber	$W \cdot m^{-2}$
$< I(z_i)_{film} >$	Irradiance profile at the reactor axial direction	$W \cdot m^{-2}$
KBr	Potassium bromide	
$Load_{P25}$	Load of photocatalytic P25	$mg \cdot cm^{-2}$
$L_{photo\text{-}TiO2}$	Load of photocatalytic TiO_2	$mg \cdot cm^{-2}$
LUMO	Lowest unoccupied molecular orbital	
MFC	Mass flow controller	
MFM	Mass flow meter	
mk-10	Montmorillonite k-10	
NECD	National Emission Ceilings Directive	
NH_3	Ammonia	
NH_4^+	Ammonium	
NHE	Normal hydrogen electrode	V
NMHCs	Non-methane hydrocarbons	
NO	Nitric oxide	
NOx	Nitrogen dioxides (NO and NO_2)	
NO_2	Nitrogen dioxide	

Abbreviations, symbols and chemicals	Definition	Units
$NO_3^{\bullet}$	Pernitrite radical	
NO_3^-	Nitrate ion	
NO_2^-	Nitrite ion	
N_2	Nitrogen	
N_2O	Nitrous oxide	
N_2O_5	Dinitrogen pentoxide	
OH_{ads}	Adsorbed OH group (on TiO_2 surface)	
OH_{ads}^-	Adsorbed negative OH group (on TiO_2 surface)	
$OH_{ads}^{\bullet}$	Adsorbed OH radical group (on TiO_2 surface)	
OH^-	Negative OH group	
O-H	General oxygen-hydrogen atoms bond	
O_3	Ozone	
$O_{2,ads}$	Adsorbed oxygen molecule (on TiO_2 surface)	
$O_2^{\bullet-}$	Superoxide ion	
PC50	A commercial grade of photocatalytic titanium dioxide	
PC500	A commercial grade of photocatalytic titanium dioxide	
PC105	A commercial grade of photocatalytic titanium dioxide	
pH	Potential of Hydrogen	
Photo-TiO_2	Abbreviation for photocatalytic TiO_2	
PM_{10}	Particulate matter with particle diameter equal or lower than 10 μm	

Abbreviations, symbols and chemicals	Definition	Units
PP	Powder pressed	
PsP	Pseudo-paint	
PVC	Pigment Volume Concentration	
P_λ	Relative spectral response of the sensor	
P25	A commercial grade of photocatalytic titanium dioxide	
RH	Relative humidity	%
$RO_2^{\bullet}$	Alkyl peroxy	
RP	Reference paint	
S	Selectivity (towards NO_3^- and NO_2^-)	%
SEM	Scanning electron microscopy	
S_{BET}	BET surface area	$m^2 \cdot g^{-1}$
SHE	Standard hydrogen electrode	V
T	Temperature	ºC
TiO_2	Titanium dioxide	
$TiO_2(h^+)$	Positive charge on irradiated titanium dioxide	
$TiO_2(e^-)$	Excited electron on irradiated titanium dioxide	
TG	Thermogravimetry/thermogravimetric	
UNEP	United Nations Environment Programme	
USY	Ultra-stable Y type zeolite	
UV	Ultraviolet light	

Abbreviations, symbols and chemicals	Definition	Units
UVLP7500	A commercial grade of photocatalytic titanium dioxide	
UV100	A commercial grade of photocatalytic titanium dioxide	
VB	Valence band	
Vis	Visible light	
VLP7000	A commercial grade of photocatalytic titanium dioxide	
VLP7101	A commercial grade of photocatalytic titanium dioxide	
VOC	Volatile organic compounds	
Vp	Pore volume	$cm^3 \cdot g^{-1}$
WHO	World Health Organization	
WMO	World Meteorological Organization	
wPP	Wet mixed powder pressed	
W_λ	Radiant power of the lamp	$W \cdot m^{-2}$
X_{NO}	NO conversion	%
XPS	X-ray photoelectron spectroscopy	
XRD	X-ray diffraction	
Y	Y type zeolite	
Z	Position in the reactor chamber	m
Zi	A certain position (axial) inside the reactor chamber	m
$Z_{initial}$	Initial position of the photocatalytic film, axial to the reaction chamber	m

Abbreviations, symbols and chemicals	Definition	Units
Z_{final}	Final position of the photocatalytic film, axial to the reaction chamber	m
$\lambda_{initial}$	Lower limit of spectral range of UV lamp	nm
λ_{final}	Upper limit of spectral range of UV lamp	nm
$\Delta_{A^+ + B \rightarrow A + B}$	Enthalpy of reaction	eV or J
ΔE	Bandgap	eV
Δ_{th}	Relative mass loss due to photodegradation after t hours;	%
$\square_P$	Average pore size	Å
$\square$	Braag angle (XRD analyses)	º
β	Beta type zeolite	

Abstract

Ambient NOx are originated from the combustion of fossil fuels in presence of N_2 and O_2, which promotes the so-called urban smog and ozone formation that have severe health impacts. Nevertheless, many cities in Europe, and namely in Portugal, are still recording NOx concentrations above the legislated limit (2008/50/EC). Therefore, technologies are required to solve this environmental problem, among which photocatalysis should play an important role.

Photocatalysis uses energy of light and a catalyst, generally nanoparticulate TiO_2 (photocatalytic TiO_2; herein called photo-TiO_2), to promote chemical reactions. However, appropriate supports for TiO_2 are required. Construction materials can be used to support photocatalytic TiO_2 for the photoabatement of atmospheric pollutants. From all possible construction materials, paint coatings present interesting advantages since almost all surfaces can be painted and their low thickness allow the use of low amounts of photocatalyst, for the same abatement capacity.

An exterior, water-based, high quality paint was selected as starting paint for the work presented in this thesis. From this paint, half of the pigmentary TiO_2 (that promotes paint opacity) was replaced by different commercially available photocatalytic TiO_2 (9 wt.%, wet based); when incorporating P25 photocatalyst this paint was named reference paint.

Part II of this dissertation focuses on the photoactivity study of paints incorporating different commercially available photocatalysts, and powder pressed films made by each photocatalyst. It was concluded that the ranking of the best photoactive paint films did not match with the ranking of the best photoactive powder pressed films.

Therefore, the influence of paint film components on the photoactivity of P25 photocatalyst was consequently studied - Part III of this dissertation. Powder films, containing only powder (mostly inorganic) paint components, and pseudo-paint films, containing also part of the

organic components, were prepared mixing stepwise components of the reference paint. It was concluded that pigmentary TiO_2 absorbing competitively the UV light, was the most critical component affecting the photocatalytic activity. Films also containing different organic components, which are added in proportions accordingly to the reference paint recipe, show different transient periods. However, similar steady state photoactivities were achieved. This was ascribed to the photoerosion of a significant fraction of the organic phase during the transient period. Powder components play a major role on light behavior of films and such fact rules the long-term photoactivity; in fact, films containing the same powder matrix but different organic composition, show the same photoerosion (ca. 25 wt.%) and therefore the very similar photoactivity.

Deposition of photocatalytic TiO_2 particles either on the internal or external surface of porous solid inorganic adsorbent materials, such as zeolites, are possible approaches for the protection of the paint matrix. If particles are deposited inside the pore structure, one can achieve paint protection avoiding direct contact of the paint matrix, namely the binder, with the photocatalytic TiO_2 particles; harmful gases can yet penetrate the support pore system and get oxidized. On the other hand, if photocatalytic TiO_2 particles are deposited on the outer surface of the support, protection can still occur once direct contact of paint and TiO_2 is reduced (dilution effect). Chapters 5 and 6 report the study of photocatalytic TiO_2 produced by ion exchange and impregnation on different supports, respectively. The highest photoactivity was observed for the TiO_2 supported on the outer surface of zeolite Y.

Sumário

Os NOx ambientais são maioritariamente provenientes da queima de combustíveis fósseis na presença de N_2 e O_2. Estes promovem a formação de *smog* urbano e ozono com consequências mais ou menos graves na saúde pública. No entanto, muitas cidades europeias, e nomeadamente em Portugal, apresentam ainda concentrações de NOx no ar acima do limite legal (2008/50/EC). São por isso necessárias tecnologias para resolver este problema ambiental; de entre as várias opções, a fotocatálise poderá desempenhar um papel importante.

A fotocatálise usa a energia da luz para promover a excitação de um catalisador, geralmente nanopartículas de TiO_2 (TiO_2 fotocatalítico, aqui também denominado de foto-TiO_2), desencadeando reacções químicas na sua superfície. São, no entanto, necessários suportes apropriados para o TiO_2 fotocatalítico. Os materiais de construção habitualmente usados podem ser utilizados para suportar o TiO_2 fotocatalítico. De todos os materiais de construção possíveis, as tintas apresentam vantagens interessantes, já que quase todas as superfícies podem ser pintadas e a sua baixa espessura permite o uso de pequenas quantidades de fotocatalisador.

Foi seleccionada uma tinta exterior, de base aquosa e alta qualidade, como ponto de partida para o trabalho apresentado nesta tese. A partir desta tinta, metade em peso do TiO_2 pigmentar (que promove a opacidade da tinta) foi substituído pela mesma quantidade de diferentes tipos de TiO_2 fotocatalítico disponíveis comercialmente (9% em peso, em base húmida); a tinta incorporando P25, um dos fotocatalisadores seleccionados, foi designada de tinta de referência.

Assim, a Parte II desta dissertação estuda a fotoactividade de filmes de tinta incorporando os diferentes fotocatalisadores disponíveis comercialmente. Estes fotocatalisadores foram também testados na sua forma pura, em filmes feitos de pó prensado. Concluiu-se que o os

fotocatalisadores mais activos quando incorporados na tinta não são necessariamente os melhores sob a forma de pó prensado.

Assim sendo, a influência dos componentes do filme de tinta na fotoactividade do fotocatalisador P25 foi estudada na Parte III desta dissertação. Filmes de pó, contendo apenas componentes inorgânicos da tinta, e filmes de pseudo-tinta, contendo também componentes orgânicos, foram preparados misturando os componentes passo a passo de acordo com a formulação da tinta. Concluiu-se que o TiO_2 pigmentar, absorvendo a luz UV competitivamente, é o componente mais crítico no que respeita ao prejuízo da actividade catalítica do P25. Os filmes contendo diferentes componentes orgânicos, que são adicionados em proporções de acordo com a formulação de tinta de base, apresentam diferentes comportamentos no estado transiente. No entanto, estes apresentam fotoactividades semelhantes no estado estacionário. Tal facto foi atribuído à fotoerosão de uma parcela semelhante da fase orgânica (25 % em massa) durante o período transiente.

A deposição de partículas fotocataliticas de TiO_2 na superfície interna ou externa de adsorventes porosos inorgânicos, tais como zeólitos, são abordagens possíveis para a protecção da tinta. Se as partículas forem depositadas dentro da estrutura de poros, pode obter-se uma protecção da tinta através do impedimento do contacto directo da tinta com as partículas de TiO_2 fotocatalítico; o NOx pode contudo difundir-se no sistema de poros do suporte adsorvente. Por outro lado, se o TiO_2 é depositado sobre a superfície externa dos adsorventes, a protecção deverá ocorrer apenas como consequência da redução desse contacto directo entre fotocatalisador e tinta. Os capítulos 5 e 6 desta tese abordam de forma breve a fotoactividade de fotocatalisadores compósitos em que o TiO_2 existem depositado na superfície interna e externa dos adsorventes. A maior fotoactividade foi observada para o TiO_2 suportado na superfície externa de zeólito Y.

Sommaire

Ambient NOx est originaire de la combustion de combustibles fossiles sous N_2 et O_2, ce qui favorise la formation du smog que l'on appelle la formation d'ozone en milieu urbain et qui ont des répercussions graves sur la santé. Néanmoins, de nombreuses villes en Europe, et notamment au Portugal, sont encore d'enregistrement des concentrations de NOx au-dessus de la limite prescrite (2008/50/EC). Par conséquent, les technologies sont nécessaires pour résoudre ce problème environnemental, dont la photocatalyse devrait jouer un rôle important.

Photocatalyse utilise l'énergie lumineuse et d'un catalyseur, généralement nanoparticulaire TiO_2 (TiO_2 photocatalytique; ci-après appelée photo-TiO_2), pour favoriser les réactions chimiques. Toutefois, soutien approprié pour le TiO_2 sont nécessaires. Matériaux de construction peuvent être utilisés pour soutenir TiO_2 photocatalytique pour la photo-oxydation des polluants atmosphériques. De tous les matériaux de construction possible, revêtements de peinture présente des avantages intéressants puisque presque toutes les surfaces peuvent être peintes et leur faible épaisseur permet l'utilisation de faibles quantités de photocatalyseur, pour la même capacité de réduction.

Un extérieur, à base d'eau, peinture de haute qualité a été choisie comme point de départ de la peinture pour le travail présenté dans cette thèse. De cette peinture, la moitié des TiO_2 pigmentaire (qui favorise l'opacité de la peinture) a été remplacé par différents disponibles dans le commerce TiO_2 photocatalytique (9% en poids, humide fondée.); Lors de l'incorporation photocatalyseur P25 cette peinture a été nommé peinture de référence.

Par conséquent, la partie II de cette thèse se concentre sur l'étude de la photoactivité de la peinture photocatalytique, en intégrant différents photocatalyseurs disponibles dans le commerce, et la poudre pressée films réalisés par chacun photocatalyseur. Il a été conclu que le classement des meilleurs films de peinture photoactifs ne correspond pas à la hiérarchie des meilleurs films de poudre pressée photoactifs.

L'influence des composantes du film de peinture sur la photo-activité des photocatalyseur P25 a donc été étudiées - Partie III de cette thèse. Films de poudre, contenant des composants de la peinture que inorganiques, et les films pseudo-peinture, contenant également une partie des composants organiques, ont été préparés par étapes de mélange des composants de la peinture de référence. Il a été conclu que TiO_2 pigmentaires absorbe la lumière UV concurrence, étant l'élément le plus important affectant l'activité photocatalytique. Films contenant également des différents composants organiques, qui sont ajoutés dans des proportions en conséquence à la recette de base de peinture, montrent différentes périodes transitoires. Toutefois, comme photoactivities l'état d'équilibre ont été atteints. Cela a été attribué à la photoerosion d'une fraction importante de la phase organique au cours de la période transitoire. Composants inorganiques jouent un rôle majeur sur photoactivité à long terme d'un film de peinture, en fait, films contenant les mêmes minéraux, mais différentes compositions organiques présentent les mêmes photoactivities l'état d'équilibre.

Le dépôt de particules de TiO_2 photocatalytique soit sur la surface intérieure ou extérieure de solide poreux inorganiques matériaux adsorbants, tels que les zéolithes, sont les approches possibles pour la protection de la matrice de peinture. Si les particules se déposent à l'intérieur de la structure des pores, on peut obtenir une protection de peinture en évitant le contact direct de la matrice de peinture, à savoir le liant avec les particules de TiO_2 photocatalytique; gaz nocifs peuvent encore pénétrer dans le système de pores de soutien et une oxydation. D'autre part, si les particules de TiO_2 photocatalytique sont déposés sur la surface extérieure du support, la protection peut encore se produire une fois contact direct de peinture et de TiO_2 est réduite (effet de dilution). Les chapitres 5 et 6 du rapport de l'étude de TiO_2 photocatalytique produite à l'intérieur qu'à l'extérieur du système de pores de supports différents, respectivement. Une plus grande photoactivité a été observée pour le TiO_2 pris en charge sur la surface externe de la zéolithe Y.

Resumen

Ambiente de NOx se origina de la combustión de combustibles fósiles en atmósfera de N_2 e O_2, que promueve el smog urbano y la formación de ozono que tienen efectos graves para la salud. Sin embargo, muchas ciudades de Europa, y especialmente en Portugal, se sigue grabando las concentraciones de NOx por encima del límite legislado (2008/50/EC). Por lo tanto, tecnologías son necesarias para resolver este problema ambiental, entre las que la fotocatálisis debe desempeñar un papel importante.

Fotocatálisis utiliza energía de la luz y un catalizador, por lo general nanopartículas de TiO_2 (TiO_2 fotocatalítica; aquí denominado foto-TiO_2), para promover las reacciones químicas. Sin embargo, los apoyos apropiados para TiO_2 son obligatorios. Los materiales de construcción se puede utilizar para apoyar fotocatalítica de TiO_2 para la foto-reducción de los contaminantes del aire. De todos los materiales de construcción posibles, revestimientos de pinturas presentan ventajas interesantes, ya que casi todas las superficies se pueden pintar y su bajo espesor permite el uso de pequeñas cantidades de fotocatalizador, por la capacidad de reducción mismo.

Una pintura exterior, a base de agua, de alta calidad ha sido seleccionada para los trabajos presentados en esta tesis. A partir de esta pintura, la mitad de los TiO_2 pigmentario (que promueve la opacidad de la pintura) fue reemplazado por diferentes TiO_2 fotocatalítica disponibles comercialmente (9% en peso, basado en mojado), Cuando la incorporación de fotocatalizador P25 esta pintura fue nombrado pintura de referencia.

Por lo tanto, la parte II de esta tesis doctoral se centra en el estudio de la fotoactividad de la pintura fotocatalítica, con la incorporación de distintos fotocatalizadores disponibles en el mercado, así como peliculas de polvo pressionado del fotocatalisador. Se concluye que el ranking de las mejores películas de pintura no se han encontrado con el ranking de las mejores películas en polvo presionado.

Por lo tanto, la influencia de los componentes de la pelicula de pintura en la fotoactividad del fotocatalizador P25 se estudió - parte III de esta tesis. Películas en polvo, que contienen componentes inórganicos de la pintura, y películas de pseudo-pintura, que contienen también parte de los componentes orgánicos, se prepararon mezclando los componentes de la pintura de referencia, paso a paso. Se concluyó que el TiO_2 pigmentario absorbe competitivamente la luz UV, siendo el componente más crítico que afecta la actividad fotocatalítica. Las películas también contienen diferentes componentes orgánicos, que se añaden en proporciones de acuerdo a la formulación de pintura de base, se muestran diferentes períodos transitorios. Sin embargo, tienen actividades similares en el estado estacionario. Esto se atribuyó a la photoerosion de una fracción similar de la fase orgánica (25 % en peso) durante el período transitorio. Componentes inorgánicos juegan un papel importante en fotoactividad a largo plazo de una película de pintura, de hecho, las películas que contienen los mismos inorgánicos, pero diferentes composiciones orgánicas, presentan similares actividades en estado estacionario.

La deposición de partículas de TiO_2 fotocatalítica en la superficie interna o externa del sólido poroso adsorbente de materiales inorgánicos, tales como las zeolitas, son los posibles enfoques para la protección de la pintura de la matriz. Si las partículas se depositan dentro de la estructura porosa, se puede lograr una protección de pintura evitando el contacto directo de la matriz de la pintura con las partículas de TiO_2 fotocatalítico; gases nocivos aún puede penetrar en el sistema de poros y seguir su oxidación. Por otro lado, si las partículas fotocatalítica de TiO_2 se depositan en la superficie externa del soporte, protección aún así puede ocurrir porque el contacto directo de la pintura y TiO_2 es reducido. Los capítulos 5 y 6 estudian la actividade del TiO_2 producido dentro y fuera del sistema de poros de diferentes soportes, respectivamente. Una fotoactividad mayor se observó para el TiO_2 soportado en la superficie externa de la zeolita Y.

Part I - *NOx and Photocatalysis*

Chapter 1 – Introduction

1.1 NOx: a priority pollutant

Anthropogenic NOx are mainly derived from combustion processes and can be divided into 3 groups according to the process of formation: - Prompt NOx; - Fuel NOx; - and Thermal NOx. Prompt NOx are produced in the fuel rich pre-combustion zone from the reaction between chemical radicals from the heated fuel with molecular nitrogen from combustion air (Fenimore mechanism) [1]. Fuel NOx result from the reaction between fuel nitrogen and molecular oxygen from combustion air. Thermal NOx, first proposed by Zeldovich [2], refers to NO and NO_2 formation via radical process from oxygen and nitrogen atoms. Such radical process is only possible at high temperatures in the flame zone and is therefore highly dependent on the combustion temperature.

Combustion flue gas is normally rich in NO; depending on the combustion technology, NO/NO_2 mixing ratio range from 500/1 up to 1000/1 (volume ratio). However, at typical atmosphere conditions $NO\text{-}NO_2$ thermodynamic equilibrium favors the formation of NO_2 (Figure 1.1), though kinetics are rather slow. NO concentration in the vicinity of the emission zone is then higher than it should be, if one consider just the thermodynamic equilibrium.

NOx have several impacts. Actually, they are related to the formation of [4]: - troposphere ozone; - secondary particulate matter; - gaseous nitric acid; - and toxic gases due to airborne reaction with volatile organic compounds (VOCs). Such processes lead to urban smog and acid rain occurrence as well as to eutrophication of water with high health and environmental impacts.

A complex net of chemical reactions involve NO and NO_2 in troposphere. Although controversy, major reaction paths can be sketched as follows, Figure 1.2.

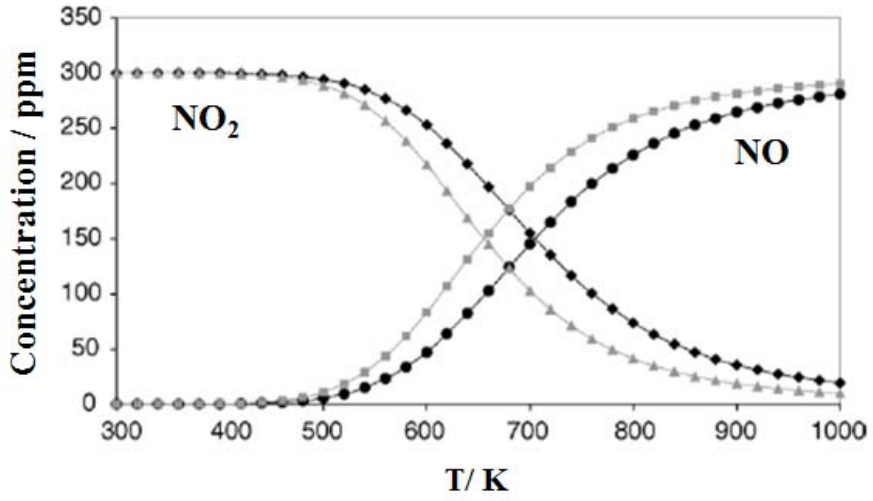

Figure 1.1 – Thermodynamic equilibrium concentration of NO (●, ■) and NO_2 (◆, ▲) starting from NO + NO_2 = 300 ppm in air (●,◆) and in oxygen depleted air (■, ▲) (adapted from [3]).

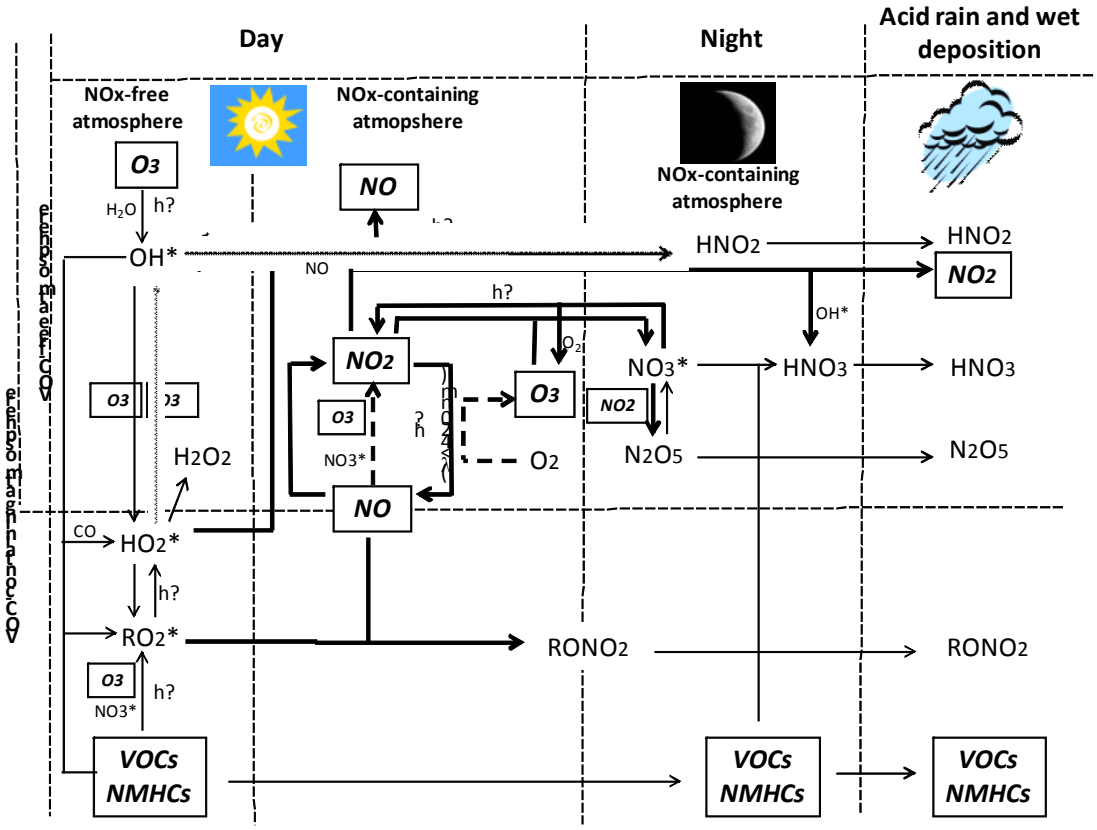

Figure 1.2 – Sketch of major reactions involving airborne NOx (rectangles represent anthropogenic primary gas emissions; bold lines represent reaction with direct involvement of NOx; NMHC – non-methane hydrocarbon; VOC – volatile organic compound) – adapted from [5, 6].

Stratosphere ozone diffusion to troposphere is responsible for O_3 ground level occurrence even in "clean" environment [5]. However, in a NOx-free atmosphere (usually below 100 ppt of NOx), ozone is constantly consumed, forming $OH^{\bullet}$, $HO_2^{\bullet}$ and $RO_2^{\bullet}$ radicals. In VOC-free, NOx-containing atmosphere, ozone reacts with NO originating NO_2. However, photolysis of NO_2 promotes the formation of ozone. These net reactions lead to null net ozone formation; though NO_2 can react with ozone to produce $NO_3^{\bullet}$ radicals, these are promptly photolysed to NO_2 again with ozone uptake [5]. In VOC and NOx-containing atmosphere, the concentration of $HO_2^{\bullet}$ radicals strongly increases, reacting with NO and interfering in the null ozone net reactions mentioned before; NO is oxidized towards NO_2 without ozone consumption. NO reactions with $RO_2^{\bullet}$ and $OH^{\bullet}$ radicals produce $RONO_2$ (gaseous or particulate) and gaseous HNO_2 and HNO_3. Ozone, $RONO_2$ and nitrogen acids are the main responsible for urban smog formation (Figure 1.2) directly related to health problems, namely lung diseases. The Great London Smog of 1952 was reported to be responsible for approximately 4000 deaths during 4 days and a further 8000 deaths in following weeks [7]. However, urban smog occurrence is still usual in the present in many cities, as in Beinjing (Figure 1.3).

Rain washout of airborne NOx and related nitrogen components (see Figure 1.2), are responsible for the acid rain. This wet deposition of nitrogen, along with dry deposition (particulate matter), promotes eutrophication of water.

NOx air concentrations and emissions started to be recorded after the Gothenburg protocol in 1972 and signatories' self-imposed NOx reductions targets. Within European Union, the National Emissions Ceiling Directive (NECD) is enforced until the end of 2010. However, taking into account last reports [8], at EU-27 only 16 countries expected to meet their NOx ceiling; France, Spain and Ireland expected to exceed their emission ceilings by 32 %, 28 % and 47 %, respectively. Road transportation is usually the main responsible for NOx emissions both in the EU and USA (Figure 1.4).

Figure 1.3 – Typical smog episodes: a) London, late of XIX century, photo and portrait by Monet; b) Beijing nowadays.

Table 1.1 shows that for usual priority gases, regarding urban air directives of international agencies, NOx are the ones with greatest troposphere ozone formation potential and secondary PM_{10} mass factor.

Therefore NOx occurrence in urban air, where 50 % of the world population lives [11], deserves special attention. Both USA Environmental Protection Agency (EPA) and European Environment Agency (EEA) established an hourly NOx air concentration limit of 0.1 ppm [12, 13]. NOx concentration still overcomes the limit allowed, even in small cities. This reflects the difficulties for problem solving; Figure 1.5 plots NOx concentration in the main avenue of Lisbon (Liberdade Avenue) in June (sunny dry month) and in December (foggy and rainy month) from 1995 until 2007. No clear reduction in NOx concentrations is observed and

$NO + NO_2$ concentration very often overcomes the maximum hourly limit of 0.1 ppm. Generally, NOx concentration is higher in the foggy rainy month of December than in June. Such fact must arise from the lower irradiance and consequent lower $OH^{\bullet}$ and $HO_2^{\bullet}$ radical production that can help the direct NOx removal (see Figure 1.2). NO concentration values higher than NO_2, highlights the kinetic constraints of NO oxidation towards NO_2 though the thermodynamic tendency towards the more oxidized species (Figure 1.1). Competitive reaction of $RO_2^{\bullet}$ with NO in comparison to reaction with ozone towards NO_2 can also play a role in NO prevalence over NO_2 (see Figure 1.2).

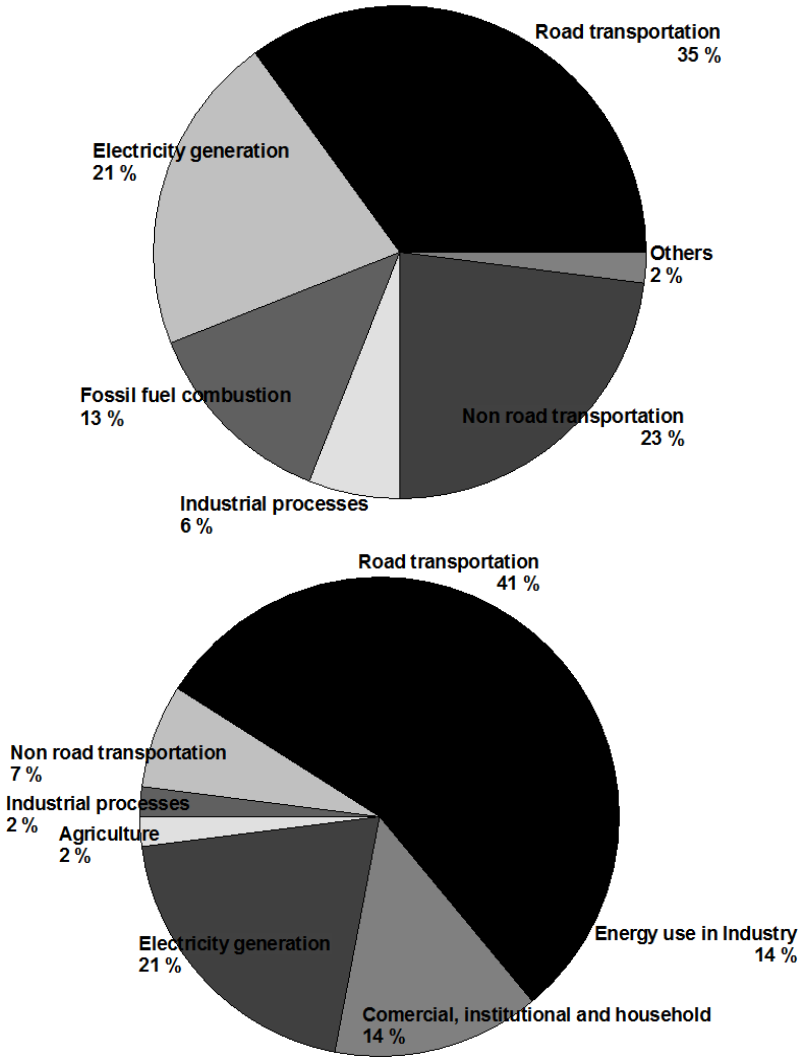

Figure 1.4 – NOx emission by source in the USA by 2005 (top) [9] and EU-27 by 2008 (bottom) [8].

Table 1.1 – Lifetime, acidity, PM_{10} mass factors and ozone formation potential for NOx and other priority pollutants [10].

Chemical	Lifetime (weeks or other)	Acidity mass factor (eq. $H^+ \cdot kg^{-1}$)	Secondary PM_{10} mass factor	Troposphere ozone formation potential
NOx	1 day	21.74	0.88	1.22[a]
SO_2	-----	31.25	0.54	-----
NH_3	-----	58.82	0.64	-----
NMVOC	< 4	-----	-----	1[a]
CO	8	-----	-----	0.11[b]
CH_4	450	-----	-----	0.014[b]

[a], responsible for short distance ozone formation; [b], responsible for transboundary ozone formation.

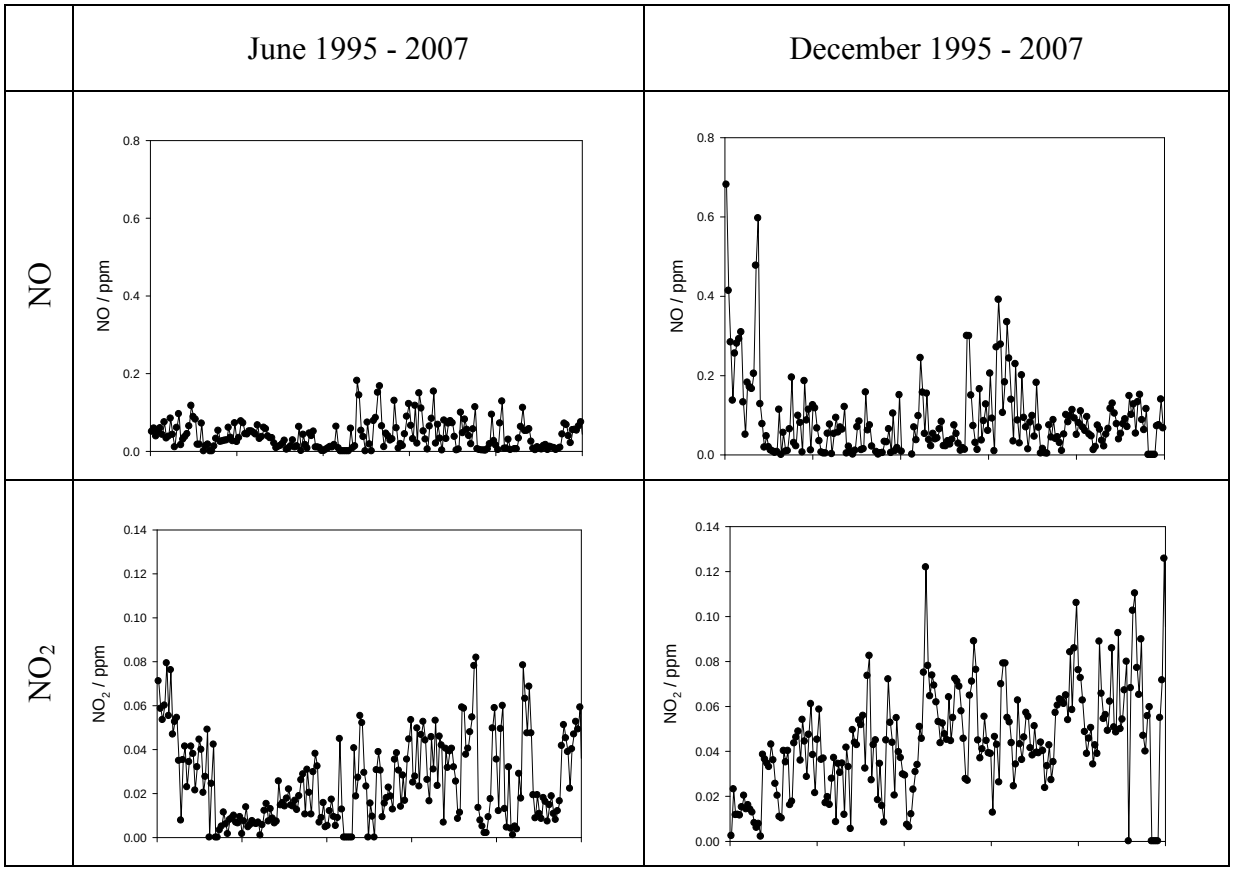

Figure 1.5 – NO and NO_2 concentrations in June and December from 1995 to 2007 at Lisbon (adapted from [14]).

1.2 From photoelectrochemistry to photocatalysis of NOx

In 1839, Becquerel [15] reported electric current production over an irradiated AgCl electrode immersed on an electrolyte and connected to a counter electrode; the phenomenum was known as Becquerel effect. Many years later, in 1972, Fujishima et. al. [16] succeed to make the water splitting using an irradiated photoanode of TiO_2. Both researchers created what it is presently known as a photoelectrochemical cell.

When two atoms get close enough to form a molecule, their atomic orbitals (valence orbitals) originate ligant and anti-ligant molecular orbitals, each containing up to two electrons (Pauli Exclusion Principle). Increasing the number of atoms in a molecule or cluster will increase the number of energy levels that a molecular orbital can have (Figure 1.6); this set of orbitals exhibits the so-called energy band. In the case of semiconductors, the valence band (lower energy) is separated from the conduction band (higher energy) by a certain energy, known as bandgap (ΔE, Figure 1.6). When an electron absorbs a photon with sufficient energy (higher than the bandgap) it moves from the valence to the conduction band; this is the so-called photoelectric effect. When an electron leaves the valence towards the conduction band, it creates an electron-hole pair (e^-/h^+, where h^+ stands for hole, the positive charge left in the valence band). These e^-/h^+ pairs can intermediate redox chemical reactions - photocatalysis. Figure 1.6 shows the potential edges and bandgaps of various semiconductors.

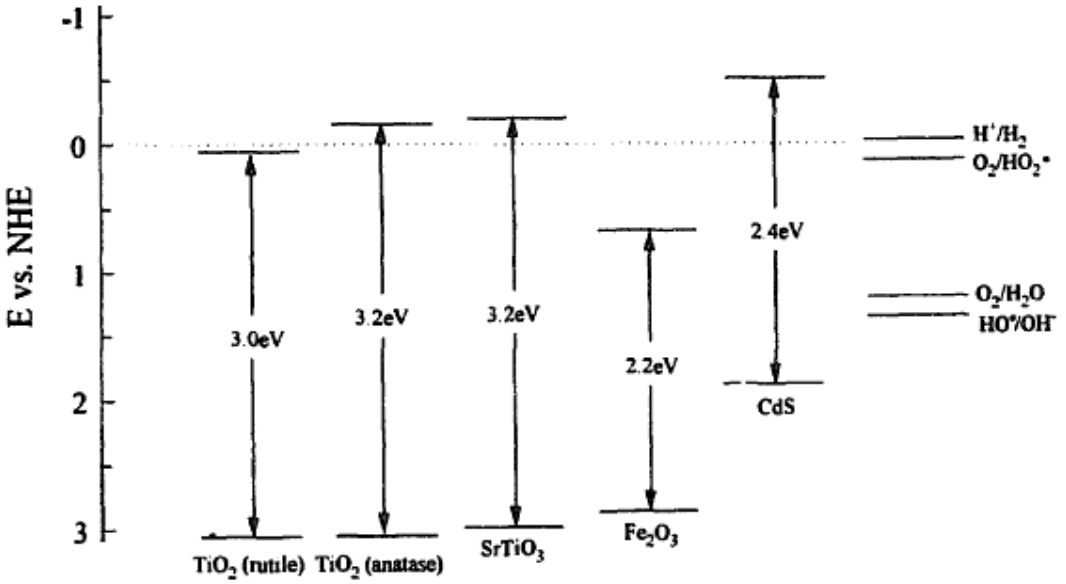

Figure 1.6 – Redox position bands of various semiconductors and their bandgaps (adapted from [17]).

Suitable photocatalysts for efficient photoabatement under solar radiation have to fulfill the following requirements:

I. Suitable bandgap and band edge positions, to have a high solar light harvest and enable reduction/oxidation of target species, respectively;
II. Efficient charge transport;
III. Low overpotentials for the reduction/oxidation reactions;
IV. High absorption of the reactants but not of the reaction products;
V. High chemical stability in the dark and under illumination;
VI. Harmless for the environment and humans;
VII. Low cost.

Photocatalytic TiO_2 has being by far the most used photocatalyst [18]. The high reduction potential of TiO_2 anatase valence band (ca. 2.7 V (NHE) at pH 7) [19] makes this semiconductor suitable for the photocatalytic oxidation of harmful species present either in gas [20, 21] or liquid [22, 23] phases. On the other hand, the reduction potential of TiO_2

conduction band is quite low (ca. -0.5 V (NHE) at pH 7) [19]. The energy band positions (band edges), which change with the pH, determines the semiconductor bandgap (3.2 eV for TiO_2 anatase). So, this semiconductor absorbs photons with energy not smaller than 3.2 eV, this means for wavelengths not longer than 387 nm (UV light). Since only ca. 5 % of the solar radiation has less than 387 nm, research is being done for producing photocatalytic TiO_2 with smaller bandgaps (i.e., with absorption at higher wavelengths, if possible in the Vis region). As illustrated in Figure 1.7, the photocatalyst promotes oxidation reactions with a reduction potential smaller than the corresponding valence band edge potential and reduction reactions with a reduction potential higher than the corresponding conduction band edge potential.

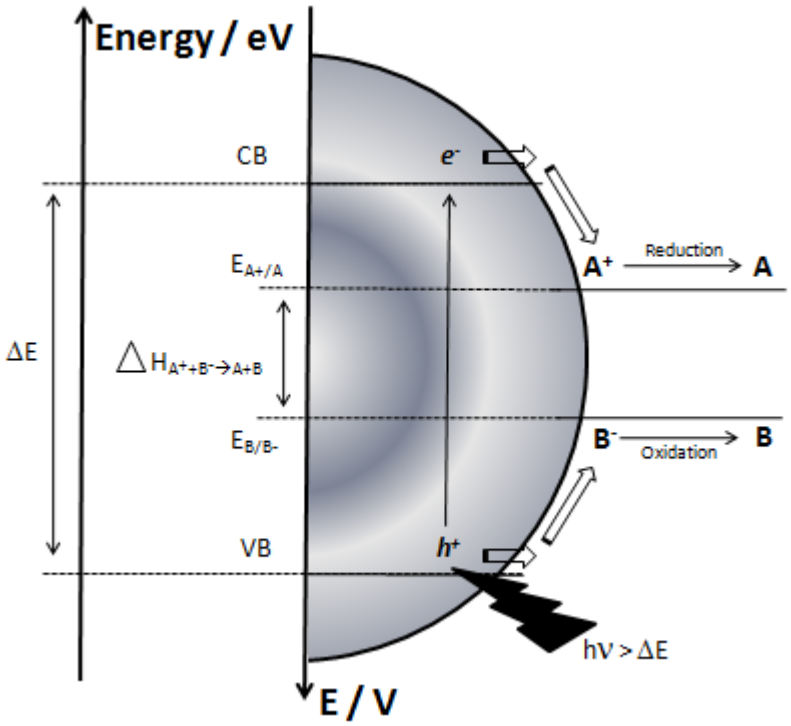

Figure 1.7 – Simplified sketch of photocatalytic phenomena over TiO_2 and relation with redox potentials and flat band energy positions.

Besides the band edges potentials, the mobility of charges also characterizes the photoactivity of a semiconductor. The e^-/h^+ pair generated in the semiconductor particle should move towards its surface. For instance, TiO_2 rutile absorbs light up to ca. 415 nm but is generally

less photoefficient than TiO_2 anatase. Indeed, the charge transport kinetics in rutile is about one order magnitude smaller than in anatase, making the recombination phenomena more probable to occur [24]. According to Kaneko and Okura [25], electron transfer at the surface of a semiconductor is normally a limiting step in photocatalytic processes. The transfer occurs due to charge accumulation on the surface of TiO_2 (depletion layer) and counter balancing charges in the surrounding of the particle (Helmholtz layer). Therefore, to promote fast reaction rates an overpotential is required [26, 27] (electron transfer overpotential), which is created by charge accumulation on the particle surface that makes, however, the recombination to increase [19]. Therefore a lower overpotential is desired. For the case of TiO_2 and under atmospheric conditions, water adsorption originates surface OH groups that can promote electron transfer to the adsorbed species [28] reducing the overpotential. When charge carrier densitiy increases, electron transfer at semiconductor surface also increases and difusion of species (reagents and products of reaction) becomes the limiting step; an even higher overpotential is required (diffusion overpotential) to counter balance the low concentration at surface [29]. In this way, adsorption and desorption kinetics of reactants and products, respectively, contributes for the efficiency of photocatalysis. Weak adsorption on TiO_2 surface is reported for the case of NO [30, 31] and NO_2 [30]. Adsorption of NOx is greatly influenced by oxygen vacancies on TiO_2 surface.

Matsuoka and Anpo [32] observed NO photocatalytic reduction towards N_2 and N_2O. For N_2O production, lateral interactions of adsorbed NO molecules must exist and are reported for a minimum surface coverage of 5.5×10^{14} molecules·cm^{-2} [32]. Higher coverage is reported to form N_2O_2, which adsorbs more strongly than NO, N_2O and NO_2 [30]. However, NOx photocatalytic reduction is commonly achieved when high partial pressures of NOx are observed along with absence of water and/or oxygen [e.g. 23]. At atmosphere conditions, the presence of water and oxygen together with low NOx partial pressures promote the NOx

photocatalytic oxidation. A dissociative adsorption of water occurs on surface defects for coverages up to 7 x 10^{13} molecules·cm^{-2} [33, 34] while molecular adsorption prevails for higher coverages, both in defects [35] and terraces [33, 34] of TiO_2 particles (Figure 1.8). A second layer is reported in a flat layer [35] with lattice oxygen interaction [33, 34, 36].

Concerning oxygen adsorption, photocatalytic [37 – 39] and co-adsorption studies with H_2O and NH_3 [40 - 42], revealed molecular oxygen adsorption centered on lattice oxygen vacancies producing extended oxygen adatoms, which help in the hydrolisys of coadsorbed water (Figure 1.9).

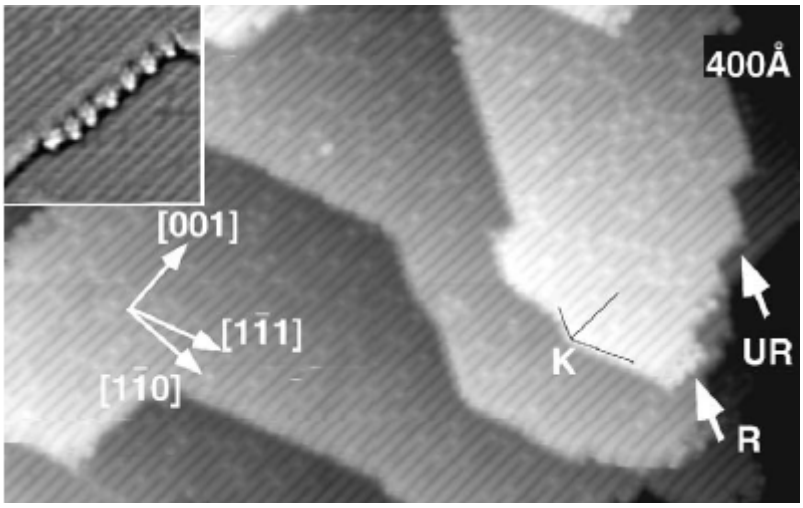

Figure 1.8 – Detail image of TiO_2 (adapted from [43]).

Adsorption also occurs on the vicinity of the oxygen vacancies towards Ti atoms. The presence of an adatom helps in the dissociation of adsorbed water on Ti^{4+} sites with formation of OH groups [43]. These OH groups are believed to have a greater contribution than adsorbed water in hydroxyl radical formation by electron donation to the hole produced on the valence band of excited TiO_2 (eqs. 1.1 – 1.2). Redox cycle closes with electron scavenging by the adsorbed oxygen reduction towards superoxide (eq. 1.3).

$$TiO_2(h^+) + H_2O_{ads} \rightarrow TiO_2 + OH_{ads}^- + H^+ \quad (1.1)$$

$$TiO_2(h^+) + OH_{ads}^- \rightarrow TiO_2 + OH_{ads}^{\bullet} \quad (1.2)$$

$$TiO_2(e^-) + O_{2ads} \rightarrow TiO_2 + O_2^{\bullet -} \quad (1.3)$$

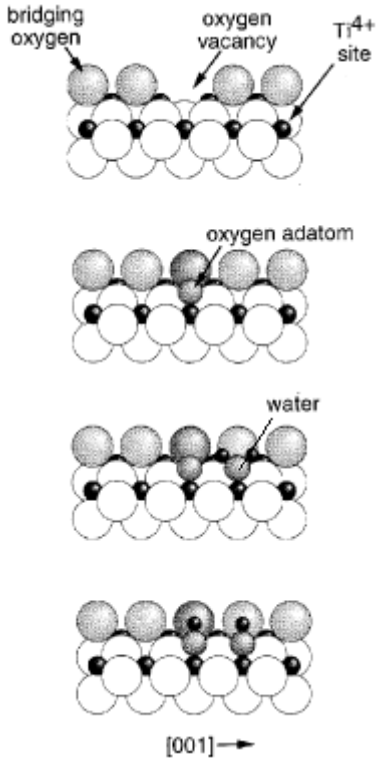

Figure 1.9 – Schematic models for O_2 and H_2O coadsorption on TiO_2 surface (adapted from [43]).

Photocatalytic oxidation is considered to occur by hydroxyl [44] and superoxide ion radicals [45]. In principle, oxidation of NO to NO_2^-, NO_2, NO_3^-, N_2O_4, N_2O_5 among other nitrogen-containing molecules is possible [3, 5, 45]. However, photocatalytic tests of NO over TiO_2 at typical atmospheric conditions reports the major formation of NO_2^-, NO_2 and NO_3^- as products of the reaction [25, 46]. In this way, one can assume that NOx photocatalytic oxidation takes place on TiO_2 surface with consequent nitrite and nitrate formation and NO_2 release. Nitrate and nitrite are strongly adsorbed on TiO_2 [44], impairing photocatalysis due to competitive adsorption or due to interference on redox chemical reactions, once the redox potentials of nitrate and nitrite are between the redox potentials of TiO_2 valence and

conduction bands (Figure 1.10). Therefore, the products of reaction nitrates and nitrites must be removed from the TiO_2 surface.

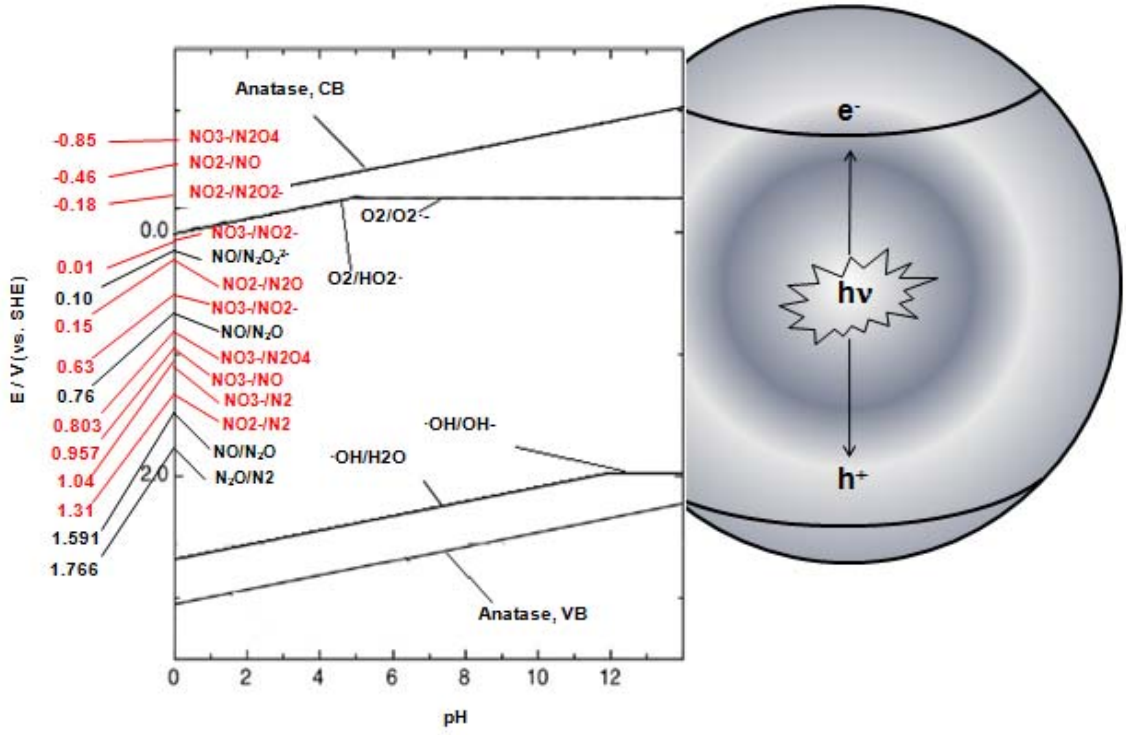

Figure 1.10 – TiO_2 anatase valence and conduction band reduction potential dependence on pH and reduction potential of some possible photocataytic reactions of NO, water and oxygen - reagents and products (adapted from [47 - 49]).

TiO_2 presents a good chemical and physical stability under dark and irradiated conditions that is important for real applications.

TiO_2 has been produced for many years and is part of the formulation of many products such has pills, paper, paint, chewing-gum, tooth-paste, among others [18]. However, recent studies with nanoparticulated TiO_2 refer possible neurons damage when in contact with brain cells [50]. This is a non-conclusive study and research is going on to assess the real harmfulness of nanoparticulated TiO_2.

The increasing interest on TiO_2 reinforced the worldwide production and prices are now lower than before. However, nanoparticulated TiO_2 (photocatalytic grade) is still a specialty, sold at ca. 150 €·kg^{-1}, compared to ca. 27 €·kg^{-1} for micron size TiO_2 [18].

1.3 Photocatalytic oxidation of NOx

1.3.1 Lab tests on pure photocatalytic TiO_2

Devahasdin et al. [44] studied the effect of irradiance, NO concentration, relative humidity (RH), and flow rate on the ability of P25 (Evonik) to photocatalyticaly oxidize NO. P25 was applied on the internal walls of a borosilicate tubular reactor by brush-coating. These authors concluded that a photocatalyst load higher than 0.7 $mg \cdot cm^{-2}$ did not improve the photoefficiency of the reactor. They referred an equilibrium limited photoefficiency for space time values greater than 12 seconds and found a strong dependence of NO conversion with the inlet concentration; the lower the NO inlet concentration, the higher the conversion for a concentration ranging from 5 ppm to 40 ppm. Devahasdin and co-authors also concluded that irradiance plays an important role on NO conversion, especially for high NO concentrations (above 40 ppm); however, for irradiances above 7 $W \cdot m^{-2}$ it was observed a constant NO conversion. Moreover, for 5 ppm NO concentration photoefficiency was found to be almost irradiance independent (irradiance from 2 $W \cdot m^{-2}$ to 7 $W \cdot m^{-2}$).

Kaneko and Okura [25] proposed a UV light controlled region for irradiances between 10^{-4} and 10^{-3} $W \cdot m^{-2}$ for solute concentrations between 1 and 10 ppm. On the other hand, Kaneko and Okura [25] reported a light controlled region for irradiances below 1 $W \cdot m^{-2}$, specifically for NO concentration of 1 ppm. These very different irradiance ranges of light controlled region point out the influence of photoreactor design on photoefficiency [51]. To allow a comparative assessment of photocatalysts and photocatalytic films performance, a standard based on the NO photocatalytic oxidation was proposed (ISO 22197-1:2007(E)) [52].

Devahasdin et al. [44] reported a positive effect of relative humidity on NO photocatalytic oxidation up to 50 % RH. However, this should depend on the adsorption properties of the used TiO_2 grade along with the NOx feed concentration. They observed the production of

NO_2 and nitrate at steady state conditions and reported 100 % selectivity towards NO_2 for NO inlet concentrations higher than 10 ppm. However, selectivity towards nitrate is 10 % and 50 % when NO inlet concentration is 6 ppm and 2 ppm, respectively, which are typical atmospheric concentrations in polluted areas. NO_2 selectivity also increases with irradiance.

Lab tests have been showing that photocatalysis using TiO_2 and under typical atmospheric conditions is able to perform NO and NO_2 abatement. Nitrate is the main product of reaction. Therefore, photocatalysis using TiO_2 can play an important role on urban air NOx depletion. Construction industry realized this and has been incorporating photocatalytic TiO_2 into their products, opening a new market segment - the photocatalytic construction materials.

1.3.2 Photocatalytic construction materials

Photocatalysis using TiO_2 presents some interesting features for atmospheric abatement of harmful gases [25, 53]:

I. The reaction is rather fast at the atmospheric pressure and room temperature;
II. It deals well with the relatively low atmospheric pollutants concentration;
III. A wide spectrum of organic contaminants can be oxidized towards harmless products;
IV. No additional chemical reactants are required;
V. Solar energy can be used as activation source;
VI. Photocatalytic TiO_2 is highly stable, both chemically and physically.

Such advantages do not disappear when incorporating photocatalytic TiO_2 in construction materials. Thus, construction materials can be used to support photocatalytic TiO_2, working as depolluting agents, especially in highly polluted urban areas.

However, radicals formed during the photocatalytic process, namely highly oxidative $OH^{\bullet}$, can increase the degradation rate of such construction materials. Kaneko and Okura [25] enumerate the requirements a support for photocatalytic TiO_2 should have:

I. Support the photocatalytic TiO_2 particles while allowing them to be photoactive;

II. Be chemically and physically stable;

III. Provide large specific surface area;

IV. Be harmless for environmental use.

Ibusuki mentioned that fluorocarbon based sheets, hardened cement paste and alkoxysilane-based paint are the most promising photocatalytic TiO_2 supports [25].

Marley Eternit [54], a UK based roofing solutions company, developed a photocatalytic roof tile, the EcoLogic. This company estimates that an average-sized roof made of EcoLogic tiles can remove an amount of NOx equivalent to that emitted by a modern car travelling 160 000 km, during its lifetime of 25 years [54].

Concerning lab scale tests, Cassar et al. [55] studied the photoefficiency of concrete in a standard-like setup. These authors observed a ca. 40 % NO conversion with a NO_2 selectivity of 70 %. On the other hand, Beeldens [56] concluded that the contact time and air turbulence are the controlling parameters of NOx photoabatement with photocatalytic concrete. Beeldens also reported a significant dependence of NOx photocatalytic conversion on the reaction chamber height.

Real scale tests are however necessary since conditions such as dust, sand and stain deposition, wind direction, typical air composition, among others, are difficult to reproduce in the lab.

In 2007, approximately 50 000 m^2 of urban surfaces were estimated to be covered with photocatalytic construction materials in Japan [57]. Kaneko and Okura [25] reports a test performed with windowed photocatalytic highway wall panels (0.6 m x 1.0 m) in Tokyo (Japan). Photocatalytic surfaces were attached to traditional panels and a borosilicate glass was used to cover them, producing a gap between the glass and the surface. Polluted air was pumped at a flow rate of 15 to 60 $L \cdot min^{-1}$ through the gap. Daylight irradiance was ca. 1

$W \cdot cm^{-2}$ at noon and an estimated amount of 113 000 vehicles crossed the 6-lane roadside per day. An average removal of 31 % to 69 % of NOx was obtained. The rate of NOx removal was calculated to be 3 $mmol \cdot m^{-2} \cdot d^{-1}$, based on the amount of nitrate washed from the panels.

Guerrini and Peccati [58] studied the NOx concentration profile as a function of the distance to a photocatalytic cementitious road; at 1.80 m high NOx concentration was 40 % higher than at 0.30 m high. The authors also showed that results are strongly dependent on weather conditions, namely wind velocity and direction [59].

Self-cleaning and antibacterial ceramic tiles, under the name Hydrotech and produced since 2000 by the Czech company Rako Rakovnik, were probably the first commercially available photoactive construction materials produced in Europe [60]. However, quality issues and a non-mature European market are responsible for the slow introduction in the market of these construction photocatalytic products.

From all possible construction materials, paint coatings present interesting advantages when used for immobilizing photocatalytic TiO_2: - almost all surfaces in urban areas can be painted; and - paints have the exact thickness for being optically opaque and then to produce photocatalysis. In this way, some European companies started to study and commercialize photocatalytic paints [61 - 63].

Bygott et al. [62] conducted a field test in a children playground in London, UK. An area of 300 m^2 of surrounding walls was painted with a silicate-based paint incorporating 7.5 wt.% of photocatalytic TiO_2. A daily abatement of ca. 4.5 g of NOx was reported from about 10 000 m^3 of air around the school playground.

When designing a paint formulation for immobilizing photocatalytic TiO_2, the following aspects should be considered:

I. Select the most suitable photocatalytic TiO_2 – particle size, bandgap and band edges, etc.;

II. Selection of photo-resistant binders – it should resist to the powerful photocatalytic oxidation promoted by TiO_2;

III. Long-term photoactivity;

IV. Degree of dispersion of photocatalytic TiO_2 in the paint;

V. Concentration of photocatalytic TiO_2;

VI. Immobilization of TiO_2 within a paint porous matrix with minimum light opacity (to maximize photo-TiO_2 light absorption) as well as free access of the chemical species to be degraded to the catalyst surface.

TiO_2 photoactivity depends on the particle diameter and crystal phase (anatase vs rutile) with anatase being usually more photoactive than rutile [25, 64 - 66]. The photocatalytic activity of micron size rutile TiO_2 is negligible [64]. On the contrary, the use of rutile pigmentary TiO_2 (micron size and coated TiO_2) together with nanoparticulate anatase TiO_2 seems to promote a feasible option for the development of self-cleaning paints and antimicrobial surfaces [67, 68].

Allen et al. [64] reported that the photocatalytic paint porosity has a positive effect on the photoactivity. The porosity allows gas diffusion through the film thickness to take better advantage of the immobilized photocatalytic TiO_2. The paint porosity is determined by the proportion between powder paint components, mainly pigmentary TiO_2 and extenders, and organic (non-powder) components, mainly the binder; porosity increases with the content on the powder components. However, Allen et al. [64] also concluded that a higher content in $CaCO_3$ and porosity promote a higher self-degradation rate of the paint.

In paint, the binder should be resistant towards the photooxidation promoted by TiO_2, hold the catalyst particles and allow them to keep their photoactivity. Kaneko and Okura [25] concluded that alkoxysilane is one of the best binders to be used in photocatalytic paint. An interesting approach to protect the paint matrix is the reduction of direct contact between the

matrix, and the photocatalytic TiO_2, which can be obtained allowing the presence of agglomerated particles of TiO_2 instead of primary particles [25, 67]. Motohashi and Inukai [65] showed that, with few exceptions, higher photoactivity is linked with higher paint degradation.

Long-term activity of a paint formulation is an important factor, enumerated above. Results obtained with an exterior, vinyl type, water-based photocatalytic paint (9 wt.% in P25) have shown a slight reversible loss of activity (Figure 1.11).

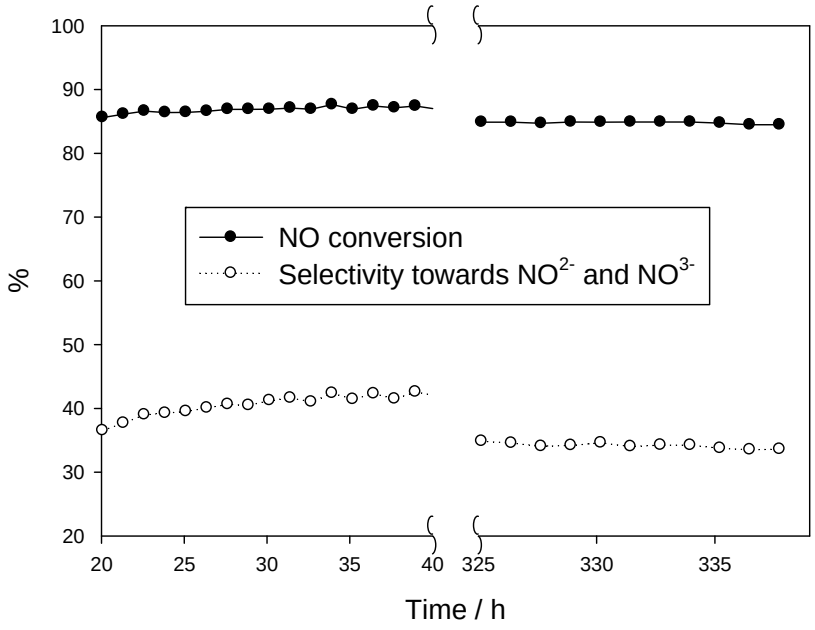

Figure 1.11 – Poison effect on photocatalytic paint films.

Decreasing the amount of photocatalytic TiO_2 in the paint would decrease self-photocatalytic degradation [68], but a loss in photoactvity towards hazardous gases would also occur. However, Ichiura et al. [69] showed that adding zeolites to photocatalytic paper allows the improvement on photoactivity towards NOx, eventhough a lower concentration of TiO_2 was used. Such approach must allow a higher paper matrix resistance, although rheological tests were not performed by the authors.

1.4 Motivation and Outline

Photocatalysis is gaining an increasing interest not only among the scientific community but also in the industry, which is coming up with technological solutions for air and water treatment, self-cleaning and microorganism photoinactivation surfaces (Figure 1.12).

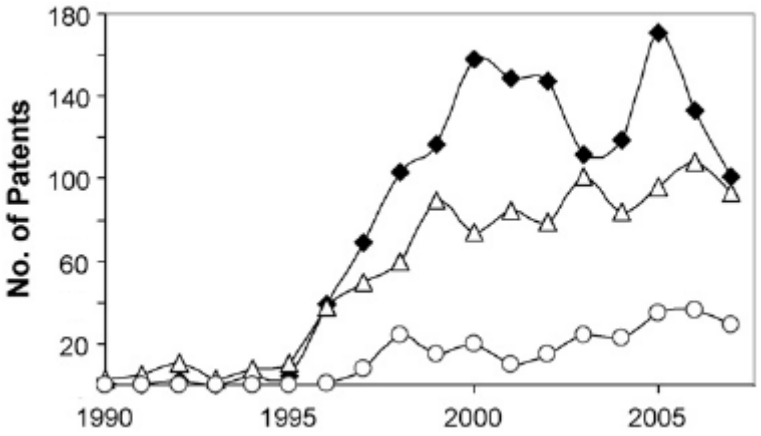

Figure 1.12 – Estimated number of patents on TiO_2 photocatalysis per year for air (filled diamond), water treatment (empty triangles) and self-cleaning surfaces (empty circles) (adapted from [70]).

Air treatment is drawing the highest attention, and the fact may be due to the increase in restricted legislation and weakness on problem solving of some harmful gases such as NOx. Construction materials, and namely paints, seem to be a good support for photocatalytic TiO_2 immobilization, acting therefore as depolluting supports.

A wide variety of TiO_2 photocatalysts are presently available in the market. From a photocatalytic paint development and commercialization point of view, it is important to know which are the most promising photocatalysts for NOx abatement. Therefore, this thesis starts by screening 10 commercially available TiO_2 photocatalysts as supplied and immobilized in a commercial paint. The photocatalytic activity was assessed based on standard ISO 22197-1:2007(E). These results are reported in chapter 2. Further on, the role of the paint matrix on photoactivity was addressed. The role of paint components that are present in the paint matrix was studied and important conclusions withdrawn. The study was focused on photocatalyst P25 (Evonik) and is presented in chapters 3 and 4.

The photocatalytic process is not selective since it normally generates free radicals, namely hydroxyl radical, that are responsible for the photodegradation of the paint matrix. The concentration of these radicals is related to the amount of TiO_2 irradiated. Therefore, photocatalytic TiO_2 was deposited and mixed with porous adsorbent particles aiming at minimize the paint matrix photooxidation and improving NO conversion and selectivity. Results are reported in chapters 5 and 6.

Finally, chapter 7 presents the conclusions of this work and suggests future developments.

References

[1] Kenneth, W., Warner, C., Davis, W., *Air Pollution - Its Origin and Control*, 3rd Edition, Prentice Hall, 1997.

[2] Nevers, N., *Air Pollution Control Engineering*, 2th Edition, McGrawHill 2000.

[3] Larrubia, M.A., Arrighi, L., Ramis, G., *Catalysis Today* 2005, 107, 139.

[4] European Environment Agency, *EEA-32 Nitrogen oxides (NOx) emissions*, Technical report No *APE002*/2010 (available at: http://themes.eea.europa.eu/IMS/IMS/ISpecs/ISpecification20080218104839/IAssessment1262689215798/view_content - accessed February 2011).

[5] Atkinson, R., *Atmospheric Environment* 2000, 34, 2063.

[6] Sadanaga, Y., Matsumoto, J., Kajii, Y., *Journal of Photochem. and Photobiol. C: Photochem. Reviews* 2003, 4, 85.

[7] Bell, M., Davis, D., Fletcher, T., *Environ. Health Perspect.* 2004, 112, 6.

[8] European Environment Agency, *European Union emission inventory report 1990–2008 under the UNECE Convention on Long-range Transboundary Air Pollution (LRTAP),* Technical report No 7/2010 (available at http://www.eea.europa.eu/publications/european-union-emission-inventory-report – accessed February 20011).

[9] http://www.epa.gov/air/emissions/nox.htm (accessed February 2011).

[10] Nikolas, N., Adams, M., in: European Evironment Agency (Eds.), *Transport Emissions of Air Pollutants (CO, NH_3, NO_X, NMVOCs, PM_{10}, SOx) by mode*, (available at:http://eea.eionet.europa.eu/Members/irc/eionet-circle/etcacc/library?l=/etcacc_ factsheets&vm=detailed&sb=Title – accessed February 2011).

[11] http://environment.nationalgeographic.com/environment/habitats/urban-profile/ (accessed February 2011).

[12] http://www.epa.gov/air/criteria.html (accessed February 2011).

[13] http://eur-lex.europa.eu/LexUriServ/LexUriServ.do?uri=OJ:L:2008:152:0001:01:EN:HTML (accessed February 2011).

[14] www.qualar.org (accessed February 2011).

[15] Becquerel, E., *C.R. Acad. Sci.* 1839, 9, 561.

[16] Fujishima, A., Kohayakawa, K., Honda, K., *J. Electrochem. Soc.* 1975, 122, 1487.

[17] Andrew, A., Le Hunt, S., *Journal of Photochemistry and Photobiology A: Chemistry* 1997, 108, 1.

[18] Robichaud, C., Uyar, A., Darby, M., Zucker, L., Wiesner, M., *Environ. Sci. Techno.* 2009, 43, 4227.

[19] Van, R., Liang, Y., Schoonman, J., *J. Mater. Chem.* 2008, 18, 2311.

[20] Anpo, M., in: Tundo, P., Anastas, P. (Eds.), *Green Chemistry*, Oxford University Press, 2000.

[21] Anpo, M., in: Corma, A., Melo, F.V., Mendioroz, S., Fierro, J.L.G., (Eds.), Proceedings of the 12th International Congress on Catalysts, Granada, *Studies in Surface Science and Catalysis* 2000, 130, 157.

[22] Ollis, D.F., AlEkabi, H., (Eds.), *Photocatalytic Purification and Treatment of Water and Air*, Elsevier, Amsterdam, 1993.

[23] Pelizzetti, E., (Eds.), *Photochemical Conversion and Storage of Solar Energy*, Kluwer Academic Publishers, Dordrecht, 1991.

[24] Kavan, L., Gratzel, M., Gilbert, S.E., Klemenz, C., Scheel, H.J., *J. Am. Chem. Soc.* 1996, 118, 6716.

[25] Kaneko, M., Okura, I. (Eds.), *Photocatalysis science and technology*, Springer, New York, 2002.

[26] Bolton, J.R., Strickler, S.J., Connolly, J.S., *Nature* 1985, 316, 495.

[27] Murphy, A.B., Barnes, P.R.F., Randeniya, L.K., Plumb, I.C., Grey, I.E., Horne, M.D., Glasscock, J.A., *Int. J. Hydrogen Energy* 2006, 31, 1999.

[28] Salvador, P., Gutierrez, C., *Chem. Phys. Lett.* 1982, 86, 131.

[29] Hamann, C.H., Hamnett, A., Vielstich, W., in: *Electrochemistry*, 2nd edition, Wiley-VCH, 2007.

[30] Sorescu, D.C., Rusu, C.N., Yates Jr, J.T., *J. Phys. Chem. B* 2000, 104, 4408.

[31] Rusu, C.N., Yates Jr, J.T., *J. Phys. Chem. B* 2001, 105, 2596.

[32] Matsuoka, M., Anpo, M., *Journal of Photochem and Photobiol C: Photochem Reviews* 2003, 3, 225.

[33] Henderson, M.A., *Surf. Sci.* 1996, 355, 151.

[34] Henderson, M.A., *Langmuir* 1996, 12, 5093.

[35] Kurts, R.L., Stockbauer, R., Madey, T.E., Roman, E., Segovia, J.L., *Surf. Sci*. 1989, 218, 178.

[36] Hugenschmidt, M.B., Gamble, L., Campbell, C.T., *Surf. Sci.* 1994, 302, 329.

[37] Lu, G., Linsebigler, A., Yates Jr, J.T., *J. Chem. Phys.* 1995, 102, 4657.

[38] Lu, G., Linsebigler, A., Yates Jr, J.T., *J. Chem. Phys.* 1995, 102, 3005.

[39] Rusu, C.N., Yates Jr, J.T., *Langmuir* 1997, 13, 4311.

[40] Henderson, M.A., Epling, W.S., Perkins, C.L., Peden, C.H.F., Diebold, U., *J. Phys. Chem. B* 1999, 103, 5328.

[41] Epling, W.S., Peden, C.H.F., Henderson, M.A., Diebold, U., *Surf. Sci.* 1998, 412, 333.

[42] Perkins, C.L., Henderson, M.A., *J. Phys. Chem. B* 2001, 105, 3856.

[43] Diebold, U., *Surf. Sci.* 2003, 48, 53.

[44] Devahasdin, S., Fan Jr., C., Li, K., Chen, D.H., *J. Photochem. Photobiol. A* 2003, 156, 161.

[45] Jourd'heuil, D., Kang D., Grisham, M.B., *Frontiers in Bioscience* 1997, 2, 189.

[46] Fujishima, A., Zhang, X., Tryk, D.A., *Surf. Sci. Rep.* 2008, 63, 515.

[47] Milazzo, G., Caroli, S., Sharma, V.K., *Tables of Standard Electrode Potentials*, Wiley, Chichester, 1978.

[48] Bard, A.J., Parsons, R., Jordan, J., *Standard Potentials in Aqueous Solutions*, Marcel Dekker, New York, 1985.

[49] Bratsch, S.G., *J. Phys. Chem. Ref. Data* 1989, 18, 1.

[50] Long, T.C., Tajuba, J., Sama, P., Saleh, N., Swartz, C., Parker, J., Hester, S., Lowry, G.V., Veronesi, B., *Environmental Health Perspectives* 2077, 115, 11.

[51] Kapteijn, F., Rodriguez-Miraso, J., Moulijn, J.A., *Applied Catalysis B: Environmental* 1996, 9, 25.

[52] International Standard Organization, *Fine ceramics (advanced ceramics, advanced technical ceramics) -- Test method for air-purification performance of semiconducting photocatalytic materials -- Part 1: Removal of nitric oxide*, ISO 22197-1:2007.

[53] Herrmann, J.-M, *Topics Catal.* 2005, 34, 49.

[54] Marley Eternit, *Ecologic Roof Tiles – Breathing Life Into the Environment* (available on: http://www.marleyeternit.co.uk/Roofing/Concrete-Tiles/EcoLogic-Ludlow-Major-Interlocking-Tile.aspx, accessed February 2011).

[55] Cassar, L., Beeldens, A., Pimpinelli, N., Guerrini, G.L., *Photocatalysis of Cementitious Materials*, International RILEM Symposium on Photocatalysis, Environment and Construction Materials, 8-9 October 2007, Florence, Italy, 131 - 146.

[56] Beeldens, A., *Air purification by road materials: results of the test project in Antwerp*, International RILEM Symposium on Photocatalysis, Environment and Construction Materials, 8-9 October 2007, Florence, Italy, 187 - 194.

[57] Osburn L., Proceedings of 5th Post Graduate Conference on Construction Industry Development, 16-18 March 2008, Bloemfontein, South Africa.

[58] Guerrini, G.L., Peccati, E., *White Cement and Photocatalysis – Part 1: Fundamentals*, International RILEM Symposium on Photocatalysis, Environment and Construction Materials, 8-9 October 2007, Florence, Italy, 179-186.

[59] http://www.picada-project.com/domino/SitePicada/Picada.nsf?OpenDataBase (accessed on February 2011).

[60] Peterka, F., Jirkovsky, J., St'ahel, P., Navrátil, Z., *Limits of application of photocatalytic technologies to construction materials, International RILEM Symposium on Photocatalysis*, Environment and Construction Materials 8-9 October 2007, Florence, Italy, 49 - 56.

[61] Paint company Sto – website for photocatalytic product Climasan (www.stoclimasan.com - accessed February 2011).

[62] Bygott, C.E., Maltby, J.E., Stratton, J.L., McIntyre, R., Photocatalytic Coatings for the Construction Industry, International RILEM Symposium on Photocatalysis, Environment and Construction Materials 8-9 October 2007, Florence, Italy, 251–258.

[63] Global Engineering - Photocatalytic building products (www.ecopurer.com - accessed February 2011).

[64] Allen, N.S., Edge, M., Verran, J., Stratton, J., Maltby, J., Bygott, C., *Polymer Degradation and Stability* 2008, 93, 1632.

[65] Motohashi, K., Inukai, T., *Self-cleaning Performance Evaluation of Commercial Photocatalyst Coating Materials Through 5 Years Outdoor Exposure*, International RILEM Symposium on Photocatalysis, Environment and Construction Materials 8-9 October 2007, Florence, Italy, 307 - 314.

[66] Solomon, D.H., Hawthorne, D.G., *Chemistry of Pigments and Fillers* 1983, Wiley-Blackwell.

[67] Fujishima, A., Hashimoto, K., Watanabe, T., TiO_2 Photocatalysis: fundamentals and applications, 1st edition, Bkc Inc., Kudanminami (Japan), 1999.

[68] Caballero, L., Whitehead, .A., Allen, N.S., Verran, J., *Dyes and Pigments* 2010, 86, 56.

[69] Ichiura, H., Kitaoka, T., Tanaka, H., *Journal of Materials Science* 2003, 38, 1611.

[70] Paz, P., Applied Catalysis B: Environmental 2010, 99, 448.

Part II – *Commercially Available TiO_2*

Chapter 2 – Photocatalytic Oxidation of NO – Screening of commercial TiO_2[1]

Abstract

The present chapter aims to evaluate the photocatalytic activity of photocatalytic TiO_2 from various producers (Evonik, Kemira, Kronos, Millennium Inorganic Chemicals, Sachtleben and Tayca), in the form of powder pressed films and upon incorporation in a water-based paint, for outdoor NO abatement. The photocatalytic activity of the different samples was evaluated in terms of NO conversion and selectivity towards nitrite and nitrate ions following approximately the ISO 22197-1:2007(E) standard.

The highest yields obtained for powder pressed films were achieved with VLP7000 (0.70), followed by VLP7101 (0.55) and UVLP7500 (0.55), all from Kronos. On the other hand, when incorporated in paint films, the highest yields were obtained with PC500 and PC105 from Millennium and UV100 from Sachtleben (ca. 0.15).

The paint matrix plays an important role on the photocatalytic activity. In particular, the time for steady state is one or two orders of magnitude higher when the photocatalysts are incorporated in paint films in relation to the powder pressed films.

The paint films were activated following the procedure recommended by the above-mentioned standard. However, the photocatalytic activity of films incorporating P25 (Evonik) was displayed only when higher power radiation and higher humidity conditions were used. This allowed for similar levels of photocatalytic activity as the other paint films.

[1] *Águia, C., Ângelo, J., Madeira, L.M., Mendes, A., Journal of Environmental Management (10.1016/j.jenvman.2011.02.010).*

2.1 Introduction

NO_x emissions have been receiving particular attention [1] as they are related to serious environmental and human health problems, namely acid rain, water eutrophication and photochemical smog formation [2, 3]. In the European Environment Agency (EEA-32) area, NOx emissions have decreased 31 % in the period 1990-2007 [4]. However, Spain is still reporting a significant increase in NOx emissions, far from the National Emissions Ceilings Directive (NECD) for the year 2010, while the emissions in Portugal have just stabilised [5]. Beyond this, it is also important to remark that although emissions have been decreasing, NOx concentration in air is still above EU legislated limit (2008/50/EC directive), especially in urban areas [6]. Therefore, the development of new technologies for NOx abatement and emissions reduction is required.

Photocatalysis using a semi-conducting material, mainly titanium dioxide, and free solar energy is a promising approach to handle with NO_X abatement. When a photon with sufficient energy is absorbed, occurs the injection of an electron to the conduction band and the consequent formation of a hole of positive charge in the valence band. The energy difference between these bands is called bandgap; for TiO_2-anatase the bandgap is 3.2 eV [e.g. 7] and only photons with less than 387 nm wavelengths have enough energy for promoting the electron injection. The hole in anatase has a high oxidation power, (2.7 V *vs.* NHE, at pH 7 [8]), which makes this semiconductor suitable for the production of highly oxidant hydroxyl radicals when in contact with water molecules or OH^- [9]. Hydroxyl radicals promote consequently the oxidation of harmful NOx, with nitrate production [10]. On the other hand, the excited electron has a high reduction power/low reduction potential (- 0.5 V *vs.* NHE, at pH 7 [8]), which forms O_2^- and contribute for the production of $HO_2^{\bullet}$ oxidant radicals [10, 11].

Presently, a range of photocatalytic TiO_2 is commercially available. Each performs differently according to their intrinsic properties, the support material and the interaction between the two [12]. Since photocatalysis deals better with low concentrations and environment temperatures [e.g. 10, 13], it is being considered to address the photoabatment of atmospheric pollutants. In this way, a number of construction materials incorporating photocatalysts are being studied for the abatement of NOx in urban areas, such as paints, glass windows and concrete for outside surfaces [14, 15]. Tests performed on a 500 meter long photocatalytic concrete pavement in an avenue of Bergamo, Italy, have led to a mean NOx concentration decrease of *ca*. 50 % [16]. On the other hand, Maggos et al. [17] reported a decrease between ca. 37 % and 82 % in a canyon-like pilot street, 2 m x 5.2 m x 18.2 m (width x height x length), in Guerville, France, coated with mortars containing 3 wt.% of photocatalytic TiO_2. Concerning the use of photocatalytic paints, Bygott et al. [18] conducted a field trial in London, close to a school children playground, where an area of 300 m^2 of walls was painted with a silicate-based paint incorporating 7.5 wt.% of photocatalytic TiO_2. These authors reported a daily NOx abatement of ca. 4.5 g in about 10000 m^3 of air around the school children playground [19].

In this work, the photocatalytic activity towards NO abatement is studied, using a paint incorporating different commercially available photocatalytic TiO_2. An exterior water-based paint was chosen, with a pigment volume concentration (PVC) slightly above the critical value (CPVC) [20]; PVC and CPVC are 62.2 and 59.3, respectively. The photocatalysts added to the paint were also evaluated directly in powder form. The photocatalytic tests followed roughly ISO 22197-1:2007(E) standard.

2.2 Experimental

2.2.1 Photocatalytic films

Different commercial photocatalytic TiO_2 grades were tested for the photooxidation of NO. Table 2.1 summarizes the main properties of the materials used, as reported by the manufacturers. The photocatalytic TiO_2 were tested in two forms: pure powder pressed film and incorporated in an exterior water-based paint (9 wt.% in wet base).

The vinyl type water-based paint used for incorporating the photocatalysts was a commercial exterior paint, from which half of the pigmentary TiO_2 was removed (this paint is hereafter named base paint). A brief description of its composition is given chapter 3 (and [20]). The same batch of the base paint was used for all experiments (unless otherwise stated). Each photocatalytic paint was then prepared by adding photocatalytic TiO_2 to ca. 50 cm^3 of the base paint and mixing for 30 min at 300 rpm in a 100 cm^3 stainless steel vessel. The final photocatalytic TiO_2 and pigmentary TiO_2 content was 9 wt.% in wet basis (*ca*. 17 wt.% in dry basis).

The photocatalytic films, either powder pressed or paint films, 0.10 m length x 0.05 m width, were applied over an aluminum slab. A draw-down bar was used to apply the photocatalytic paint films, producing wet films *ca*. 200 μm thick (varying slightly accordingly to the rheology of each film). Photocatalytic paint films were dried at lab conditions for one day; drying for longer periods showed no differences in terms of photoactivity.

Powder pressed films were obtained pouring the photocatalytic TiO_2 powder evenly over the aluminum slab and then pressing at ca. 5 bar for 7 min. This procedure yielded homogeneous powder films *ca.* 0.5 mm thick. The exact amount of photocatalytic TiO_2 poured over the support was obtained gravimetrically (using an analytical balance). The final load of photocatalytic TiO_2 (mass of photo-TiO_2 per area of film) was around 2 $mg \cdot cm^{-2}$ and 60 $mg \cdot cm^{-2}$ for paint and powder pressed films, respectively (except for powder pressed films of P25, for the reasons mentioned below – section 2.3.1.2).

Table 2.1 – Properties of the photo-TiO_2 used (data provided by the manufacturers).

Sample #	Photo-TiO_2 (manufacturer)	Crystal structure	Crystal Size (nm)	Surface area ($m^2 \cdot g^{-1}$)	Particle diameter (μm)
1	ANX type PA (Kemira)	Anatase	7 - 25	100 - 250	2 - 6
2	PC500 (Millennium)	> 99 % Anatase	5 - 10	345	1.2 - 1.7
3	PC50 (Millennium)	> 99 % Anatase	20 - 30	50	1.5
4	PC105 (Millennium)	> 99 % Anatase	15 - 25	86	1.2
5	P25 (Evonik)	80 % Anatase 20 % Rutile	25	50	n.p.
6	UV100 (Sachtleben)	Anatase	10	250	n.p.
7	UVLP7500 (Kronos)	Anatase	15	> 250	n.p.
8	VLP7000 (Kronos)	Anatase	15	> 250	n.p.
9	VLP7101 (Kronos)	Anatase	15	> 150	n.p.
10	AMT100 (Tayca)	Anatase	6	267	n.p.

n.p. – not-provided.

2.2.2 Experimental setup

The experimental setup used is depicted in Figure 2.1 and implements roughly ISO 22197-1:2007(E) standard.

It comprehends basically a photocatalytic reactor inserted in a thermostatic cabinet, a feed system and a NOx analyzer (Thermo Scientific 42C). The photoreactor is made of aluminum, with internal dimensions 0.05 m x 0.23 m x 0.005 m (width x length x height) and is equipped with a borosilicate glass window (Präzisions Glas & Optik GmbH) 0.005 m thick, at the top face (because the film is only 0.10 m long, a loading of 200 m^2/m^3 was used – photocatalytic film area per photocatalytic chamber volume). The borosilicate window has an overall light transmittance of more than 90 % between 330 nm and 400 nm; during 2 years of usage no solarisation effect was observed. The gas entrance and exit of the reactor is made via two mixture chambers that connect with the internal reaction chamber through 5 holes with 1 mm diameter, allowing an homogeneous gas flow across the reactor width (see Figure 2.2 for details). Two thermocouples were inserted at the entrance and exit of the internal reaction chamber to better assess the temperature (by means of a NI USB-9211A DAQ board with 24 bits).

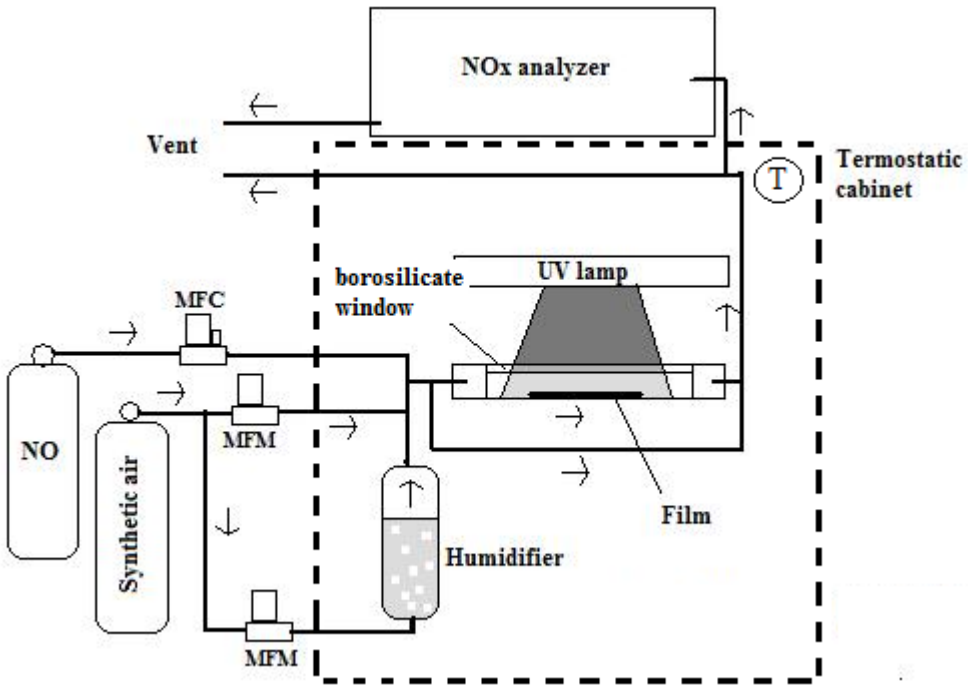

Figure 2.1 – Sketch of the experimental setup used for the photocatalytic tests (arrows represent the gas flow direction).

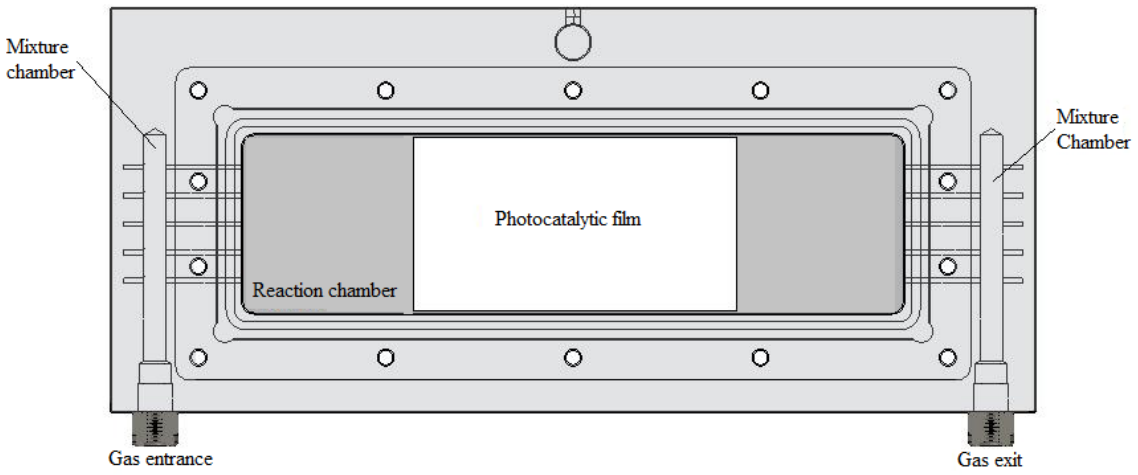

Figure 2.2 – Schematic representation of the photoreactor (top view).

The feed system is composed of two mass flow meters (MFM) and one mass flow controller (MFC) (Hi-Tech Bronkhorts, MFM 0-1 $L_N \cdot min^{-1}$ and MFC 0-0.1 $L_N \cdot min^{-1}$, with a precision of ±0.5 % FS) and a humidifier – Figure 2.1. The relative humidity (RH) of the air stream is adjusted by mixing dry and water-saturated synthetic air streams.

In the present study, a 50 % RH feed stream was supplied (Hydrogat 20; accuracy ±2 % RH), containing 1 ppm of NO in synthetic air at 25 ºC, in agreement with the above-mentioned standard; however, a flow rate of 0.7 $L_N \cdot min^{-1}$ (residence time of 2.1 s; equivalent to an air change rate of 1680 h^{-1}) was used instead of the 3 $L_N \cdot min^{-1}$ recommended by the standard.

The NO was added to the previously humidified synthetic air stream, from a gas cylinder containing ca. 45 ppm of NO in nitrogen (Linde – 2 % accuracy). In order to obtain a NO concentration of 1 ppm, it was necessary to add 2.3 % of this NO gas mixture to the synthetic air stream. The by-pass line to the reactor (see Figure 2.1) was used to calibrate the NOx analyzer at the beginning and to check the calibration at the end of each experiment; the maximum relative difference was always smaller than 1 %. The experimental setup was controlled using a data acquisition board system (Advantech PCI 1710HG and PCLD 8710) and an in-house developed program written in Labview (National Instruments).

2.2.3 UV lamp system

The UV lamp system (*Vilbert Lourmat* - BLB 365 nm, 2 x 6 W lamps) was placed over the borosilicate glass window of the reactor in a support that allows tuning the irradiance by changing the distance of the lamp to the reactor.

For the present tests, an irradiance of 7 $W \cdot m^{-2}$ was used (instead of the 10 $W \cdot m^{-2}$ recommended by the standard), which corresponds to a distance between the lamp and the reactor of ca. 0.20 m. The spectrum of the UV lamp system ranges from $\lambda_{initial}$=315 nm to λ_{final}=390 nm. The irradiance was measured across the reactor, at 7 equally spaced positions along the axial direction of the gas flow (z_i). These measurements were made at the transversal centre of the reactor, under the borosilicate glass window. A radiometer set (*Delta Ohm HD 2102.2* equipped with a *LP471UVA* sensor – maximum uncertainty of 5 %) was used for reading the irradiance per position during 60 min ($< I(z_i)_{read} >$). The UV lamp was allowed to stabilise for 30 min before the measurements. Transversal irradiance showed no significant variation. The irradiance reaching the surface of the photocatalytic films at a certain axial position z_i of the reactor, accounting for the borosilicate glass transmittance, the relative spectral response of the sensor (P_λ) and the radiant power of the lamp (W_λ) for each wavelength, averaged for the entire wavelength range, is given by [21]:

$$< I(z_i)_{film} >=< I(z_i)_{read} > \times \frac{\int_{\lambda_{initial}}^{\lambda_{final}} w_\lambda \, d\lambda}{\int_{\lambda_{initial}}^{\lambda_{final}} w_\lambda \times P_\lambda \, d\lambda} \qquad (2.1)$$

The irradiance profile at the reactor axial direction $< I(z_i)_{film} >$ is shown in Figure 2.3.

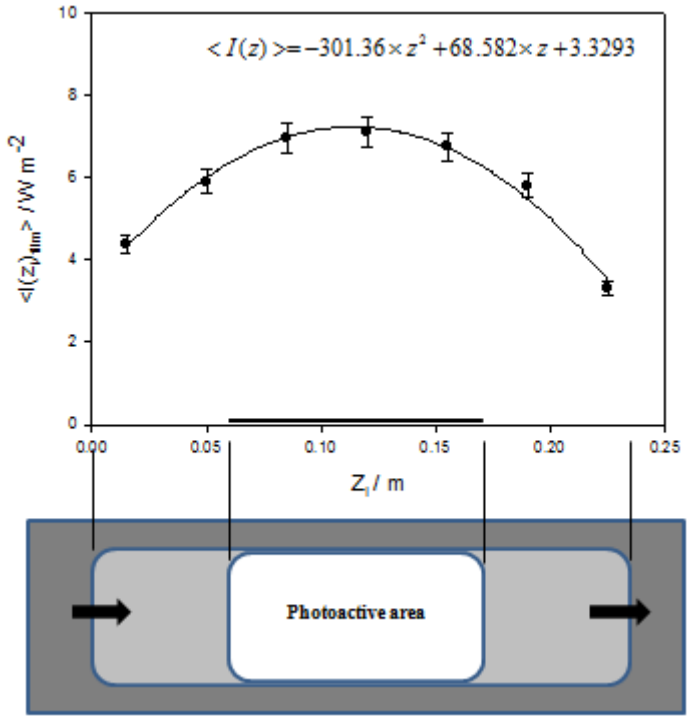

Figure 2.3 – Irradiance as a function of the position inside the photoreactor and respective uncertainty (maximum 5% considered); irradiance obtained with eq.(2.1) (full circles) and the corresponding interpolation curve (continuous line).

The average irradiance reaching the photocatalytic film ($< I_{film} >$) was calculated based on the irradiance profile over it:

$$< I_{film} > = \frac{\int_{z_{initial}}^{z_{final}} < I(z_i)_{film} > \mathrm{d}z}{z_{final} - z_{initial}} = 7 \ \mathrm{W \cdot m^{-2}} \qquad (2.2)$$

where active area of the photoreactor begins at $z_{initial} = 0.065$ m and ends at $z_{final} = 0.165$ m.

2.3 Results and discussion

2.3.1 Photocatalytic tests

Photocatalysis can originate the reduction [22] or the oxidation [10] of NO. However, photoreduction is commonly achieved when high partial pressure of NOx and/or reducing agents are present (CO, NH_3, etc.), and in the absence of water and/or oxygen [23]. For the operating conditions used, NO photocatalytic oxidation has been reported to originate only

nitrite (NO_2^-), nitrate (NO_3^-) and nitrogen dioxide (NO_2) [10], which were therefore considered to be the only reaction products in the present work. Since NO_2 is more harmful than NO for human health, the desired reaction products are the ionic species. In this way, two parameters were used to characterize the photoactivity towards the abatement of NO: NO conversion (eq. 2.3) and selectivity towards the formation of the ionic species NO_2^- and NO_3^- (eq. 2.4):

$$X_{NO} = \left(\frac{C_{NO}^{in} - C_{NO}^{out}}{C_{NO}^{in}} \right) \times 100 \quad (2.3)$$

$$S = \left(1 - \frac{C_{NO_2}^{out}}{C_{NO}^{in} - C_{NO}^{out}} \right) \times 100 \quad (2.4)$$

where C_{NO} and C_{NO_2} stand for the concentration of NO and NO_2, respectively, and the superscripts (*in* and *out*) refer to the reactor's inlet and outlet streams.

The steady state was considered to be achieved whenever NO conversion and selectivity do not vary more than ±2.5 percentage points for 5 h.

Before initiating the characterization of the photoactivity of the materials, the ability of the powder pressed films to adsorb NO and the ability of the base paint (containing no photocatalytic TiO_2) to photo-oxidize or adsorb NO was evaluated. With the UV light turned off, a negligible decrease in the exiting NO concentration was observed for all tests, indicating no significant NO adsorption (as compared to photocatalytic activity, due to the high flow rates used), either in powder pressed or paint films. No photoactivity of the base paint was also observed, even after 24 hours of activation under 90 % of RH and 30 $W \cdot m^{-2}$ (harsher activation protocol as detailed in section 2.3.1.1).

For the specific case of photocatalytic paint incorporating P25 the PVC was 62.4 and the critical one (CPVC) 55.0.

2.3.1.1 Effect of the activation step on the photoactivity

The initial photoactivity of the fresh photocatalytic films was improved after an activation period; the following operating conditions were chosen for activating the films (hereafter referred as standard activation): 25 ºC, 50 % RH, 7 $W \cdot m^{-2}$ and 0.7 $L_N \cdot min^{-1}$ using a synthetic air stream (with no NO gas) for 5 h. In the case of paint films incorporating photocatalyst P25, the activation procedure had to be harsher in order to obtain photoactivity. In this case the following operating conditions were employed: 90 % RH and 30 $W \cdot m^{-2}$ for 24 hours (this procedure is hereafter referred as harsher activation).

Figure 2.4 shows the NO conversion and selectivity histories obtained with three different films made of the same photocatalytic paint batch produced with photocatalyst ANX type PA. The results were obtained using the same operating conditions but activated differently, i.e., with no activation, and employing standard and harsher activation procedures.

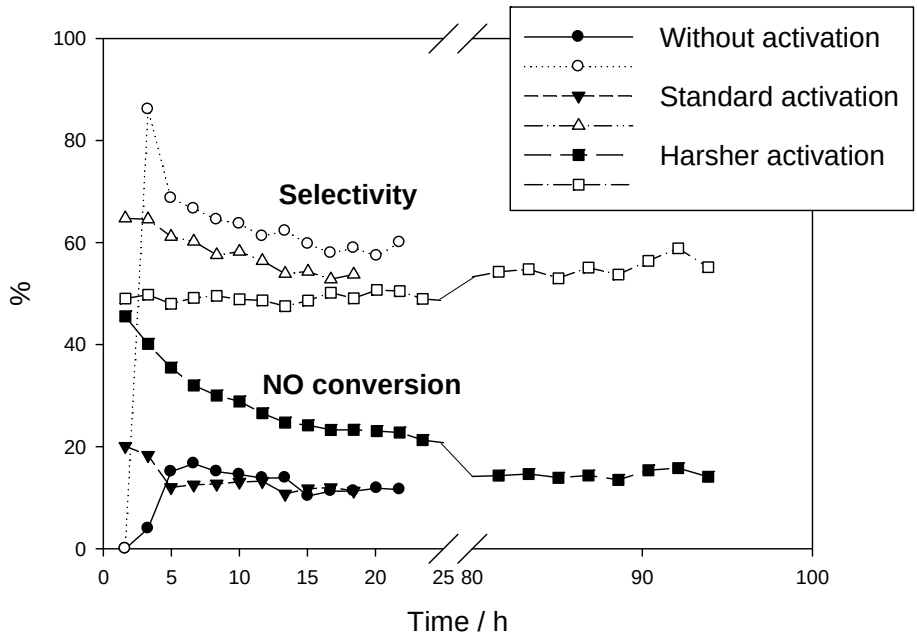

Figure 2.4 – NO conversion (full symbols) and selectivity (empty symbols) histories as a function of the activation protocol for paint films incorporating ANX type PA.

All the films showed different transient behaviors concerning the conversion and selectivity histories. The non-activated film showed no photoactivity for about 4 hours. After this period, it became photoactive, showing approximately the same steady state performance as the remaining samples (Figure 2.4). On the other hand, the harsher activated film showed a transient photoactivity that exceeded the steady state during a long period of time, ca. 90 hours; the standard activated film exhibited an intermediate photoactivity history. After the transient behavior, the steady state performance of all three photocatalytic films was approximately the same. Similar behavior was observed for other photocatalytic paint films; the steady state is approximately the same, no matter the activation protocol used and consequent transient behavior. Despite, in real tests other variables may play a role affecting the steady state performance, such as chalking with possible photocatalyst washout and dirty that can impair light absorption.

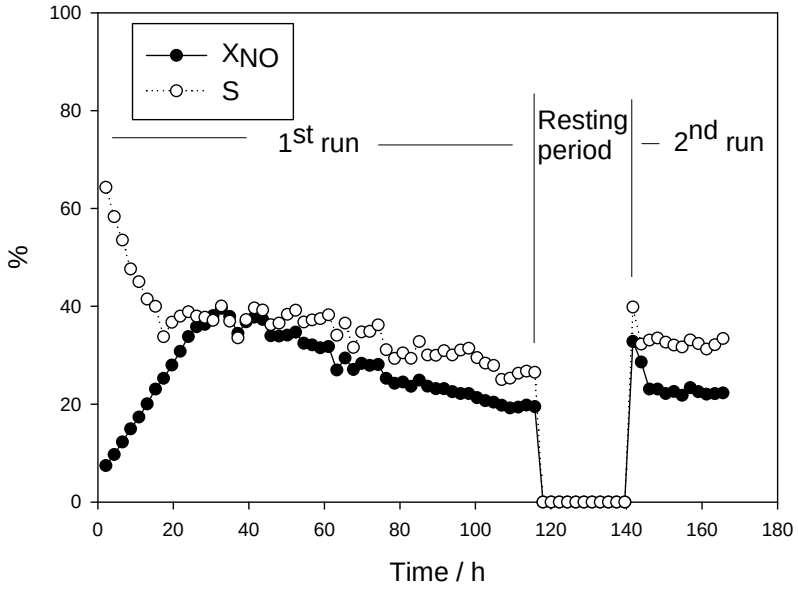

Figure 2.5 – NO conversion (full symbols) and selectivity (empty symbols) histories in two consecutive runs, with 24 hours resting period, with a photocatalytic paint film incorporating UVLP7500.

Figure 2.5 shows the history of NO conversion and selectivity of the paint film produced with photocatalyst UVLP7500, after the standard activation. This figure illustrates two consecutive runs; the paint sample was withdrawn from the photoreactor and reinserted back after one day. It can be seen that the steady state conversion and selectivity are approximately the same, showing a stable performance for the photocatalytic film after the steady state has been reached. This same behavior was observed for paint films made with other photocatalysts (data not shown). The steady state performance of a photocatalytic paint film seems therefore to be independent of the history.

Regarding the powder pressed films, no noticeable differences were observed for each sample as a function of the activation protocol, in both transient and steady state photoactivity (data not shown). In the following sections, standard activation was used, unless otherwise stated.

2.3.1.2 Repeatability and effect of photo-TiO_2 load

Repeatability of the photoactivity performance on the powder pressed and paint films and the effect of photocatalytic TiO_2 load in the photoactivity of powder pressed films were assessed using P25 and VLP7101. Table 2.2 shows the steady state NO conversion and selectivity for these tests. Powder pressed films made of P25 and VLP7101 show very different loads (Table 2.2) for similar thicknesses because P25 bulk density is very low when compared to the density of VLP7101.

The NO conversion and selectivity at steady state in powder pressed films with different photocatalyst loads are very similar (Table 2.2). This should indicate that the film is optically thick (constant optical thickness despite the film thickness and TiO_2 load); this was also concluded from spectrophotometer contrast ratio tests.

Table 2.2 – Steady state NO conversion and selectivity of powder pressed and photocatalytic paint films of P25 and VLP7101 photo-TiO_2 – study of repeatability and load effect.

Film type	**Run #**	**Photo-TiO_2**	**$L_{photo\text{-}TiO2}$ (mg·cm^{-2})**	**X_{NO} (%)**	**S (%)**
Powder pressed	1	P25	13.5	81	47
	2		18.4	81	44
	3		23.7	80	48
	4	VLP7101	61.6	94	61
	5		67.2	90	60
Paint	6	P25	2.30	25	30
	7		2.30	24	21
	8(1)		2.27	29	30
	9	VLP7101	2.23	27	40
	10		2.35	25	40

(1) Paint produced with a different base paint batch.

Figure 2.6a shows that for P25 pressed films the steady state condition was attained after a short transient period of *ca.* 5 h. On the other hand, the steady state photoactivity of the corresponding paint film, Figure 2.6b, was achieved after a much longer operation period of *ca*. 100 to 200 h, variable according to the batch of base paint used; paint films exhibited a less reproducible transient behavior even when the same batch of base paint was used, which highlights the interference of the paint matrix with the photocatalytic process. Generally, for the case of paint films, more than 100 hours were required to attain the steady state, with exception for the paint film incorporating ANX type PA which required only ca. 10 h (Figure 2.4). About 5 to 10 percentage points of variation in steady state NO conversion and selectivity within paint films can be generally considered as result of experimental errors (Table 2.2).

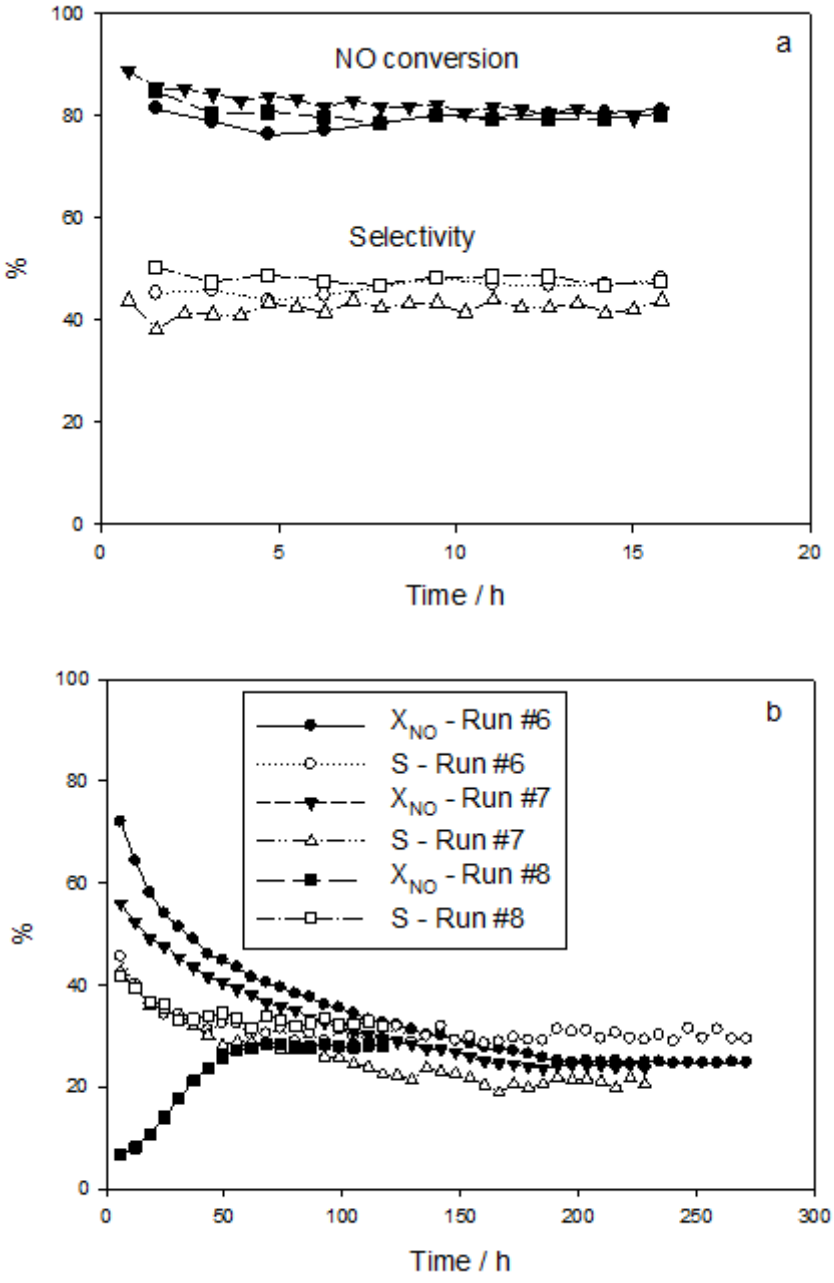

Figure 2.6 – NO conversion (full symbols) and selectivity (empty symbols) for (a) powder-pressed films of P25 (Runs #1-3) and (b) photocatalytic paint films of P25 (Runs # 6-8), as described in Table 2.2.

2.3.1.3 Steady state photoactivity of the powder pressed and paint films

Table 2.3 shows the load of photo-TiO_2 in powder pressed and paint films, which photoactivity results at steady state are presented in Figures 2.7 and 2.8. Figure 2.7 shows the steady state NO conversion and selectivity values obtained for all samples.

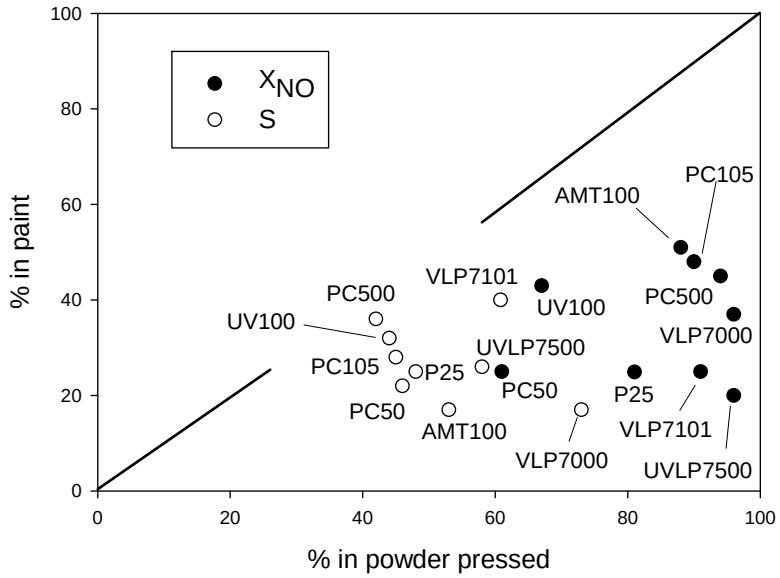

Figure 2.7 – Steady state NO conversion (full circles) and selectivity (empty circles) for all tested powder pressed (X axis) and paint (Y axis) films.

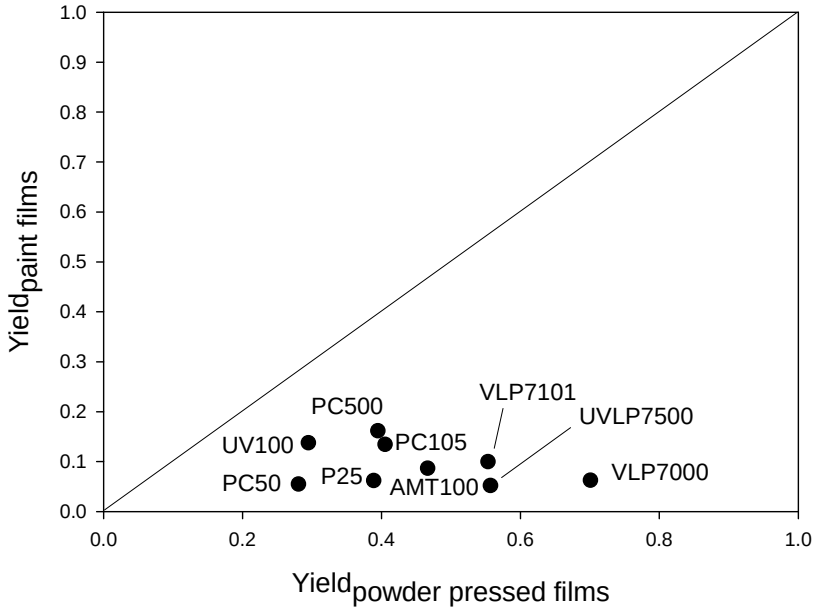

Figure 2.8 – Yield (product of NO conversion and selectivity) obtained at steady state for all tested powder pressed (X axis) and paint (Y axis) films.

The photocatalytic yield is the product of the NO conversion and selectivity, weighting this way the two characterizing parameters. Figure 2.8 shows the steady state yield obtained with the powder pressed and paint films, therefore condensing the information given in Figure 2.7. It was not possible to make a powder pressed film with ANX type PA because this material has a very low cohesion. Even though the paint films were formulated with the same mass fraction of each commercial TiO_2, they exhibit different photocatalytic TiO_2 loads because of the differences in the film thicknesses.

Table 2.3 – Photo-TiO_2 loads of the powder pressed and paint films shown in Figure 2.7.

	$L_{photo\text{-}TiO2}$ (mg·cm^{-2})	
Photo-TiO_2	**Powder pressed films**	**Paint films**
ANX type PA	n.p.	1.91
PC500	60.3	1.97
PC50	79.0	1.66
PC105	71.3	2.33
P25	18.4	2.30
UV100	65.9	2.00
UVLP7500	50.4	2.27
VLP7000	57.7	2.23
VLP7101	61.6	2.35
AMT100	67.1	2.23
Average	**64.2**[1]	**2.13**
Standard deviation	**8.7**[1]	**0.23**

n.p. – not-performed; (1) - P25 was not included in this calculation because of its relative lower load (see section 2.3.1.2 for details).

Figure 2.7 shows that NO conversion values obtained with powder pressed films are generally above 80 %; only PC50 and UV100 exhibit lower NO conversions, in the range of 60 - 70 %. When incorporated in paint, PC500, PC105, UV100 and AMT100 revealed the highest NO conversion values (ca. 40 - 50 %), while ANX type PA had the lowest one (15 % - Figure 2.4, not shown in Figure 2.7 due to lack of results in powder pressed form).

For each commercial photocatalytic TiO_2, the NO conversion was always higher for the powder pressed than for the paint films. These differences should result from the much higher photocatalyst loads and the hiding and impairing effects of the paint matrix.

Figures 2.7 and 2.8 also show that there is no apparent relationship between photoactivity of the commercial samples in powder *vs.* paint films (i.e., the less or more active materials in powder pressed films are not necessarily the same in paints); so, the interaction between the paint matrix with each photocatalytic TiO_2 must play a role on the photoactivity of the paint films.

It is worth mentioning that the paint film added with P25 showed no photoactivity when activated following the standard protocol, becoming photoactive only after the harsher activation protocol. This behavior should be related to the higher dispersion of the photocatalyst in the paint films, as discussed below (see Figure 2.11). As shown by Fujishima and co-workers, a better dispersion of photocatalytic TiO_2 in the matrix of the support lead to a greater interference of the matrix in the photocatalytic process [12].

It is also important to remark that photocatalyst UV100 exhibited the smallest NO conversion difference when comparing paint and powder films – respectively 40 % and 65 %. Such fact highlights the importance of better understanding the interactions between paint components and photocatalytic TiO_2; it was shown, for example, that there is a significant competitive absorption of UV by the pigmentary TiO_2 of the paint (chapter 3 and 4 and [20]).

Concerning the selectivity obtained with the powder pressed films, VLP7000 showed the highest value (ca. 75 %) followed by VLP7101 and UVLP7500 (ca. 60 %); the selectivity obtained with the remaining materials lied in the range of 40 % to 55 % (Figure 2.7). Regarding the selectivity obtained with paint films, ANX Type PA showed the highest value (ca. 55 % - Figure 2.4), exhibiting however the lowest NO conversion (15 %). VLP7101, PC500 and UV100 showed the second highest selectivity (30 % to 40 %).

No clear relationship was found between the photocatalytic TiO_2 properties - Table 2.1 - and their photoactivity, either in powder pressed or paint films (Figures 2.7 and 2.8).

The highest yields for powder pressed films were obtained with photocatalysts VLP7000 (0.70), VLP7101 and UVLP7500 (ca. 0.55), while for paint films the highest yields were achieved with PC500, UV100 and PC105 (ca. 0.15). The yield obtained with the photocatalytic paint containing ANX type PA was 0.06 (data not shown).

2.3.2 Diffuse reflectance and SEM analyses

Light interaction with an optically thick powder pressed film of photocatalytic TiO_2 particles results in absorption and scattering. The intensity of each phenomenon varies accordingly to the wavelength used, particle diameter and nature, film morphology, crystal-lattice, temperature and pressure [24]. The photoactivity depends on the nature and morphology of the photocatalyst but also on the powder pressed film ability to absorb effectively the incident light. Figure 2.9a shows the incident light spectrum used on the photocatalytic tests and the diffuse reflectance of the powder pressed films tested (data not shown for ANX type PA because it was not possible to obtain stable powder pressed films). The diffuse reflectance data were obtained using a Perkin Elmer lambda 750 spectrophotometer, equipped with a 60 mm integrating sphere and using Spectralon^{TM} as 100% reflectance standard. The powder samples were supported on the above-mentioned aluminum slabs.

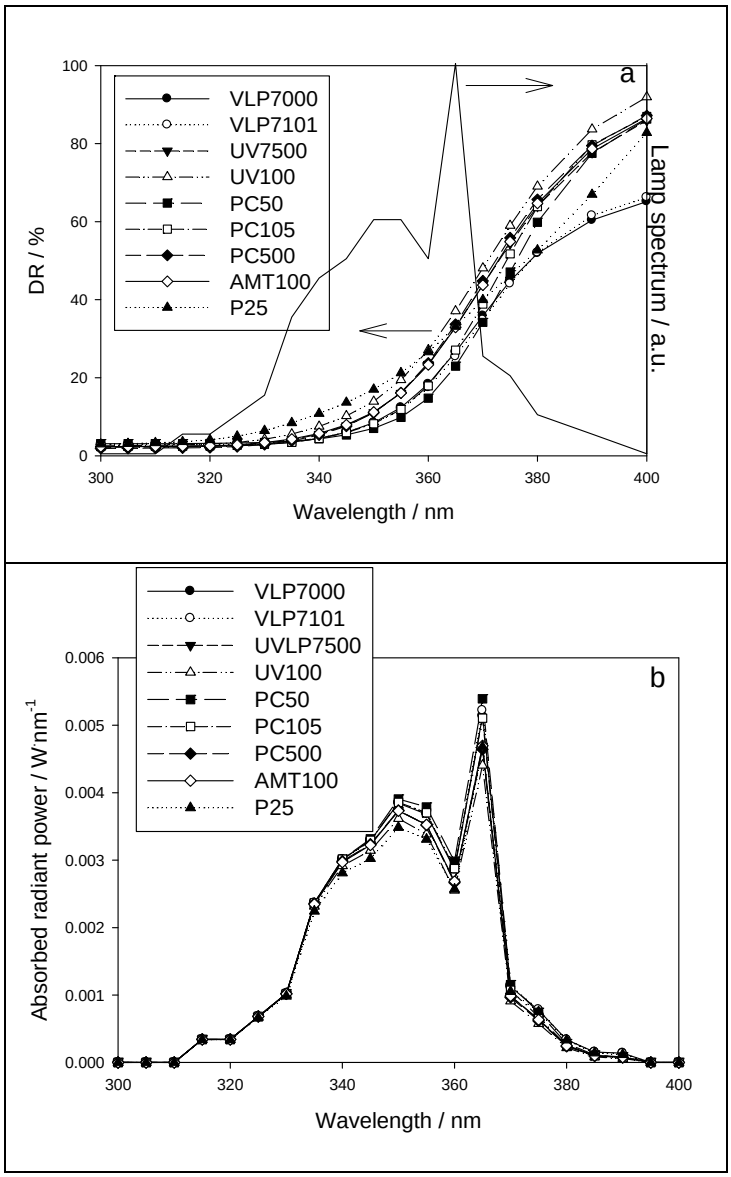

Figure 2.9 – Diffuse reflectance (DR) of powder pressed films and incident UV lamp spectrum (a) and absorbed spectral radiant power for the same powder pressed films (b).

Figure 2.9a shows that VLP7000 and VLP7101 have the lowest diffuse reflectance above 380 nm, with ca. 65 % reflectance at 400 nm, in opposition to ca. 80 % for the remaining photocatalysts, indicating the ability of VLP samples to effectively absorb visible light [25]. These results are in good agreement with the data reported by the manufacturer.

The "absorbed radiant power" (Figure 2.9b) was calculated based on the light intensity per wavelength reaching the film subtracted by the corresponding reflectance, which is shown in Figure 2.9a. It is possible to see that most of the differences among the samples lie between

the wavelengths from 335 nm to 365 nm, which corresponds to the range of the maximum radiant power of the lamp used (cf. Figure 2.9a). Figure 2.10 shows the NO conversion and selectivity as a function of the total absorbed radiant power (integral of the "absorbed radiant power"); no clear trend was observed indicating that either the energy differences are not significant or other variables are playing a significant role.

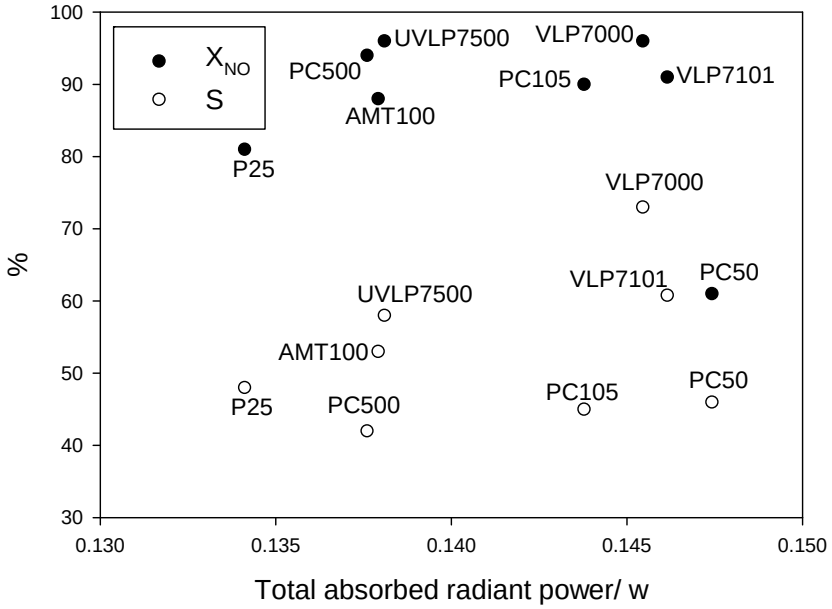

Figure 2.10 – NO conversion and selectivity as a function of the total absorbed radiant power by the powder pressed films between 315 nm and 390 nm.

SEM images of some photocatalytic films are shown in Figure 2.11; left side images show powder pressed films while right side ones show paint films. In this Figure, there are visible agglomerates of primary particles with dimensions in good agreement with the values provided by the manufacturers, cf. Table 2.1 and Table 2.4. P25 (Figure 2.11c and d), PC500 (Figure 2.11e and f) and the remaining photocatalytic TiO_2 tested show uniform-size agglomerates, while VLP7101 (Figure 2.11a) and PC50 exhibit two distinct particle morphologies: the smaller primary particles form agglomerates while the bigger ones do not agglomerate. Despite these behaviors, the EDS analyses indicates that in both cases

agglomerates and individual particles are only made of TiO_2 (data not shown). In Figure 2.11b there are visible smooth round hollow spheres. These spheres are a polymeric extender used for increasing the paint contrast ratio (opacity). Besides these spheres, Figure 2.11 shows that the morphology of the photocatalytic TiO_2 is similar when analysed in powder pressed films (Figure 2.11c and e) or when incorporated in paint films (Figure 2.11d and f).

Table 2.4 – Particle diameter and shape of the photo-TiO_2, obtained by SEM.

Photo-TiO_2	**Particle diameter (μm or specified)**	**Shape**
ANX type PA	2 to 6	Agglomerates
PC500	1.5	Agglomerates
PC50	~ 0.1 and ~ <1.5	Single large particles and agglomerates
PC105	1.5	Agglomerates
P25	25 nm	Primary particles
UV100	1 to 3	Agglomerates
UVLP7500	1 to 3	Agglomerates
VLP7000	1 to 3	Agglomerates
VLP7101	~ 0.1 and ~ 1	Single large particles and agglomerates
AMT100	< 2	Agglomerates

P25 was the photocatalyst that showed the highest dispersion in paints among all the photocatalysts tested (see Figure 2.11). This higher dispersion exposes the photocatalyst to the direct contact with the paint matrix, and then to possibly more severe photocatalytic hindering effects. As mentioned before, this might be the reason why a harsher activation was needed for this material.

Powder	Paint
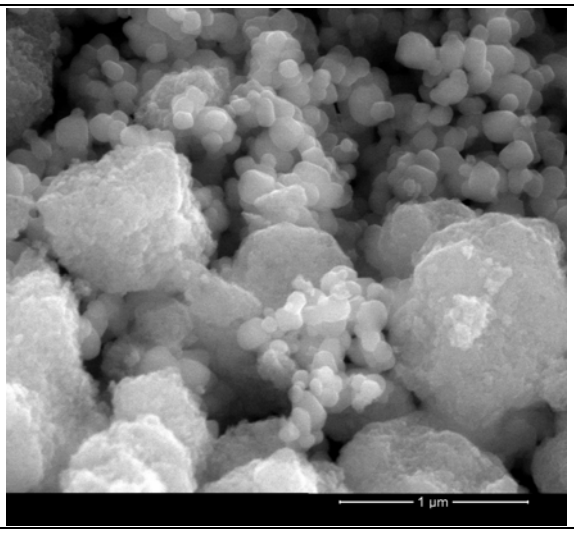	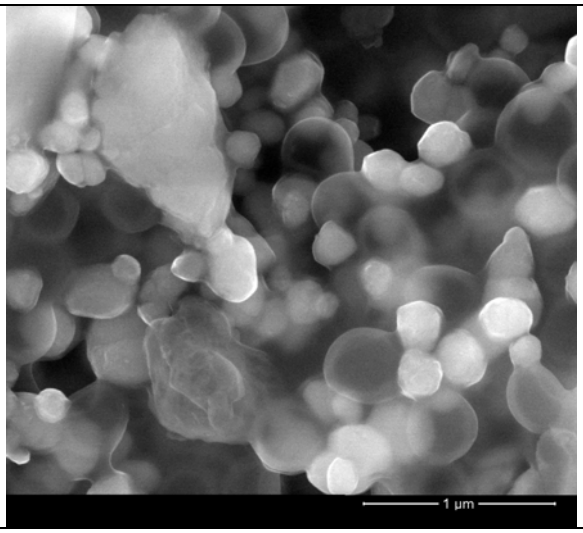
a) VLP7101	b) Base paint
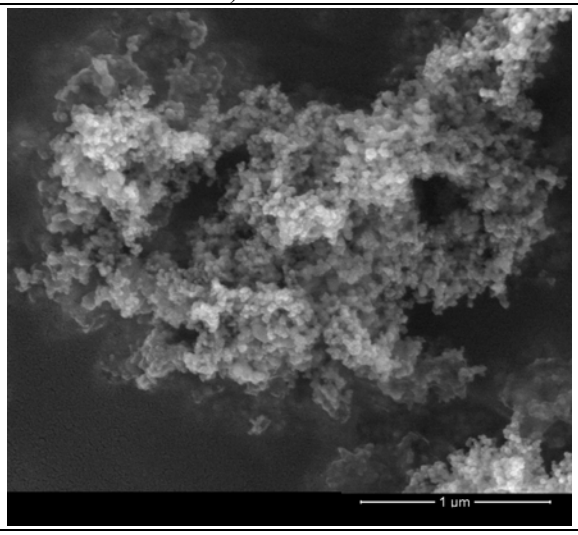	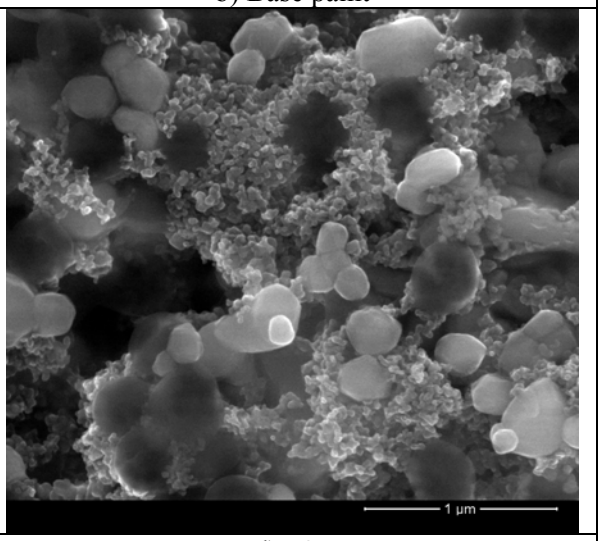
c) P25	d) P25
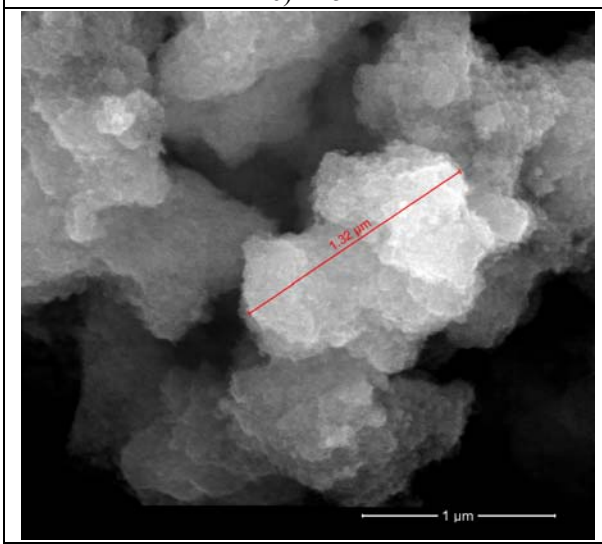	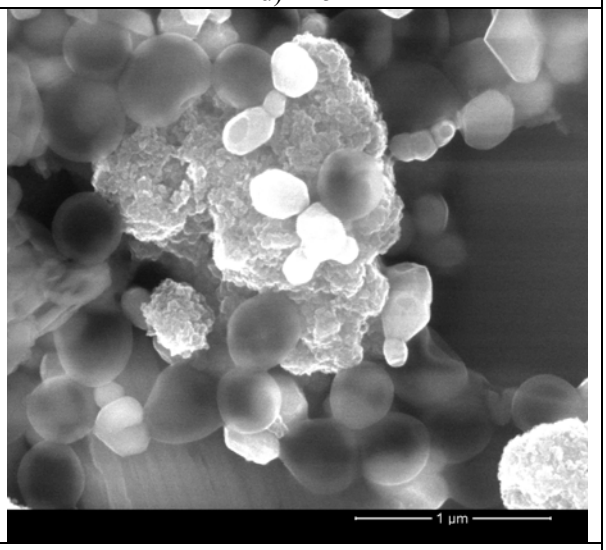
e) PC500	f) PC500

Figure 2.11 – SEM images of the photo-TiO_2 in powder (left images) and paint (right images) films – 100 000x mag.

2.4 Conclusions

In the present study 10 commercial photocatalytic TiO_2 samples were tested for NO abatement. The photoactivity was assessed following approximately ISO 22197-1:2007(E) standard. The photocatalysts were tested as powder pressed films and incorporated in a water-based paint, with a content of *ca.* 9 wt.% (wet base). For this, an exterior water-base paint with PVC slightly above the critical value was used.

In the photocatalytic tests, the steady state conversion and selectivity were attained faster with the powder pressed films than with the paint films: respectively within *ca*. 5 hours and generally after more than 100 hours. No clear relation was found between the photoactivity of the commercial photocatalytic TiO_2 in powder and when incorporated in the paint film; i.e., the best performing photo-TiO_2 in powder form was not the best when incorporated in the paint. Such fact indicates that the paint support plays an important role in the photoactivity of the tested materials, as shown elsewhere (chapters 3 and 4 and [20]).

The photocatalytic TiO_2 in powder form exhibited always a higher photoactivity than when incorporated in the paint. This can be partially explained by the photocatalytic content: 100 wt.% when in the powder form compared with ca. 17 wt.% (dry base) when incorporated in paint. The highest yields were obtained with powder pressed films of photocatalysts VLP7000 (0.70), VLP7101 (0.55) and UVLP7500 (0.55), while the highest yields obtained with paint films were achieved with PC500, UV100 and PC105 (ca. 0.15).

The powder pressed films showed a very reproducible photoactivity that was not influenced by the activation step. On the other hand, the photoactivity of the paint films showed a great dependence on the activation protocol, affecting the time needed to reach the steady state. However, the steady state photoactivity of a given photocatalytic paint was the same, independently of the activation protocol, within the accepted variation of 5 to 10 percentage points. Moreover, after attaining the steady state a paint film held the photoactivity even after

a resting period. Such fact confirms the steady state results as more adequate for photocatalytic TiO_2 screening than initial or transient values.

References

[1] European Commission, *Attitudes of European Citizens Towards the Environment*, Special Eurobarometer 295/Wave 68.2 – TNS Opinion & Social, March 2008 (available at: http://ec.europa.eu/public_opinion/archives/ebs/ebs_295_en.pdf – accessed February 2011).

[2] United States Environmental Protection Agency, *How nitrogen oxides affect the way we live and breathe*, EPA-456/F-98-005, September 1998 (available at: http://www.cleanairaction.org/pubs/pdfs/old_pubs/noxfldr.pdf - accessed February 2011).

[3] Leeuw, F.A.A.M., *Environ Sci Policy* 2002, 5, 135.

[4] – European Environment Agency, - EEA-32 Nitrogen oxides (NOx) emissions, Technical report, APE002/2010 (available at: http://themes.eea.europa.eu/IMS/IMS/ISpecs/ISpecification20080218104839/IAssessment1262689215798/view_content - accessed February 2011).

[5] European Environment Agency, *NECD: Member State Country-Profiles*, 2007 (available at: http://www.eea.europa.eu/themes/air/nec-directive-member-state-country-profiles/nec-directive-member-state-country-profiles - accessed February 2011).

[6] Riga-Karandinos, A.-N., Saitanis, C., *Chemosphere* 2005, 59, 1125.

[7] Fujishima, A., Zhang, X., Tryk., D. A., *Surf. Sci. Rep.* 2008, 63, 515.

[8] Krol, R., Liang, Y., Schoonman, J., *J. Mater. Chem.*2008, 18, 2311.

[9] Diebold, U., *Surf. Sci. Rep.* 2003), 48, 53.

[10] Devahasdin, S., Fan Jr., C., Li, K., Chen, D.H., *J. Photochem. Photobiol. A* 2003, 156, 161.

[11] Gerischer, H., Heller, A., *J. Phys. Chem.* 1991, 95 5261.

[12] Fujishima, A., Hashimoto, K., Watanabe, T., *TiO_2 PhotocatalysisFundamentals and Applications*, 1st ed., BKC Inc., Tokyo (Japan), 1999.

[13] Herrmann, J.-M., *Appl. Catal. B: Environ*. 2010, 99, 461.

[14] Paint company Sto – website for photocatalytic product Climasan (www.stoclimasan.com - accessed February 2011).

[15] Global Engineering - Photocatalytic building products (www.ecopurer.com - accessed February 2011).

[16]. Guerrini, G.L, Peccati, E., *White Cement and Photocatalysis – Part 1: Fundamentals*, International RILEM Symposium on Photocatalysis, Environment and Construction Materials, 8-9 October 2007, Florence, Italy, 179-186.

[17] Maggos, Th., Plassais, A., Bartzis, J.G., Vasilakos, Ch., Moussiopoulos, N., Bonafous, L., *Environ. Monit. Assess.* 2008, 136, 35.

[18] Bygott, C.E., Maltby, J.E., Stratton J.L., McIntyre, R., *Photocatalytic Coatings for the Construction Industry*, International RILEM Symposium on Photocatalysis, Environment and Construction Materials, 8-9 October 2007, Florence, Italy, 251-258.

[19] Koleske, J.V., *Paint and coating testing manual*, 14th ed., Gardner-Sward Handbook, Philadelphia, 1995.

[20] Águia, C., Ângelo, J., Madeira, L.M., Mendes, A., *Catal. Today* 2010, 151, 77.

[21] Salvad-Estivill, I., Hargreaves, D.M., Puma, G.L., *Environ. Sci. Technol.* 2007, 41, 2028.

[22] Matsuoka, M., Anpo, M., *J. Photochem. Photobiol. C*, 2003, 3, 225.

[23] Bowering, N., Walker, G.S., Harrison, P.G., *Appl. Catal. B – Environ* 2006, 62, 208.

[24] Siegel, R., Howell, J.R., *Thermal radiation heat transfer*, 4th ed., Taylor & Francis, New York, 2002.

[25] Blöß S.P., Elfenthal, L., *Doped Titanium Dioxide as a Photocatalyst for UV and Visible Light*, International RILEM Symposium on Photocatalysis, Environment and Construction Materials, 8-9 October 2007, Florence, Italy, 31-38.

Part III – *The Paint Matrix*

Chapter 3 – Influence of Paint Components on P25 Photoactivity – Powder and organic paint components[2]

Abstract

The present chapter studies the effect of the components of a photocatalytic paint towards the photooxidation of NO. A high quality vinyl exterior paint, modified with photocatalyst P25, was used. NO conversion and selectivity towards nitrate and nitrite were obtained in an experimental photocatalytic reactor that implements essentially the standard ISO 22197-1:2007(E).

It is concluded that the paint matrix plays an important role on the photocatalytic activity: pigmentary TiO_2 absorbs competitively the UV light, being the most critical component affecting the photocatalytic activity; extenders, such as $CaCO_3$, impair the photoactivity, especially when water is involved in mixing the paint components; organic components mostly affect the performance of the paint during a transient period time of *ca.* 100 - 250 hours.

[2] *Águia, C., Ângelo, J., Madeira, L.M., Mendes, A., Cataysis Today 2010, 151, 77.*

3.1 Introduction

Air pollution has been calling the attention of the public in general [1]. Amongst numerous air pollutants, hazardous gases for human health are of particular concern, mainly in urban and industrial areas.

Presently, more than a half of the population in developed countries lives in highly dense traffic cities. Such way of living exposes people to toxic gases like carbon monoxide and nitrogen oxides (NO + NO_2). End of pipe technologies developed over the last decades have been particularly important to decrease the emission of hazardous gases to the atmosphere. However, some gases are still present in the atmosphere above their legal limits; NOx, mainly produced by vehicles, is one of such examples. NOx concentrations are above the legal limits established by the European Commission (2008/50/EC) not only in big cities but even in small cities with relative low traffic such as Guimarães (Portugal), Patras and Volos (Greece), among others [2, 3]. It is therefore necessary to improve and develop new de-pollution technologies.

Photocatalysis is an attractive technology for de-pollution proposes because it uses solar radiation and works at ambient temperatures and at typical low airborne concentrations [4, 5]. In a simple way, photocatalysis can be described as a redox process that uses a catalyst activated by photonic energy (photocatalyst).

Photocatalysts have been incorporated into construction materials so they can act as de-polluting agents. They have been incorporated into cement/mortars pavements [e.g. 6, 7], coatings [8 - 12], among others. Maggos et al. [9], for instance, reported a NO photoabatement of *ca.* 40 % to 80 % in a canyon pilot street under real weather conditions using mortar panels. Bygott et al. [11] conducted a field trial in London, close to a children playground, where an area of 300 m^2 of walls was painted with a silicate-based paint loaded

with 7.5 wt.% of photocatalytic TiO_2. It was reported a daily abatement of *ca.* 4.5 g of NO_X from about 10 000 m^3 of air around the school playground [11].

In order to be commercially attractive, a photocatalytic paint should exhibit a high photoactivity while preventing its own degradation. However, typical photocatalysts processes involving hydroxyl radicals are generally non-selective and strategies for minimizing paint photodegradation must be developed. At the same time, paint components can impair photoactivity concerning the abatement of target pollutants. This can be due to several factors such as blockage of radiation and/or blockage of the gas pollutants itself towards the photocatalyst, electron-hole external recombination or preferential photooxidation of organics present in the paint.

In a previous work by the authors, various commercially available photocatalytic TiO_2 materials were incorporated in an exterior water-based paint [12]. In this study it was noticed a strong influence of the paint components on the NO photooxidation [12]. Paint film incorporating the photocatalyst P25 (Evonik) was, among those tested, the only one requiring a harsher activation procedure to become promptly active. In this way, this work aims to study the influence of paint components on the photoactivity of P25.

3.2 Experimental

3.2.1 Photocatalytic films

The paint formulation used in the present work is based on exterior water-based vinyl paint. This paint formulation was modified and half of the pigmentary TiO_2 was replaced by P25 (producing a photocatalytic paint hereafter referred as reference paint – denoted as RP#).

Paint components were here divided in powder components – pigmentary and photocatalytic TiO_2, extenders and powder thickener – and non-powder or water-dispersed components

(hereafter referred as organic components, for simplicity) –binder (resin) and additives such as thickener, dispersing agents and coalescent.

For evaluating the role of each paint component in the photoactivity of the paint, a series of experiments with increasing number of component were performed – see Table 3.1. For simplicity, whenever the films are formed by just powder components, they are called powder pressed films (denoted as PP#); the others are called pseudo-paint films (denoted as PsP#). The mass proportion of each component in the final paint was mostly kept in the powder and pseudo-paint films.

The powder mixtures were obtained by hand-shaking for 5 min. The powder mixtures were then evenly poured over an aluminum slab and pressed at *ca*. 5 bar for 7 min; the film was then tested for NO photoactivity as described below.

In the case of PP5 (Table 3.1) the powder mixture was obtained stirring 10 g of the powder mixture used in PP4 into 50 cm^3 of distilled water applying 300 rpm for 30 min followed by sonication for 5 min (Hielscher UIP1000hd, at 90 % of amplitude). The slurry was then deposited over a glass plate and dried for 1 day at lab conditions and 1 more day at 50 ºC (temperature already higher than the typical maximum a paint usually face). It was then powdered and the powder applied in an aluminum slab, as described before.

In the case of the pseudo-paint films, the powder and organic components were mixed in a 100 cm^3 vessel with 50 cm^3 distilled water, applying 300 rpm for 30 min. Wet films were produced with the help of a drawn down bar over the aluminum slab and let to dry for 1 day at lab conditions, producing therefore the pseudo-paint films.

All films have an area of *ca*. 10 x 5 cm^2. PP# and PsP# / RP# films have approximately 0.5 mm thickness (estimated using a micrometer) and 60 μm dry thickness (estimated by SEM images), respectively. The initial composition of the pseudo-paint films and their rheology yield different P25 loads in the film. For the case of pseudo and reference paint experiments,

the fraction of volatile substances present in each organic component and the amount of water added for stirring were considered, along with the film mass, to estimate the final P25 load (mass of P25 per area of film) reported in Table 3.1.

UV/Vis Diffuse reflectance analysis of the films were made using a Perkin Elmer lambda 750 spectrophotometer equipped with a 60 mm integrating sphere and Spectralon^{TM} as reflectance standard.

3.2.2 Experimental setup

The aluminum slabs above referred used to support the testing films were introduced in the down part of the interior of the photoreactor, sketched in Figure 3.1.

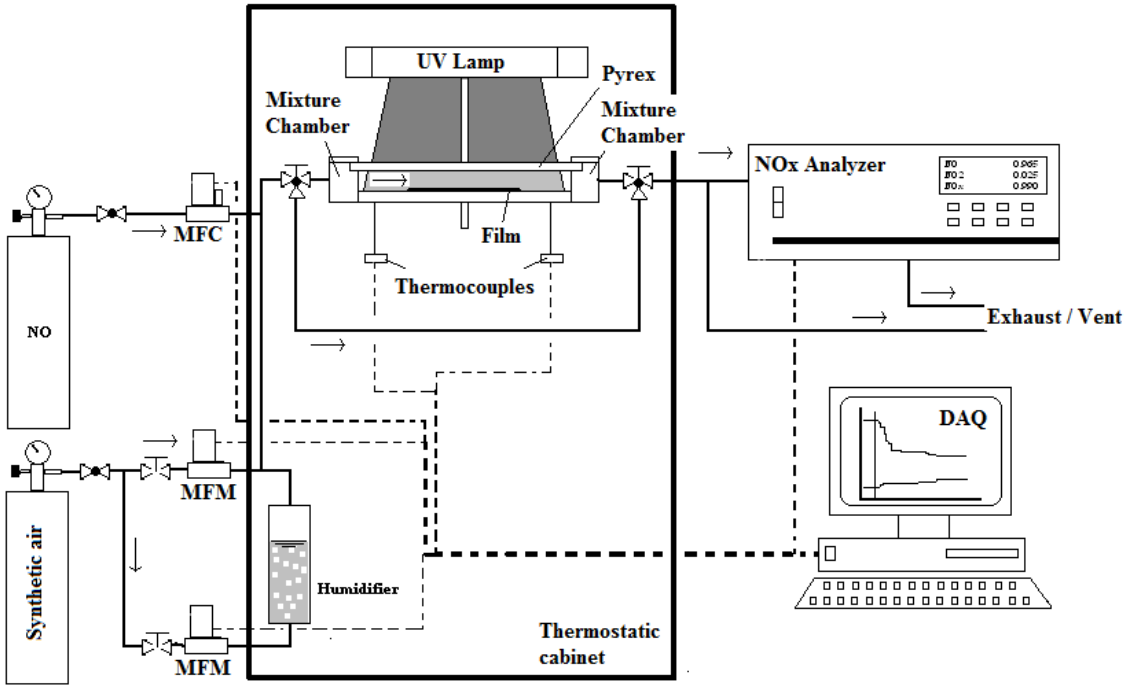

Figure 3.1 – Sketch of the experimental setup used for the photocatalytic tests (arrows represent the gas flow direction).

The photoreactor has a borosilicate window (overall light transmittance of 90 % over 330 nm) at the top face, above which is placed a UV lamp system (Vilbert Lourmat - BLB 365 nm, 2 x 6 W lamps). These units were assembled inside a thermostatic cabinet for temperature control.

Table 3.1 – Mass fraction (with two decimal places) of paint components in the film used in each experiment, load of P25 and content of powders and organic components (dry basis).

			Mass fraction in dry film basis (wt.%)											
			Powder pressed films						***Pseudo-paint films***					***Reference paint film***
	Component paint functionality	***Description***	***Run PP0***	***Run PP1***	***Run PP2***	***Run PP3***	***Run PP4***	***Run PP5[1]***	***Run PsP6***	***Run PsP7***	***Run PsP8***	***Run PsP9***	***Run PsP10***	***Run RP11***
Powders	**Photocatalyst**	Photo-TiO_2 P25	100.00	25.44	25.44	25.44	25.43	25.43	25.40	25.34	25.34	24.93	18.28	17.45
	Extender	$CaCO_3$	-----	74.56	-----	-----	1.63	1.63	1.60	1.59	1.60	1.56	1.12	1.02
	Extender	$BaSO_4$	-----	-----	74.56	-----	-----	-----	-----	-----	-----	-----	-----	-----
	Extender	Silicates	-----	-----	-----	-----	46.93	46.93	46.89	46.78	46.66	45.86	33.57	32.56
	Pigment	Pigmentary TiO_2	-----	-----	-----	74.56	25.18	25.18	25.16	25.10	25.04	24.60	18.01	17.45
	Additive	Powder thickener	-----	-----	-----	-----	0.83	0.83	0.83	0.84	0.83	0.82	0.60	0.58
Organics	**Extender pigment**	Opaque polymeric particles	-----	-----	-----	-----	-----	-----	-----	-----	-----	-----	5.11	4.69
	Additive	Biocides	-----	-----	-----	-----	-----	-----	-----	-----	0.41	0.02	-----	0.24
	Additive	Antifoam	-----	-----	-----	-----	-----	-----	0.12	0.12	0.12	0.13	-----	0.08
	Additive	Amine	-----	-----	-----	-----	-----	-----	-----	0.23	-----	0.29	-----	0.16
	Additive	Dispersing agent	-----	-----	-----	-----	-----	-----	-----	-----	-----	1.79	-----	1.26
	Additive	Coalescent	-----	-----	-----	-----	-----	-----	-----	-----	-----	-----	3.34	4.10
	Additive	Thickener	-----	-----	-----	-----	-----	-----	-----	-----	-----	-----	-----	0.53
	Binder	Resin	-----	-----	-----	-----	-----	-----	-----	-----	-----	-----	19.97	19.88
		$Load_{P25}$ ($mg \cdot cm^{-2}$)	**13.5**	**13.9**	**13.6**	**13.4**	**9.7**	**14.5**	**2.6**	**2.6**	**3.1**	**6.1**	**1.8**	**2.3**
		Powders (wt.%)	**100.0**	**100.0**	**100.0**	**100.0**	**100.0**	**100.0**	**99.9**	**99.6**	**99.5**	**97.8**	**71.6**	**69.1**
		Organics (wt.%)	**0.0**	**0.0**	**0.0**	**0.0**	**0.0**	**0.0**	**0.1**	**0.4**	**0.5**	**2.2**	**28.4**	**30.9**

[1] equivalent to run PP4 but sonicated in a slurry, dried and powdered in mortar (see section 3.2.1)

The setup comprehends also a feed system and a NOx analyzer (Thermo Scientific 42C). The feed is ensured by a set of mass flow meters and one controller (Hi-Tech Bronkhorts) and the corresponding relative humidity is adjusted by mixing dry and water-saturated synthetic air streams (the latter obtained allowing the gas to bubble through a water column – referred as humidifier, Figure 3.1).

The photoactivity was assessed by means of NO conversion (eq. 3.1) and selectivity towards ionic species (eq. 3.2), i.e. nitrate and nitrite ions.

$$X_{NO} = \left(\frac{C_{NO}^{in} - C_{NO}^{out}}{C_{NO}^{in}} \right) \times 100 \qquad (3.1)$$

$$S = \left(1 - \frac{C_{NO_2}^{out}}{C_{NO}^{in} - C_{NO}^{out}} \right) \times 100 \qquad (3.2)$$

In these equations C_{NO} and C_{NO_2} stand for the concentration of NO and NO_2, respectively, while the superscripts *in* and *out* refer to the inlet and outlet streams of the reactor.

The operating conditions used were the following: 50 % relative humidity (RH), 25 ºC, 7 $W \cdot m^{-2}$ of irradiance and total feed flow rate of 0.7 $L_N \cdot min^{-1}$ containing 1 ppm of NO. Prior to the photocatalytic tests, the films were let to activate for 5 hours in the same operating conditions but in absence of NO. This procedure follows roughly the standard ISO 22197-1:2007(E). For the case of RP, a harsher activation was required (similar to the one above referred but with 90 %RH, 30 $W \cdot m^{-2}$ and for 24 hours). The steady state was considered to be achieved whenever NO conversion and selectivity do not vary more than ±2.5 percentage points for 50 hours.

3.3 Results and discussion

3.3.1 UV/Vis diffuse reflectance

The light that reaches a film can be reflected, absorbed or transmitted. According to the chemical and physical properties of the films, the contribution of each of these three phenomena may vary. Figure 3.2 presents the diffuse reflectance of powder pressed (PP) films tested in the photoreactor, in which transmittance of radiation is negligible, as discussed below.

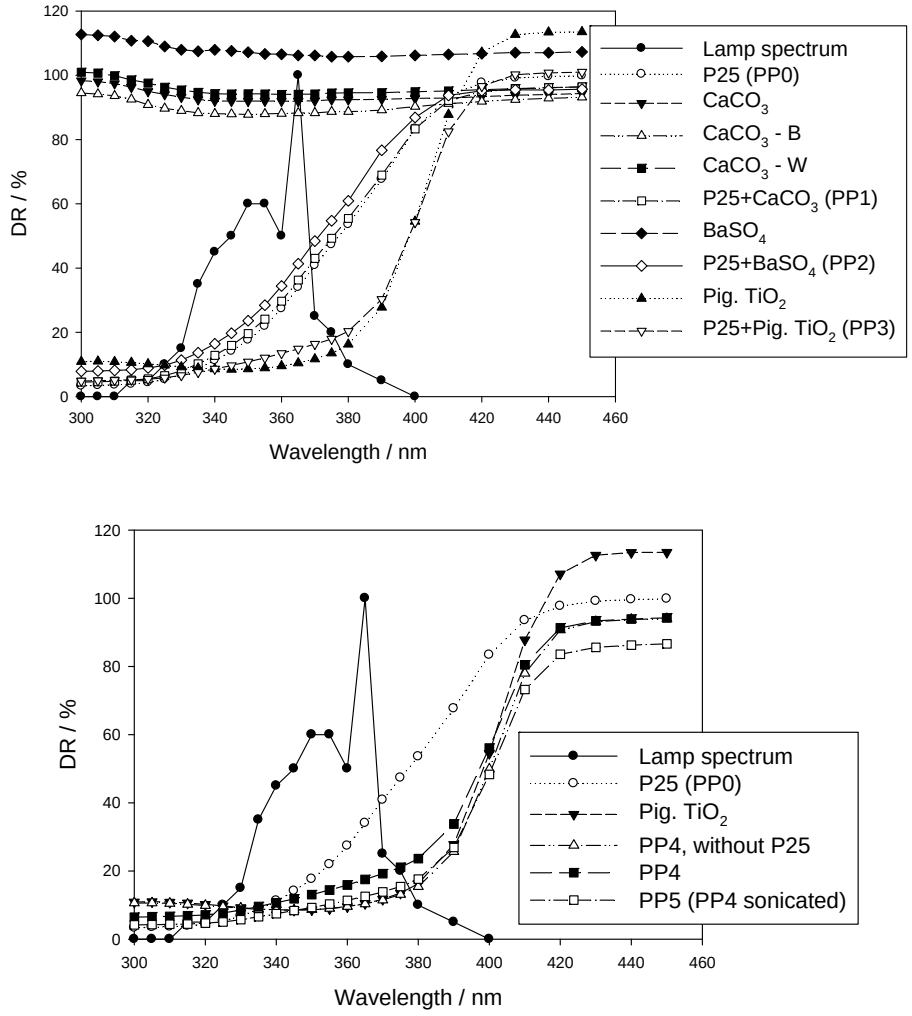

Figure 3.2 – Diffuse reflectance (DR) of pure powder films of P25, $CaCO_3$, $BaSO_4$, pigmentary TiO_2 and films tested in the photoreactor (Table 3.1); it was used an aluminum support for powder deposition except for $CaCO_3$ – B (black support - Leneta test charts) and $CaCO_3$ – W (white support - Leneta test charts).

P25 absorbs light up to the wavelength of 415 nm. However, it is known that the efficiency of the photocatalyst to absorb light decays near to the longest wavelength that it can absorb [5]; accordingly, the diffuse reflectance analysis of P25 PP film exhibits a sigmoid-like curve with no significant reflection up to 320 nm (Figure 3.2). The reflectance intensity starts then to increase up to the 415 nm wavelength, the minimum energy able to excite electrons in rutile crystal form of P25 (values above 100 % are related to the higher reflectance of the powder film compared to the reference material, Spectralon^{TM}).

The spectrum obtained with pigmentary TiO_2 reveals an increase in diffuse reflectance with the wavelength, again with a sigmoid-shape, particularly in the range 360 nm – 450 nm. The low reflection of this material at wavelengths lower than 360 nm arises from the ability of light absorption by TiO_2 (rutile crystalline form).

P25 behaves similarly to pigmentary TiO_2, but the reflectance in the UV region is generally higher. For this difference account several properties of the two materials, namely: the particle diameter (25 nm vs. 360 nm, respectively, probably with an higher dispersion of the primary particle diameter in the first case) and the crystal structure (80 % anatase and 20 % rutile for P25 and pure rutile for pigmentary TiO_2). Apart of such differences, pigmentary TiO_2 has also a surface treatment of alumina and amorphous silica (5.5 wt.%) for minimizing the photocatalytic activity, which otherwise would degrade the paint.

The UV/Vis diffuse reflectance analysis shows that extenders $CaCO_3$ and $BaSO_4$ have a high reflectance in the wavelength range analysed (Figure 3.2). The spectra of $CaCO_3$ PP films are mostly independent of the support used (B – black, or W – white), indicating a negligible transmittance of these films. This effect was also observed for the remaining films, indicating that they are optically thick (i.e. their corresponding optical thickness is lower than the film thickness).

When mixing $CaCO_3$ or $BaSO_4$ with P25 (experiments PP1 and PP2, Table 3.1), films reveal similar spectra as pure P25 (Figure 3.2). Diffuse reflectance spectrum of the PP3 film (P25 + pigmentary TiO_2) lies in general between those of the pure components, but in the wavelength region of concern for photocatalysis (majority of irradiance promoted by the UV lamp system is in between 330 nm and 380 nm), reflectance lies closer to the one of pigmentary TiO_2. Such fact highlights the competitive absorption of photons by both components of this mixture.

Diffuse reflectance of film PP4 (see Table 3.1 and Figure 3.2) reveals a higher UV reflectance than pigmentary TiO_2, which is consistent with the presence of P25; the spectrum of PP4 lies between the one of pigmentary TiO_2 and that of P25.

Analysis of siliacates was impossible to perform due to lack of powder cohesion, however their pure analyses shows that they must act as reflectors as $CaCO_3$ and $BaSO_4$.

Film PP5 shows a lower diffuse reflectance compared to PP4, particularly up from 340 nm, being more similar to the spectra of pigmentary TiO_2 in the UV region, while revealing the lowest reflectance in visible region. Such result highlight the procedure interference on film behavior towards light, which can account for its photoactivity.

3.3.2 Photoactivity of powder pressed (PP) films

Figure 3.3 shows the NO conversion and selectivity histories on three different powder pressed films of P25. It can be seen that the steady state conversion and selectivity towards nitrate and nitrite were reached after *ca.* 5 hours, *ca.* 80 % and 45 %, respectively. Figure 3.3 also shows that tests performed with different P25 films show good repeatability.

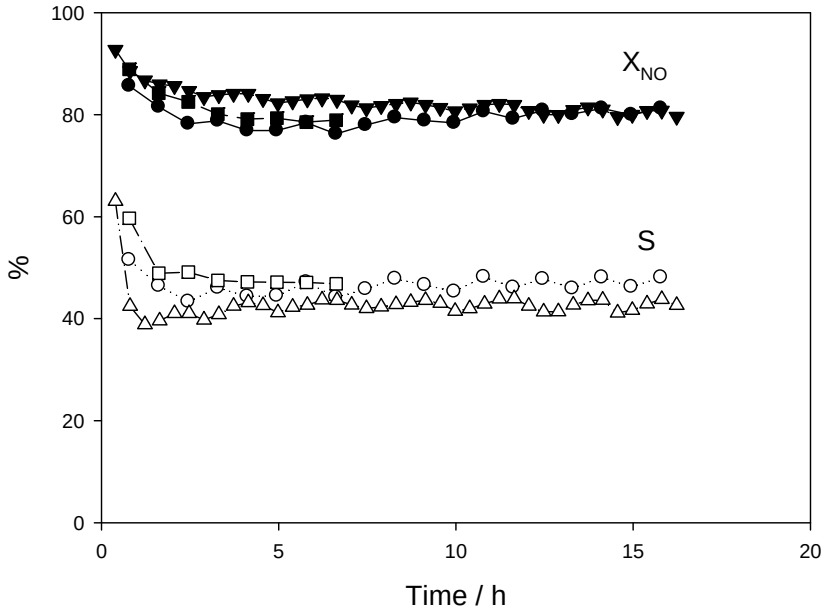

Figure 3.3 – Conversion (full symbols) and selectivity (empty symbols) histories on 3 different powder pressed films of pure P25 (experiment PP0).

Tests performed with powder films of pure P25 (experiment PP0) with different thicknesses (and therefore different loads of P25) have shown no differences in either diffuse reflectance or photoactivity at steady state (Figure 3.4). This allows concluding that only a fraction of the P25 in PP0 films becomes photoactive. Consequently, it is not totally possible to establish a direct correlation between photocatalyst load and photoactivity of the film.

Contrarily to the load, photoactivity of the powder film P25 is particularly affected by the film length, which is related to the NO contact time in the photoreactor. It can be seen that not only the conversion is smaller, but also it seems that the selectivity becomes smaller (Figure 3.4). Such fact highlights once again that photocatalyst load is not the unique parameter playing a role, as the 6 x 5 cm^2 film has the same load as one of the 10 x 5 cm^2 films and a lower conversion.

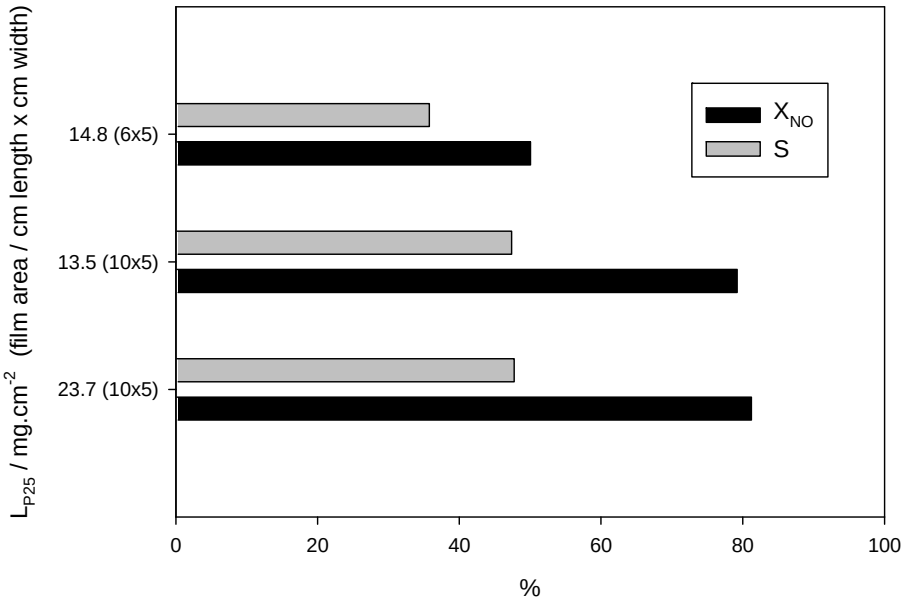

Figure 3.4 – Steady state conversion and selectivity on PP0 films with different loads and areas of P25: 14.8 (6x5) – 14.8 mg·cm^{-2} and 6 x 5 cm^2 (length x width); 13.5 (10x5) – 13.5 mg·cm^{-2} and 10 x 5 cm^2 and 23.7 (10x5) – 23.7 mg·cm^{-2} and 10 x 5 cm^2.

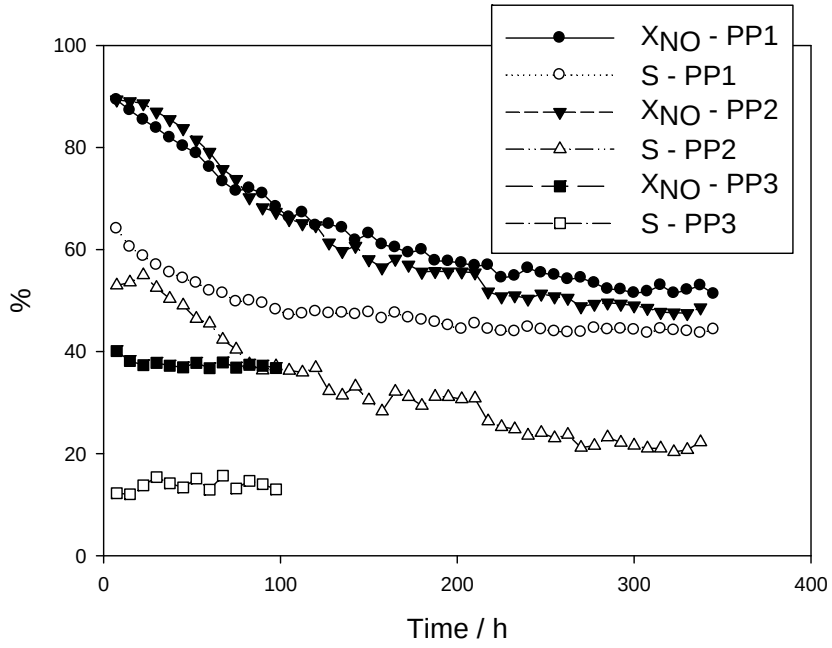

Figure 3.5 – Conversion (full symbols) and selectivity (empty symbols) history for experiments PP1, PP2 and PP3.

Figure 3.5 presents the photocatalytic results of P25 mixed separately with $CaCO_3$, $BaSO_4$ and pigmentary TiO_2 (experiments PP1 to PP3, respectively, cf. Table 3.1). The formers are extenders typically used in paints while the latter is the most typical opacifier in the visible light region of the electromagnetic spectrum used in paint industry. Among all, only $BaSO_4$ does not enter in the reference paint formulation used herein. However, since it is a usual paint component, it was decided to use it for comparing with $CaCO_3$ in terms of the film photoactivity. NO steady state conversion on films containing $CaCO_3$ and $BaSO_4$ are similar, *ca.* 55 %. The mass fraction of P25 in these films was 25 % (cf. Table 3.1), thus it possibly explains the smaller NO conversion when compared to the one obtained with the PP0 film (pure P25 – X_{NO} = 80 %). Films made with $CaCO_3$ and $BaSO_4$ (PP1 and PP2) also show a similar NO conversion history (Figure 3.5). The lower NO steady state conversion obtained with PP3 (*ca.* 40 %) should be due to the competitive light absorption between pigmentary TiO_2 and P25, as discussed before. From these results one can conclude that $CaCO_3$ and $BaSO_4$ are not bottlenecks in terms of lower photocatalytic oxidation rates obtained with reference paint film obtained in chapter 2. On the other hand, pigmentary TiO_2 must play an important role.

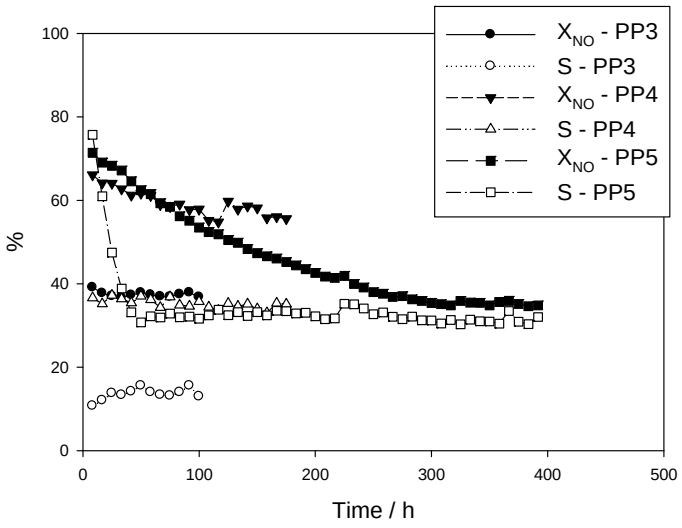

Figure 3.6 – Conversion (full symbols) and selectivity (empty symbols) history for experiments PP3, PP4 and PP5.

Figure 3.6 presents the NO conversion and selectivity on films PP4 and PP5 (conversion and selectivity obtained on film PP3 are reprinted for convenience). Film PP4 contains all powder components used in the formulation of the reference paint; basically, 66 wt.% of pigmentary TiO_2 present in PP3 have been replaced by extenders and powder thickener (cf. Table 3.1). The lower pigmentary TiO_2 concentration on PP4 should result in less competitive absorption of UV light and then on higher NO conversion compared to PP3. PP5 has the same composition as PP4 but the powder components were mixed in an aqueous suspension followed by sonication, drying, powdering and application over the aluminum slab, following the same procedure as for PP4. Despite the similarities between the two experiments, it was observed a significant decrease in the steady state NO conversion (from *ca*. 55 % to *ca*. 35 %). Such fact highlights the interference of paint production procedure on the photoactivity of the final product; in fact, film PP5 shows a stronger impair effect on light absorption by P25, as discussed on chapter 3.3.1 (Figure 3.2). It is worth noting the increase on the transient period observed for experiments on films PP1 to PP5 compared to film PP0, revealing an interference of the powder components; ionic chromatography did not reveal the presence of dissolved anions or cations on the water used for PP5 film production.

3.3.3 Photoactivity of pseudo-paint (PsP) films

Figures 3.7 - 3.10 show the NO conversion and selectivity histories on pseudo-paint films PsP6-PsP10 and on RP11. The organic paint components were added step by step (cf. Table 3.1) and the photoactivity of the corresponding pseudo-paint films evaluated. First of all, a slurry was made with all powder components.

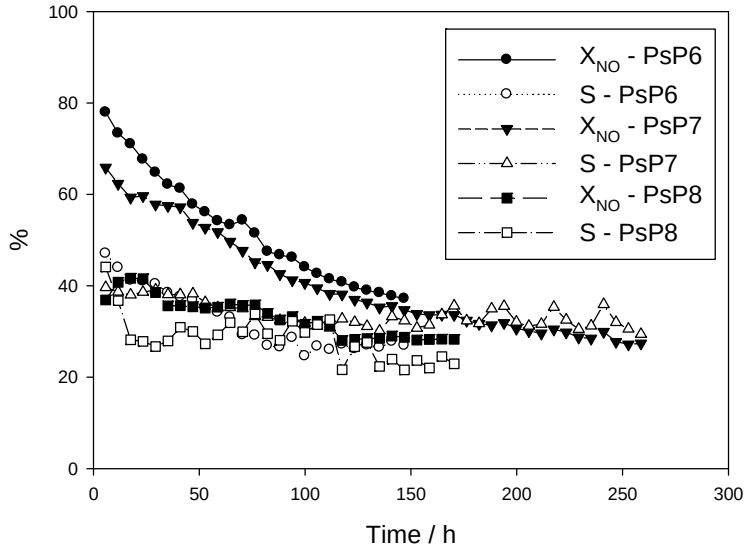

Figure 3.7 – Conversion (full symbols) and selectivity (empty symbols) history of experiments PsP6, PsP7 and PsP8.

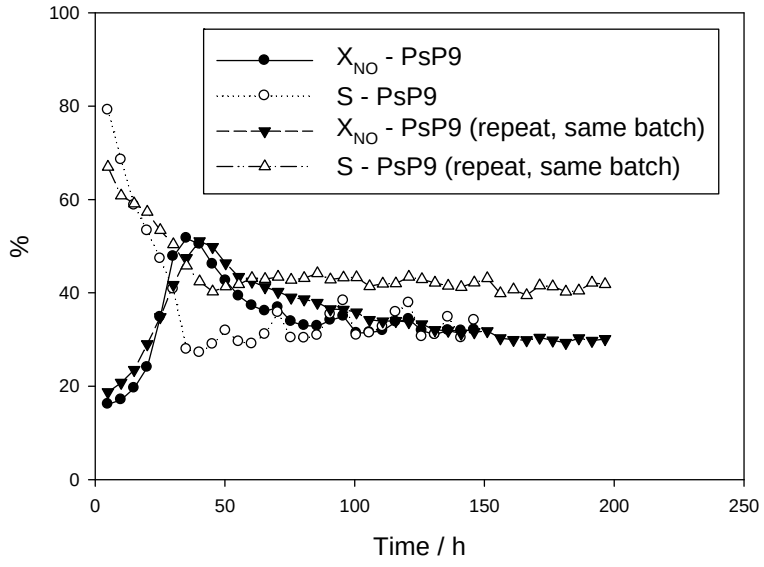

Figure 3.8 – Conversion (full symbols) and selectivity (empty symbols) history of experiment PsP9, employing fresh and 6 months in-can pseudo-paint.

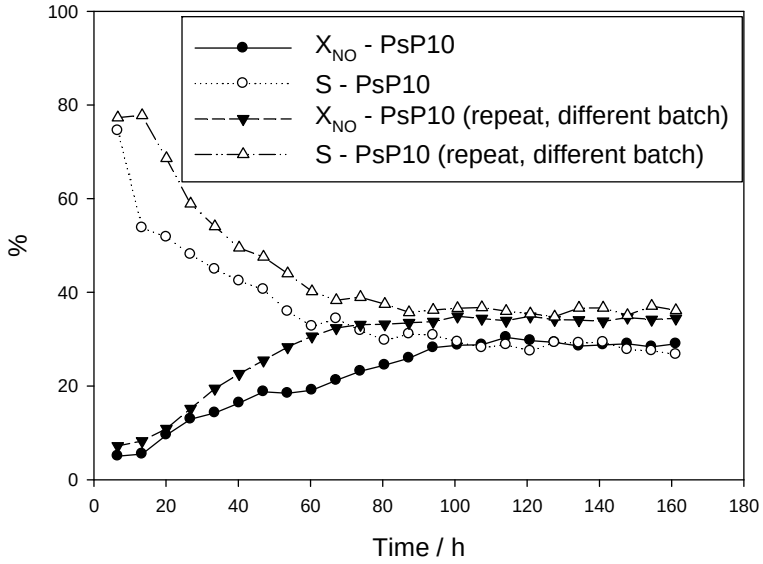

Figure 3.9 – Conversion (full symbols) and selectivity (empty symbols) history of experiment PsP10, using pseudo-paints produced from two different batches.

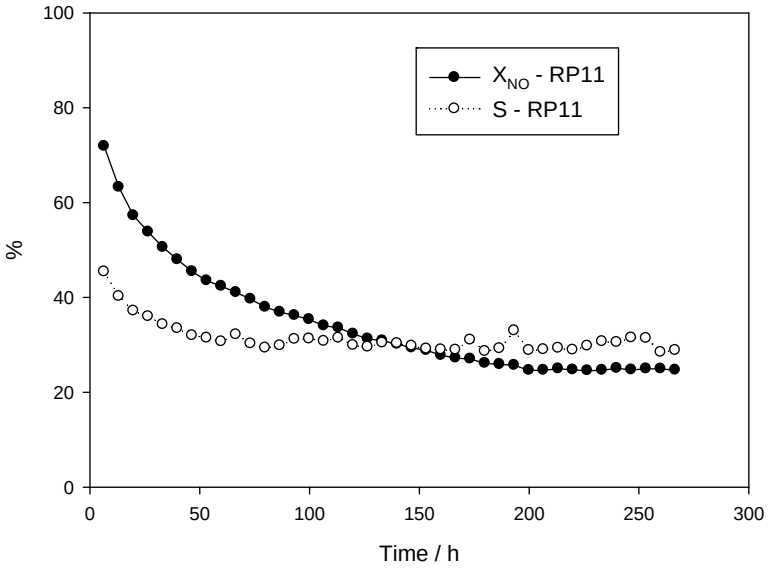

Figure 3.10 – Conversion (full symbols) and selectivity (empty symbols) history of experiment RP11, after harsher activation.

To this slurry it was added and mixed antifoam (PsP6), antifoam and amine (PsP7), antifoam and biocides (PsP8), antifoam, amine, biocides and dispersing agents (PsP9) and antifoam, opaque polymeric particles, resin and coalescent (PsP10). Figure 3.7 presents the NO conversion and selectivity histories obtained for experiments PsP6-PsP8. Although the load of

P25 is higher for the case of PsP8, the initial NO conversion is lower than for PsP6 and PsP7. This might arise from the stronger detrimental influence of the biocides on the photoactivity but also from the presence of a greater amount of organic *vs*. powder components. In fact, the initial NO conversion decreases with the amount of organic components in the formulation (cf. Table 3.1).

However, steady state conversion and selectivity values are nearly the same for these experiments and also for experiment PP5 (Figures 3.6 and 3.7), *ca.* 30 %, which may indicate that the surface of P25 is free of these organics (and products of reaction) at this stage.

PsP6 was performed in order to compare the influence of the antifoam in the transient behavior in comparison to antifoam + amine (PsP7) and antifoam + biocides (PsP8), being therefore a reference for both tests. Figure 3.7 evidences that PsP6 shows a similar transient behavior as PsP7, indicating a major effect of the antifoam compared to the amine one, the former one present in smaller concentration (Table 3.1). Comparing PsP6 with PsP8, one can refer the greater impairment by the biocides during the transient period. However, the higher amount of biocides can be here playing an important role.

Similar tests performed with fresh PsP9 exhibited a low initial NO conversion, Figure 3.8. Comparing with experiments PsP6 to PsP8 (Figure 3.7), it becomes apparent that again such fact should arise from the higher organic content and namely from dispersing agents (see Table 3.1). However, the steady state conversion is again *ca.* 30 %. Experiment PsP9 was repeated with the pseudo-paint after its rest in-can for about 6 months (Figure 3.8), producing close steady state results. This indicates also the good stability of the formulation.

Steady state conversion and selectivity obtained with PsP10 films were also *ca.* 30 % (Figure 3.9), which is in line with the results obtained for PP5 to PsP9. For PsP10, the initial conversion was the lowest of all experiments and, as referred above, such fact should arise from the highest content in organic components (cf. Table 3.1 and Figures 3.7 – 3.9).

Repeatability assessment made to different films from different batches of PsP10 produce similar results, especially at the steady state (Figure 3.9).

In line with this, the reference paint (which has the maximum content of organic components, Table 3.1) does not show any photoactivity after the normal activation protocol. The ratio of the pigment volume concentration (PVC) to the critical PVC [13] is 2.1 for PsP9 and 1.2 for PsP10 and RP11. Consequently, there is a larger porosity and lower coverage of P25 by organic components in PsP9 film (therefore higher initial activity) compared to PsP10 and RP11. Compared to PsP10, RP11 contains more only the organic additives that account only for *ca.* 2.5 wt.%. However, PsP10 showed initial photoactivity while RP11 did not; it was necessary a harsher activation procedure (see section 3.2.2) to make it photoactive, Figure 3.10. Consequently, the lowest initial photoactivity of RP11 points out to a synergetic hiding effect of the paint components towards the photocatalyst obtained after all components being present. After the harsher activation protocol the steady state NO conversion obtained is similar to the one obtained for all PsP films, *ca.* 30 % (Figure 3.10).

3.4 Conclusions

Photocatalytic powder pressed and pseudo-paint films were produced and tested towards NO abatement. Paint components (powder and organic compounds) were progressively added, giving rise to more complex films that ended with the reference photocatalytic paint. The photoactivity of each film was assessed and the interference of each paint component in P25 photoactivity evaluated.

The load of P25 photocatalyst explains only partially the different photoactivity of the films produced, as the composition of the film itself influences the larger or shorter penetration depth of light through the film and therefore the real active load (photoactivated photocatalyst mass *vs*. total mass of photocatalyst). When $CaCO_3$ was mixed with P25 alone (25 wt.% of

P25), it was observed an improvement of selectivity towards more oxidized species (nitrate and nitrite). On the other hand, the film containing pigmentary TiO_2 has shown the worst photoactivity of all, which is due to the competitive absorption of photons in the UV region.

The production of a slurry of distilled water with the powder components deeply interfered with the photoactivity of P25.

Although the amount of organic paint components (films PsP6 to RP11) plays a major role on initial NO conversion, steady state photoactivity is mostly independent of this amount, tending to the same NO conversion of *ca.* 30 %, whatever the species initially present (dispersing agents, resin, antifoam, antifoam plus amine, etc). Such fact should be related to the oxidation of organic species initially wrapping the photocatalytic TiO_2 particles, which after being oxidised allow the NO reaction to proceed freely.

The NO conversion and selectivity histories on films produced from different batches were reproducible. The reference paint showed no photoactivity after being submitted to the normal activation procedure and needed to be activated under hasher conditions to produce conversion and selectivity values in line with experiments PsP6 to PsP10. It is suggested that there should be a synergetic effect when all paint components are present in the formulation, that wrap more closely the photocatalytic TiO_2 particles leading to no initial photoactivity.

References

[1] European Commission, *Attitudes of European Citizens Towards the Environment*, Special Eurobarometer 295/Wave 68.2 – TNS Opinion & Social, March 2008 (available at: http://ec.europa.eu/public_opinion/archives/ebs/ebs_295_en.pdf accessed February 2011).

[2] Agência Portuguesa do Ambiente – online database on air quality (www.qualar.org , accessed on February 2011).

[3] Riga-Karandinos, A., Saitanis, C., *Chemosphere* 2005, 59, 1125.

[4] Devahasdin, S. Fan Jr., C., Li, K., Chen, D. H., *J. Photoch. Photobio. A* 2003, 156, 161.

[5] Herrmann, J.-M., *Top. Catal.* 2005, 34, 49.

[6] Italcementi Group Press Release, *Urban photocatalysis comes to city roads and facades with Italcementi*, (available at: http://www.italcementigroup.com/NR/rdonlyres/2062CB8F-6FAB-4C3B-86EB-28AE17D68913/0/Comunicato_TXActive_UK.pdf - accessed on February 2011).

[7] Guerrini, G.L., Peccati, E., *White Cement and Photocatalysis – Part 1: Fundamentals*, International RILEM Symposium on Photocatalysis, Environment and Construction Materials, 8-9 October 2007, Florence, Italy, 179-186.

[8] Paint company Sto – website for photocatalytic product Climasan (www.stoclimasan.com - accessed February 2011).

[9] Maggos, Th., Plassais, A., Bartzis, J. G., Vasilakos, Ch., Moussiopoulos, N. Bonafous, L., *Environ. Monit. Assess.* 2008, 136, 35.

[10] Fujishima, A., Hashimoto, K., Watanabe, T., *TiO_2 Photocatalysis – Fundamentals and Applications*, BKC, Inc., Tokyo, 1999.

[11] Bygott, C.E., Maltby, J.E., Stratton, J.L., McIntyre, R., Photocatalytic Coatings for the Construction Industry, International RILEM Symposium on Photocatalysis, Environment and Construction Materials 8-9 October 2007, Florence, Italy, 251–258.

[12] Águia, C., Xamena, F.X.L., Dominguez, E., García, H., Madeira L. M., Mendes, A., Photocatalytic Paint Production for the Abatement of Nitrogen Oxides, 10th International Chemical and Biological Engineering Conference, 4-6 September 2008, Braga, Portugal, 117-118 (CD: pp. 277-282).

[13] Koleske, J. V., *Paint and Coating Testing Manual*, 14th edition of the Gardner-Sward Handbook, Philadelphia, 1995.

Chapter 4 - Influence of Paint Components on P25 Photoactivity – Wet effect and paint matrix degradation[3]

Abstract

The present chapter studies the interference of paint components on the photoactivity of P25 photocatalyst towards NO abatement. Paint components are divided in two major groups: powder inorganic components and organic components. Two types of films were then prepared, powder pressed films and films made of pseudo-paints, and their photoactivity assessed following approximately standard ISO 22197-1:2007(E). Powder pressed films were obtained by mixing stepwise powder components of the base paint; pseudo-paint films involved mixing stepwise the powder components with families of organic components present in the original photocatalytic paint formulation.

Concerning powder pressed films, it was concluded that the morphology of the film influences the photoactivity while $CaCO_3$ and silicates, which are extenders, have a smaller impact on P25 photoactivity compared to pigmentary TiO_2, even when water is involved in the production procedure.

Pseudo-paint films containing the same proportion of powder components as powder pressed films displayed different transient behaviors but similar steady state photoactivities, regardless the presence of organic components such as the binder. This was assigned to the photoerosion of a significant fraction of the organic paint components during the transient period. Therefore, after reaching steady state, NO photooxidation could proceed freely as if only

[3] *Águia, C., Ângelo, J., Madeira, L., Mendes, A., Polymer Degradation and Stability (10.1016/j.polymdegradstab.2011.01.032).*

inorganic paint components were present. An average of ca. 25 wt.% of organic phase erosion was observed and more severe erosion should occur closer to the top of the paint film.

4.1 Introduction

NOx emissions and corresponding atmospheric concentration have been legislated all over the world due to environmental and health effects of these contaminants. Tropospheric NOx contribute for water eutrophication, promotion of ozone and particulate matter formation, with consequent development of urban smog and increase number of lung diseases. In fact, NOx are one of the anthropogenic contaminants present in atmosphere with greatest impact on aerosol and particulate matter formation [1, 2]. Legislation regarding NOx emissions and atmospheric concentration are leading to technological improvements; however, recent surveys in urban areas showed that NOx concentrations are still above the legislated limits [3-5]. Therefore, efforts for continuous reduction on NOx emissions and greater atmospheric abatement are expected in the next years.

Photocatalytic TiO_2 has been increasingly studied and used for NOx photoabatement [6-9]. At atmospheric conditions (low partial pressure of NOx, low temperature and presence of water and oxygen) the reaction mechanism of NOx photoabatement follows the oxidation path. Photooxidation of hazardous compounds occurs over the photocatalytic TiO_2 surface or in the neighboring of the particle [10]. At atmosphere conditions, the photocatalysis of NOx produces mostly nitrate ions that can be easily washed out from the photocatalyst surface [11]. Photocatalytic oxidation using photocatalytic TiO_2 presents some advantages compared to other processes for the abatement of atmospheric contaminants, such as [12-15]: - the reaction is rather fast at atmospheric pressure and room temperature; - it deals with the low atmospheric pollutants concentration; - a wide spectrum of organic contaminants can be completely oxidized towards non-toxic products; - no additional chemical reactants are required; - it makes use of a relative low cost material; - it can use solar energy as activation source; - it shows high chemical and physical stability; and – it allows the formation of

thermodynamically disfavored products, overcoming large activation barriers in a short period of time.

Photocatalytic TiO_2 can be immobilized in different construction materials for the photoabatement of atmospheric NOx. For example, approximately 50 000 m^2 of urban surfaces are estimated to be already covered with photocatalytic construction materials in Japan [16]. Kaneko and Okura [13] reported a windowed photocatalytic highway wall panels (0.6 m x 1.0 m) tested in Tokyo, where photocatalytic surfaces were attached by adhesive tape to the panels. A borosilicate glass window was used to cover the painted panels forming a gap through which polluted air was pumped at 15 to 60 $L \cdot min^{-1}$. Daylight irradiance was ca. 1 $W \cdot m^{-2}$ at noon and an average of 113 000 vehicles crossed the 6-lane roadside per day. An average NOx removal of 31 % to 69 % was observed, which corresponded to a rate of ca. 3 $mmol \cdot m^{-2} \cdot d^{-1}$ based on the amount of nitrate washed from the panels [13]. On the other hand, Marley Eternit [17], a roofing solutions company based in the UK, developed a photocatalytic roof tile - the EcoLogic. This company estimates that an average-sized roof made of EcoLogic tiles can remove during its lifetime an equivalent amount of NOx to that emitted by a modern car travelling 160 000 km and it claims that the photocatalytic activity should last for 25 years [17].

From all possible construction materials, paint coatings have several advantages when used for immobilizing photocatalytic TiO_2, since almost all surfaces in urban areas can be painted. Moreover, paints have the exact thickness for being opaque and then to produce photocatalysis taking full advantage of the solar radiation. Bygott et al. [18] conducted a field test in a children playground in London. 300 m^2 of surrounding walls were painted with a silicate-based paint loaded with 7.5 wt.% of photocatalytic TiO_2. A daily abatement of ca. 4.5 g of NOx is reported from about 10 000 m^3 of air around the school playground.

Photocatalytic paints must keep their properties along time in terms of photoactivity and mechanical stability. However, few studies concerning the aging of photocatalytic paints or the formulation influence on photocatalytic activity are available. Allen et al. [9] studied the effect of adding $CaCO_3$ to a polysiloxane paint incorporating photocatalytic TiO_2. This extender is reported to have the capacity to react with the nitric acid formed in the NOx photooxidation process, cleaning the surface of the photocatalyst. These authors concluded that a higher content in $CaCO_3$ resulted in a higher NOx removal. They attributed this effect to the higher porosity of the paint films, which allows an efficient mass transport towards the photocatalyst surface. On the other hand, these authors concluded that increasing the concentration of $CaCO_3$ and photocatalytic TiO_2 results in an increase of paint self-degradation rate.

In the previous chapter (and [19]) the authors reported the strong impairment of pigmentary TiO_2 on the photoactivity of P25 in powder pressed films. Such impairment was attributed to the competitive photonic absorption between the two types of TiO_2 (photocatalytic TiO_2 and pigmentary TiO_2). It was also concluded that the photoactivity of powder pressed films depends whether the mixture was obtained via dry or wet mode. The present study aims to further address these issues and to study the effect of the paint components on the photoactivity of P25-based films on NO abatement. Special attention is given to the aging of the photocatalytic films tested.

4.2 Experimental

4.2.1 Photocatalytic films

An exterior water-based matt paint with a pigment volume concentration (PVC) higher than the critical value (CPVC) [20] was used as starting paint. From the original formulation, half of the pigmentary TiO_2 (9 wt.% in wet base) was removed; this paint is hereafter referred as

base paint (BP). The photocatalytic paint was subsequently formulated adding 9 wt.% (wet base) of photo- TiO_2 P25 (Evonik) to the BP; this paint is hereafter referred as reference paint (RP).

The BP is formulated with inorganic (in powder form) and organic components (mostly dispersions). The powder components are pigmentary TiO_2 and extenders, which include $CaCO_3$ and silicates. Organic components are the binder, dispersing agents, the coalescent, thickeners, additives (anti-foam, pH-stabilizer and biocides), and the polymer extender slurry. Table 4.1 gives briefly BP and RP formulations.

Procedures used to prepare the photocatalytic coatings are sketched in Figure 4.1.

Powder mixtures used in the powder pressed films were obtained by dry mixture and wet mixture, whether water was or not involved in mixing the powder components, respectively. Wet mixed powder pressed films and dry mixed powder pressed films are denoted wPP# and PP#, respectively. Pseudo-paint films, incorporating all powder as well as some organic dispersion components, were applied using a draw down bar and are denoted PsP# (pseudo-paint films, meaning that are formulated with fewer components than the reference paint); RP and BP films were also applied using this technique.

The powder mixtures of PP films (Runs PP0 - PP4, Table 4.2) were prepared by hand-shaking the relevant powder components together with P25 for ca. 5 minutes, followed by powder pouring over an aluminum slab and further compression at 5 bar for 7 min (see also Figure 4.1), originating an effective area of 10 x 5 cm2 and a film thickness of ca. 0.05 cm.

On the other hand, powder mixtures of wPP films (runs wPP0 – wPP4, Table 4.2) were obtained by dispersing the relevant powders in distillate water, mixing mechanically for 30 min and applying ultra-sounds 5 times for 1 min with 1 min of dwell (Hielscher UIP1000hd, at 90 % of amplitude - 1.8×10^7 $W \bullet m^{-3}$) – cf. Figure 4.1.

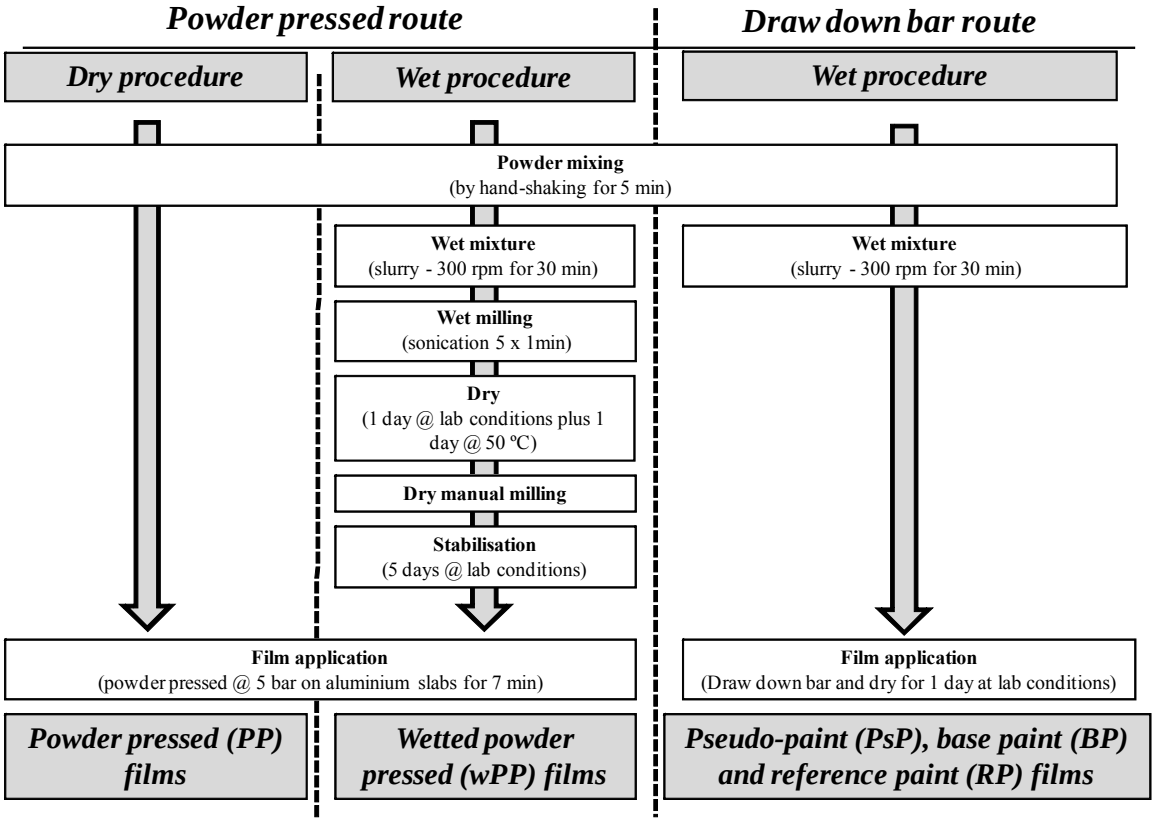

Figure 4.1 – Schematic representation of the production procedure of photocatalytic films prepared.

Table 4.1 –Base and reference paint formulations (wt.% are given for the specific case of reference paint).

Component	wt.%
Water	30
Extenders ($CaCO_3$ and silicates)	18
Pigmentary TiO_2	9
Polymer extender slurry	8
Binder slurry	20
Dispersing agents, coalescent, thickeners and other additives (in slurry)	6
Photo-TiO_2 P25	9[a]

[a] – not used in base paint.

Table 4.2 – Mass fraction (with two decimal places) of powder paint components and load of P25 for films prepared via the powder pressed route.

		Powder and wetted powder pressed films									
	Description (functionality in paint)	**Run PP0**	**Run wPP0**	**Run PP1[a]**	**Run wPP1**	**Run PP2**	**Run wPP2**	**Run PP3**	**Run wPP3**	**Run PP4**	**Run wPP4**
Mass fraction in film (wt.%)	P25 (photocatalyst)	100.0		25.44		25.44		25.44		25.26	
	Silicates (extenders)	-----		74.56		-----		-----		47.78	
	$CaCO_3$ (extender)	-----		-----		74.56		-----		1.64	
	Pigmentary TiO_2 (pigment)	-----		-----		-----		74.56		25.32	
	$Load_{P25}$ ($mg \cdot cm^{-2}$)	**13.5**	**14.2**	**-----**	**15.3**	**13.9**	**14.3**	**13.4**	**15.1**	**9.5**	**14.4**

[a] – not performed due to lack of powder aggregation.

The powders were subsequently dried at lab conditions for one day and at 50 °C for one more day, followed by hand milling the resulting powder mixture. The powder mixture was then let to rest for 5 days at lab conditions. Subsequently, the application over aluminum slabs was performed (effective area of 10 x 5 cm^2 and ca. 0.05 cm thick) in the same way as mentioned for PP films. Pseudo-paint (PsP1 and PsP2, Table 4.3), RP and BP films were applied coating an effective area of 10 x 5 cm^2 with a wet thickness of 200 μm. The influence of drying period on the photoactivity was assessed and it was concluded that 1 day at lab conditions was sufficient to obtain reproducible results.

The original mass proportions of each component in the PsP formulations are the same as in the RP. However, since these films include fewer components, mass fraction and final load (mass per film area) of photocatalytic TiO_2 in the reactor varies from film-to-film (Table 4.3). Moreover, the final concentration of each component in the dry paint film was computed

taking into account the evaporation of the water added to the mixture and the volatiles present in the dispersions of each individual organic component used.

Table 4.3 – Mass fraction (with two decimal places) of all components in the paint films used in each experiment, load of P25 and content of powders and organic components (dry basis).

			Base paint	**Pseudo-paint films**		**Reference paint**
		Description (functionality in paint)	**Run BP**	**Run PsP1**	**Run PsP2**	**Run RP**
Mass fraction in dry film base (wt.%)	**Powders**	P25 (photocatalyst)	-----	24.93	18.28	17.45
		Silicates (extenders)	39.26	45.86	33.57	32.56
		Pigmentary TiO_2 (pigment)	21.03	24.60	18.01	17.45
		$CaCO_3$ (extender)	1.23	1.56	1.12	1.02
		Thickener (additive)	0.70	0.82	0.60	0.58
	Organics	Antifoam, biocide, and pH controllers (additives)	0.77	0.44	-----	0.48
		Dispersing agents (additives)	1.52	1.79	-----	1.26
		Opaque polymeric particles (extender pigment)	5.66	-----	5.11	4.69
		Coalescent (additive)	4.95	-----	3.34	4.10
		Resin (binder)	23.97	-----	19.97	19.88
		Thickener (additives)	0.91	-----	-----	0.53
		$Load_{P25}$ ($mg \cdot cm^{-2}$)	**0.0**	**6.1**	**1.8**	**2.3**
		Powders (wt.%)	**62.2**	**97.8**	**71.6**	**69.0**
		Organics (wt.%)	**37.8**	**2.2**	**28.4**	**31.0**

4.2.2 Photocatalytic tests

The performance was assessed based on the NO conversion (eq. 4.1):

$$X_{NO} = \left(\frac{C_{NO}^{in} - C_{NO}^{out}}{C_{NO}^{in}} \right) \times 100 \qquad (4.1)$$

and selectivity towards ionic species (eq. 4.2), i.e. nitrate and nitrite ions:

$$S = \left(1 - \frac{C_{NO_2}^{out}}{C_{NO}^{in} - C_{NO}^{out}}\right) \times 100 \qquad (4.2)$$

where C_{NO} and C_{NO_2} are the gas phase concentration of NO and NO_2, respectively, and the superscripts refer to the inlet and outlet streams of the photocatalytic reactor.

Figure 4.2 sketches the photocatalytic reactor used, which is described in detail in chapter 2 (and [19]). A 0.7 $L_N \cdot min^{-1}$ flow rate of synthetic air containing 1 ppm of NO and 50 % relative humidity (RH) at 25 ºC was fed to the reactor, irradiated with an average irradiance of 7 $W \cdot m^{-2}$ [21] (Vilbert Lourmat lamp system – UV BLB 365 nm). NO and NO_2 were analyzed on-line by chemiluminescence (Thermo Scientific 42C).

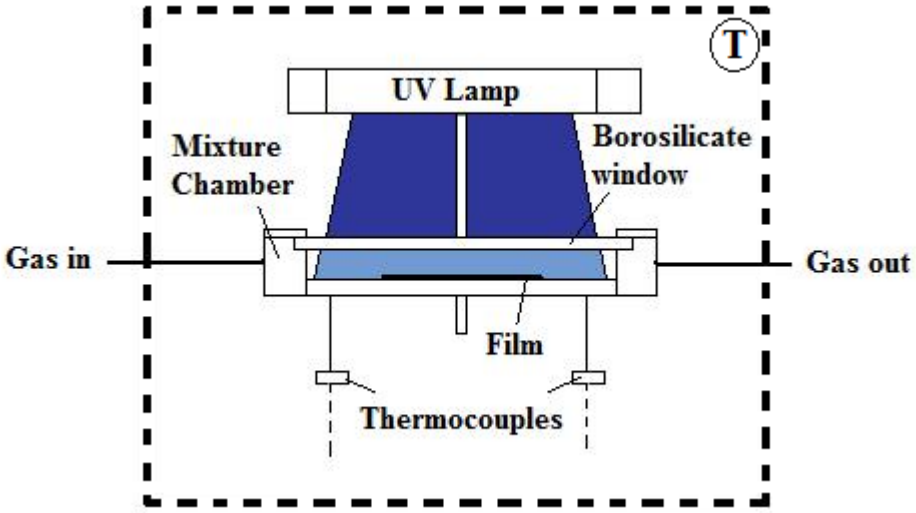

Figure 4.2 – Schematic representation of the photocatalytic reactor.

Prior to the photocatalytic tests all films produced were activated for 5 hours in the same operating conditions used for photoactivity assessment but in the absence of NO (standard activation). When required, a harsher activation protocol was used with a higher relative humidity (90 % RH) and irradiance (30 $W \cdot m^{-2}$) and for a longer period (24 hours); this activation protocol is hereafter referred as harsher activation. Steady state was considered to be achieved when NO conversion and selectivity did not vary more than ±2.5 percentage points for 5 hours.

4.2.3 Physicochemical characterization

Thermogravimetric (TG) analyses were carried out to assess the content of organic components on dried fresh films of PsP#, BP and RP as well as after their exposition to UV light for 24 hours and for 150 hours (UV aging); the above referred standard activation conditions were used. The paint and pseudo-paint films were applied in contrast ratio charts (Form 2A by Leneta). After activation, the films were easily removed from the support by means of a bistoury and dried at 110 ºC for 2 h. TG analyses were then carried out in a Netzsch TG 209 F1 Iris thermo gravimetric balance with $\pm 10^{-5}$ g precision, using a platinum crucible. A heating rate of 3 ºC·min^{-1} was used (from 20 ºC up to 900 ºC) under 30 $mL_N \cdot min^{-1}$ of synthetic air.

UV/Vis diffuse reflectance (DR) spectra were obtained using a Perkin Elmer lambda 750 spectrophotometer, equipped with a 60 mm integrating sphere, using Spectralon™ as standard.

High-resolution X-ray photoelectron spectroscopy (XPS) analyses were performed under high vacuum in an ESCALAB 200A (Thermo VG Scientific) equipment with an aluminum anode source (*E*o = 15 kV – 300 W), energy step of 0.1 eV and 1000 ms dwell time.

The crystalline phases of pure P25 were obtained using a Bruker AXS D8 Discover x-ray diffractometer equipped with a Göbel mirror with Cu K radiation in locked couple mode.

4.3 Results and discussion

4.3.1 Photoactivity of powder pressed (PP) films

Figure 4.3 plots the NO conversion and selectivity histories obtained for P25 powder pressed films PP0 and wPP0. Steady state NO conversion and selectivity are higher for wPP0, the powder pressed film prepared via wet mixture.

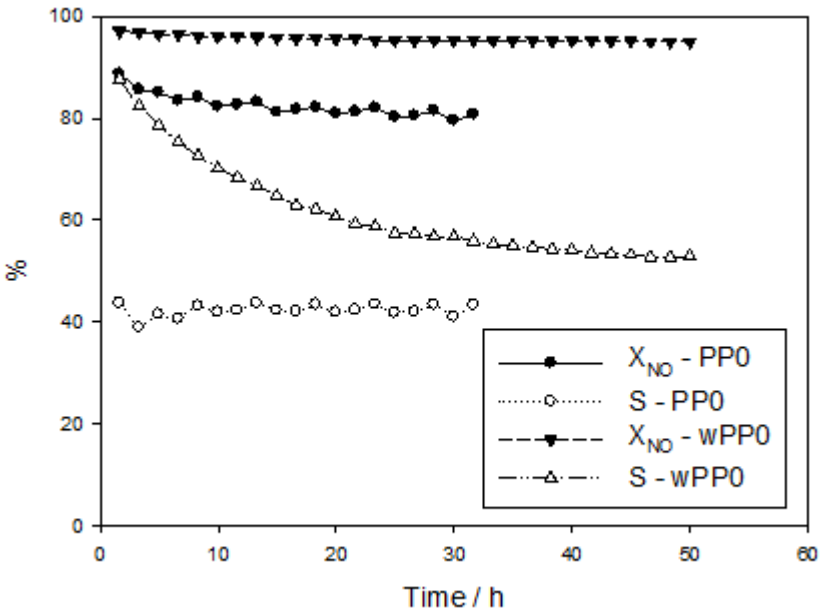

Figure 4.3 – NO conversion (full symbols) and selectivity (empty symbols) histories obtained with powder films PP0 and wPP0.

Such improvement should be related to chemical or physical changes of either P25 or the morphology of the photocatalytic film. Table 4.4 presents X-ray diffraction (XRD) patterns of fresh P25 and P25 after wet mechanical mixture followed by sonication. It can be concluded that the size and nature of P25 mostly did not change after the complete wet mixing procedure. Results of XPS analyses made to these samples are shown in Figure 4.4 and Table 4.5 and indicate a change of 3 percentage points concerning the number of OH groups bounded to the photocatalyst surface (which is within the technique uncertainty). Yu et al. [22] reported significant photoactivity improvement of P25 after hydrothermal treatment but these authors observed an increase of OH surface groups of 14 percentage points. The morphology of the film should therefore play a significant role; simple density measurements showed that wPP0 powder is ca. 5 times denser than fresh P25. Figure 4.5 plots the diffuse reflectance spectra of PP0 and wPP0 films. A different behavior of the films towards irradiation is observed, with a higher reflectance for the non-humidified one. Therefore, differences obtained in the photoactivity of PP0 and wPP0 should be assigned to different

scattering behavior of the films instead of bandgap changes. Different scatter behavior can modify the optical thickness of the film [23], and therefore the amount of UV-activated photocatalyst (effective load). These results evidence the influence of the photocatalytic film preparation protocol on the photoactivity, yielding a better steady state performance when wet protocol is used, although with a longer transient period (Figure 4.3).

Table 4.4 – Crystalline phase fraction, density, particle diameter and crystallographic net parameters of fresh P25 and P25 after mechanical mixture and sonication, obtained by XRD.

P25 Sample	**Crystalline form**	**% phase (v/v)**	**Density ($g \cdot cm^{-3}$)**	**Particle diameter (nm)**	**Lattice constant *a* (Å)**	**Lattice constant *b* (Å)**
PP0 (fresh)	Anatase	88.5	3.896	25	3.7805	9.4942
	Rutile	11.5	4.266	35	4.5893	2.9530
wPP0 (mixed & sonication)	Anatase	88.7	3.906	26	3.7821	9.4982
	Rutile	11.3	4.266	39	4.5902	2.9556

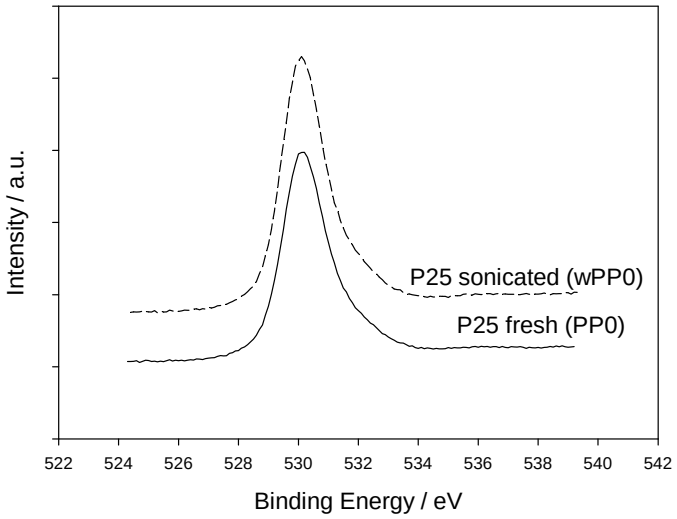

Figure 4.4 - High-resolution XPS spectra at O1s region for powders of fresh P25 and P25 after mechanical mixture and sonication.

Table 4.5 - Results of curve fitting of high-resolution XPS spectra at O1s region of fresh P25 and P25 after mechanical mixture and sonication (percentage of Ti-O vs. O-H bonds obtained by peak deconvolution).

P25 Sample	Data	O1s (Ti-O)	O1s (O-H)
PP0 (fresh)	E_b (eV)	530.12	531.65
	fwhm	1.60	1.74
	(%)	87	13
wPP0 (mixed & sonication)	E_b (eV)	530.12	531.65
	fwhm	1.60	1.74
	(%)	90	10

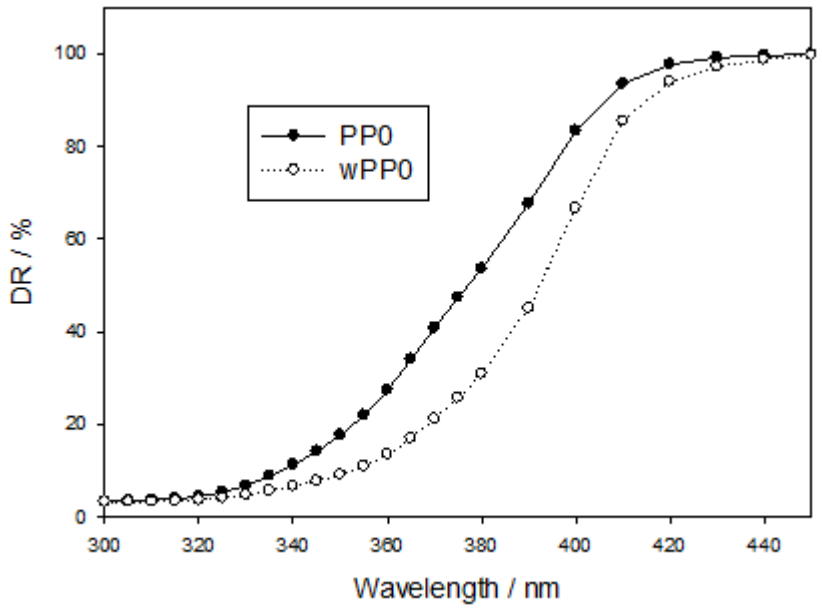

Figure 4.5 – Diffuse reflectance (DR) spectra of powder pressed films PP0 and wPP0.

Since the preparation protocol of the photocatalytic paint RP involves wet mixing, the effect of P25 wetting with different powder paint components was also studied. In chapter 3 (and [19]), the effect of wet mixing P25 with the rest of the paint powder components was reported as having a negative impact on the steady state photoactivity; the corresponding powder film

originated a NO conversion of about 40 % (in line with results of reference paint) whereas a powder film obtained via dry mixture originated a NO conversion of ca. 60 %.

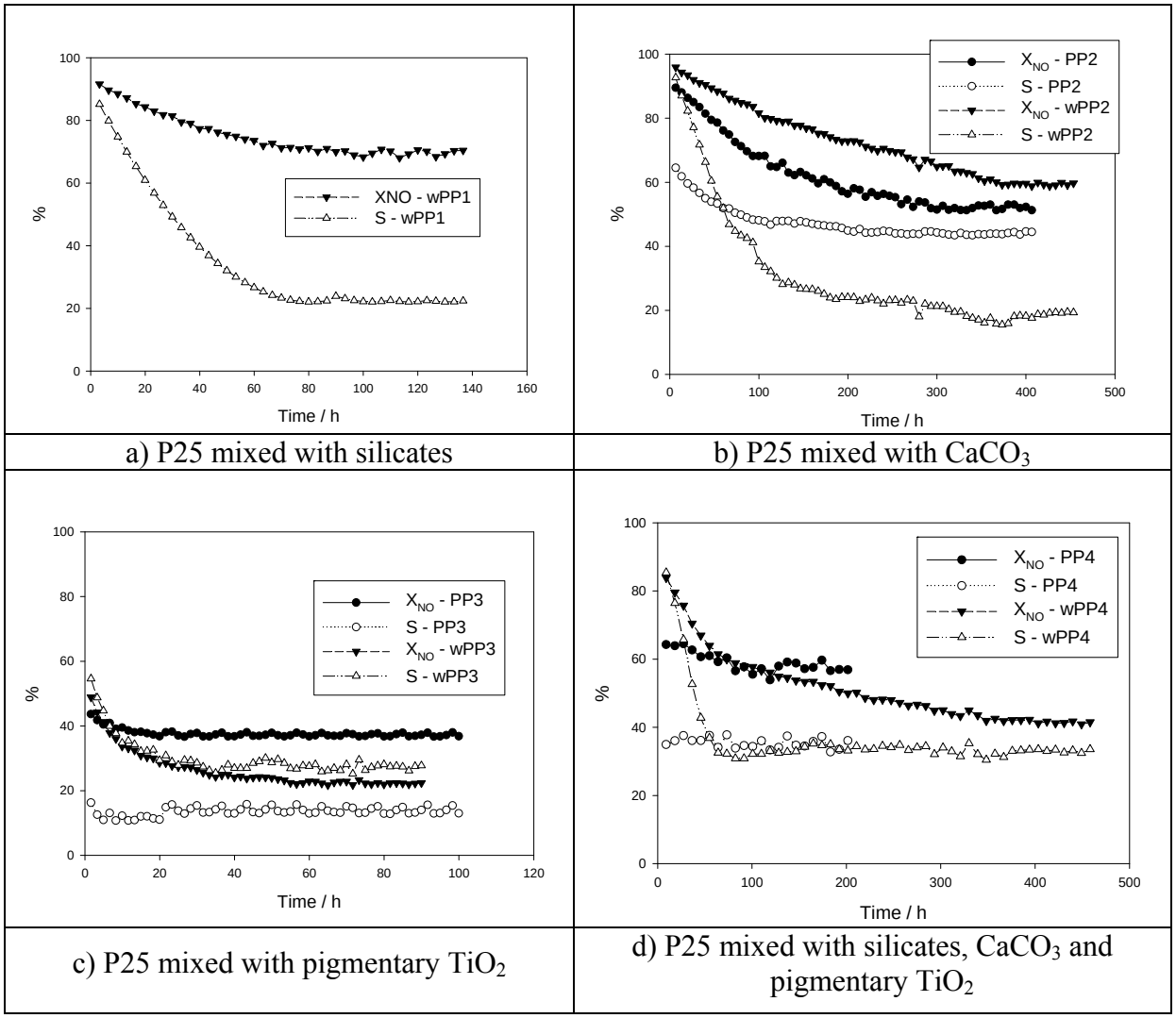

Figure 4.6 - NO conversion (full symbols) and selectivity (empty symbols) histories obtained with PP# (circles) and wPP# (triangles) films of P25 mixed with: a) silicates; b) $CaCO_3$; c) pigmentary TiO_2 and d) all powder components (silicates, $CaCO_3$ and pigmentary TiO_2).

Figure 4.6 plots the NO conversion and selectivity histories for powder films PP2 to PP4 (sample PP1 did not form a stable powder film) and wPP1 to wPP4. It can be seen that extenders do not impair the NO conversion as much as pigmentary TiO_2 does. Figure 4.6a plots the history of NO conversion and selectivity for film wPP1. This film exhibits a steady state conversion of NO of ca. 70 % and selectivity of ca. 20 %, showing that the silicate extenders do not impair significantly the NO photoconversion - cf. Figure 4.3 (one should

take into account that wPP1 film contains ca. 25 wt.% of photocatalytic TiO_2 while wPP0 contains 100 % – Table 4.2). Similar conclusion can be drawn for extender $CaCO_3$ (Figure 4.6b) where it was obtained a steady state NO conversion of ca. 55 % and 65 % for the dry and wet mixed films, respectively. $CaCO_3$ is often referred in literature as being involved in the removal of nitrous and nitric acids (nitrate and nitrite ions) from the surface of photocatalytic TiO_2 during NOx photocatalytic oxidation, forming the corresponding calcium salts [11, 18]. However, concerning wPP2, it was not observed a significant difference, neither in terms of conversion nor in terms of selectivity, compared to the performance of wPP1, which contains silicates instead of calcium carbonate. Finally, Figure 4.6c illustrates the effect on the powder film photoactivity of the pigmentary TiO_2, which seems to be the main responsible among all powder components for impairing the photoactivity of P25; such impairing effect is even higher when water is involved in the production procedure compared to pure dry mixture as shown in chapter 3.

Figure 4.6b shows that the presence of $CaCO_3$ makes the transient period up to steady state to be very long, ca. 400 h, compared to that when using silicate extenders (Figure 4a) or just in the presence of pigmentary TiO_2 (Figure 4.6c). On the other hand, the steady state activity when all powder components are present, including 1.64 wt.% of $CaCO_3$, is achieved after ca. 100 h in the case of dry mixture and ca. 400 h in the case of wet mixture (Figure 4.6d). Although no clear evidence was found for this observation, it is proposed that the photocatalyst surface after contacting with calcium carbonate becomes modified in such a way that it allows the slower accumulation of reaction products, making the conversion and selectivity to decrease accordingly until the steady state. Finally, it is worth mentioning that the wet mixture protocol led to powder films that in some cases exhibited better NO conversions than the non-wet films (e.g. Figure 4.3) but in other cases the opposite behavior was observed (e.g. Figure 4.6c). Such fact must be addressed in future studies.

4.3.2 Photoactivity of pseudo-paint (PsP) films

In the previous chapter (and [19]), the initial NO conversion of pseudo-paint films was inversely related to the amount of organic components; however, the preparation protocol may also affect the initial photoactivity [21]. Figure 4.7 shows the NO conversion and selectivity histories for pseudo-paint films PsP1 and PsP2 and for the reference paint RP (compositions shown in Table 4.3). It can be seen that after a transient period of ca. 150 hours the NO conversion concerning films PsP2 and RP are similar and the NO conversion of PsP1 only slightly higher; selectivities of all films are similar. The base paint showed no photoactivity because it has no P25 (only pigmentary TiO_2).

The possible existence of parallel photocatalytic reactions involving oxidation of NOx and organic components of the photocatalytic paint during the transient period was postulated in the previous chapter (and [19]).

As mentioned before, standard activation was not sufficient to activate the RP film and a harsher activation protocol had to be applied. The amount of the organic components photooxidized after UV aging was computed from thermogravimetry (TG) data. The UV aging was performed under the same operating conditions as for the standard activation, during 24 hours or 150 hours (see section 4.2.3).

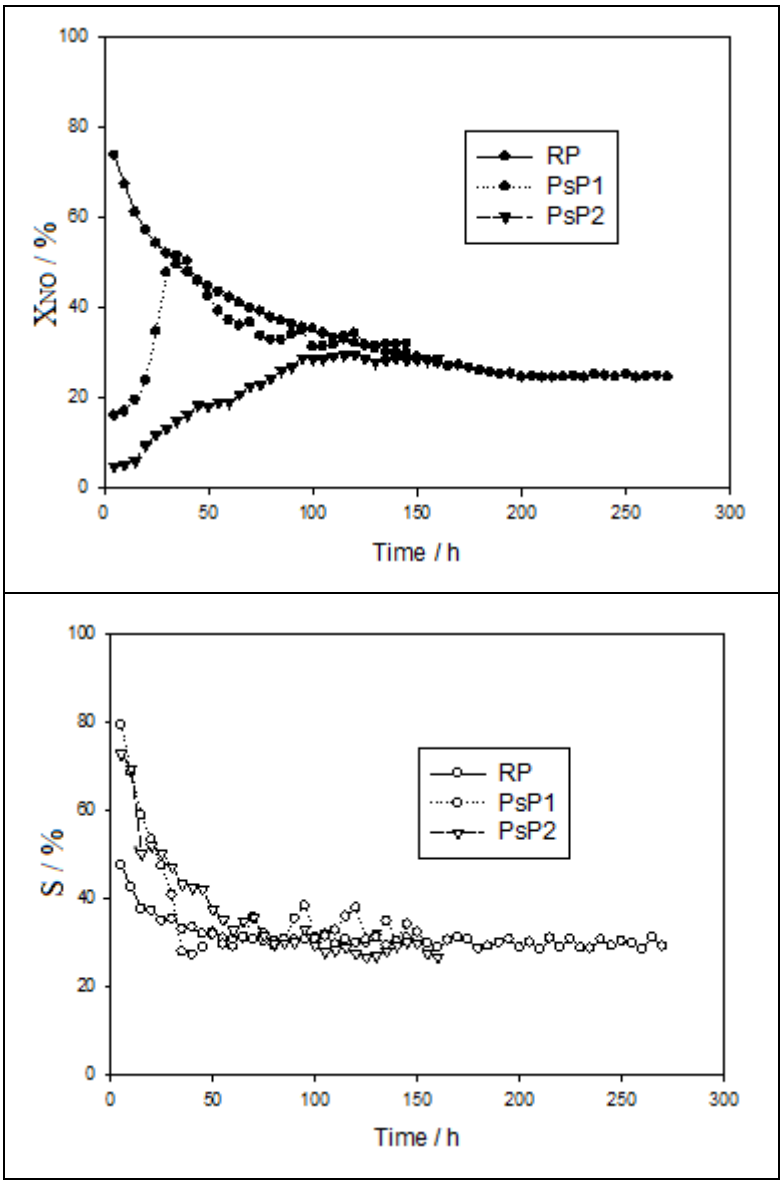

Figure 4.7 – NO conversion (top graph) and selectivity (bottom graph) histories on films PsP1, PsP2 and RP (the later with hasher activation).

Figure 4.8 presents the TG plots obtained for PsP#, RP and BP films. Although the samples were previously dried, a slight mass loss was observed for temperatures below 100 ºC. It was then used the mass at 120 ºC for normalizing the mass loss as a function of temperature (Δ_{th}). The samples were heated up at a constant rate under an atmosphere of air with consequent organic phase degradation and mass loss. Figure 4.8 compares the TG plots for the PsP1, PsP2, BP and RP films. It may be concluded that samples containing photocatalytic TiO_2 exhibit less mass loss, especially after 150 h of aging.

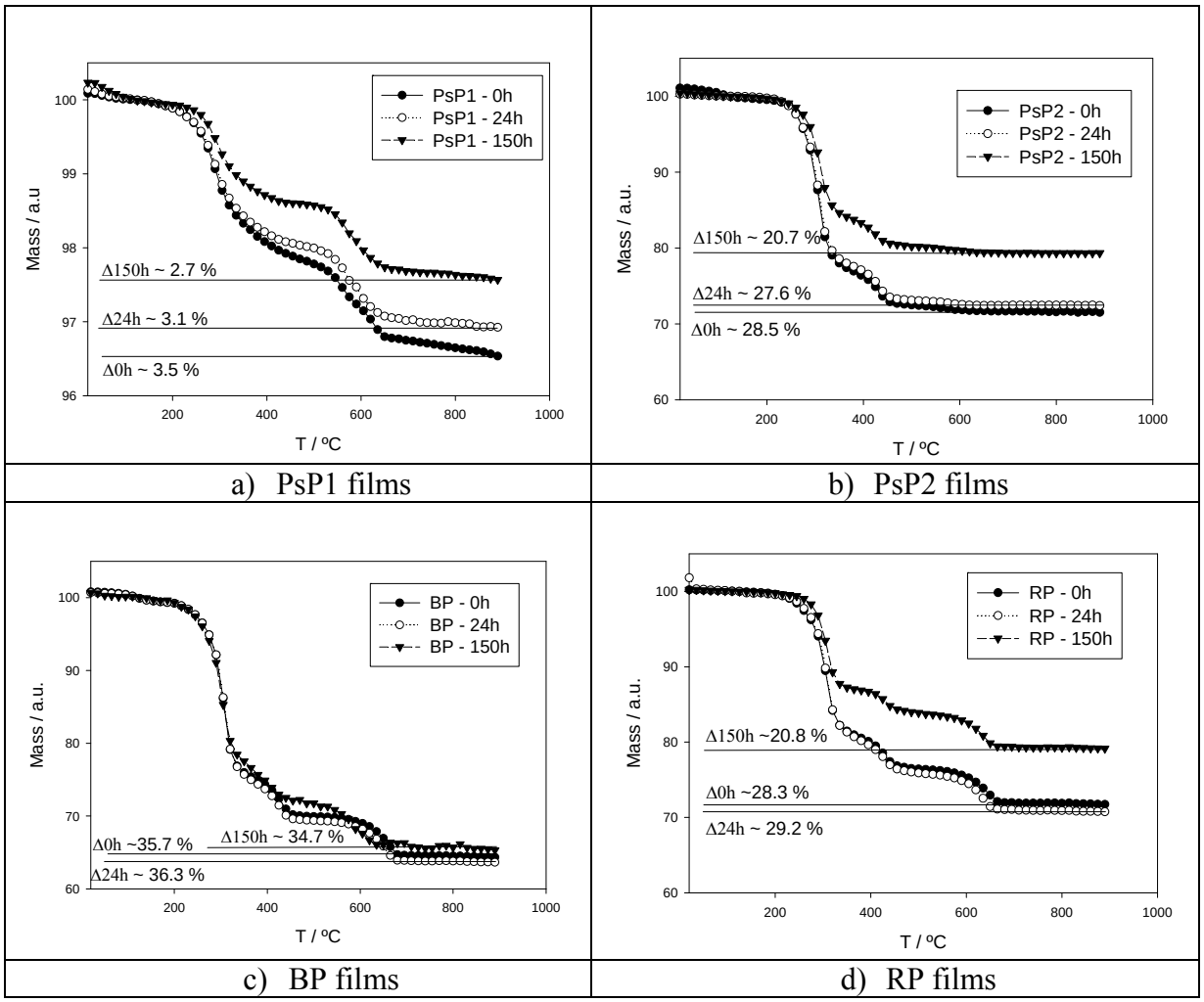

Figure 4.8 – TG analysis of PsP1, PsP2, BP and RP films without (0 h) and with (24 h and 150 h) UV aging (mass were calculated with base 100 at 120 ºC).

This means that during the UV aging stage a fraction of the organic phase was degraded and the oxidation products vented out; Table 4.6 summarizes these results. The relative mass loss due to the photodegradation occurred during the aging stage was computed as follows:

$$\text{Photodegradation}_{th} = \frac{\left(\Delta_{th} - \Delta_{0h}\right)}{\Delta_{0h}} \times 100 \qquad (4.3)$$

where t refers to 24 h or 150 h of aging. The organic content of each paint film is given by the TG mass loss at 900 °C (Δ_{0h}), which are in close agreement with data in Table 4.3.

Table 4.6 – TG mass losses at 900 °C of fresh and aged samples for 24 h and 150 h and relative mass loss due to photodegradation during UV aging.

Film	**Δ_{0h} (%)**	**Δ_{24h} (%)**	**Photodegradation$_{24h}$ (organic phase loss / wt.%)**	**Δ_{150h} (%)**	**Photodegradation$_{150h}$ (organic phase loss / wt.%)**
PsP1	3.5	3.1	-11.4	2.7	-23.2
PsP2	28.5	27.6	-3.1	20.7	-27.4
BP	35.7	36.3	1.9	34.7	-2.7
RP	28.3	29.2	3.4	20.8	-26.3

PsP2 film exhibits a lower photodegradation than PsP1 after 24 hours UV aging (3.1 % compared to 11.4 %, respectively). This is consistent with the smaller initial photoactivity shown by PsP2, 6.5 % of NO conversion, compared to 18 % for PsP1 film, respectively – Figure 4.7. Indeed, PsP2 film contained originally a higher amount of organic phase (Table 4.3), responsible for hiding the photoactivity. The full photoactivity of samples such as PsP2 or RP is only revealed after degrading a significant amount of the organic phase. This degraded organic phase should be initially wrapping photocatalytic TiO_2 particles and preventing them to photooxidize NO.

TG mass loss of BP and RP films after 24 hours of UV aging present a slight increase compared to fresh films (Table 4.6 and Figures 4.8c and d), which might be related to the precision error in TG analyses. Allen et al [9] observed a similar behavior for photocatalytic siliconised polyester coatings aged in QUV weatherometer. These results are in good agreement with the photo inactivity exhibited by the RP, even after 24 h of standard activation. This result contrasts with the photoactivity exhibited by PsP2 film that has the same composition as RP except for the dispersants (cf. Table 4.3). Indeed, the dispersants should provide a better contact of the binder with the photocatalytic TiO_2 particles, preventing the photoactivity until a stronger activation protocol is applied – Figure 4.7. Alone, however,

i.e. without other organics, the dispersants do not provide this strong photoactivity barrier since film PsP1 exhibited photoactivity right after being submitted to a standard activation procedure – Figure 4.7.

After 150 h of UV aging, BP film shows a marginal photodegradation (Figure 4.8c and Table 4.6) since it has no P25. All photocatalytic films (PsP1, PsP2 and RP) after 150 h of aging show ca. 25 wt.% of photodegradation of the organic phase (Figure 4.8c and Table 4.6). Such photoerosion should occur to a larger extend close to the film surface; thus, their photocatalytic performances towards NO abatement became quite similar after around 150 h – Figure 4.7.

The steady state photoactivity achieved for wPP4 film, containing all powder components as RP (X_{NO} ~40 %; S ~30 % – Figure 4.6d), is comparable to the ones achieved for PsP1, PsP2 and RP films (X_{NO} ~30 %; S ~30 % – Figure 4.7). Organic components show a small UV light absorption, which is supported by a similar diffuse reflectance of wPP4 film compared to RP film – Figure 4.9.

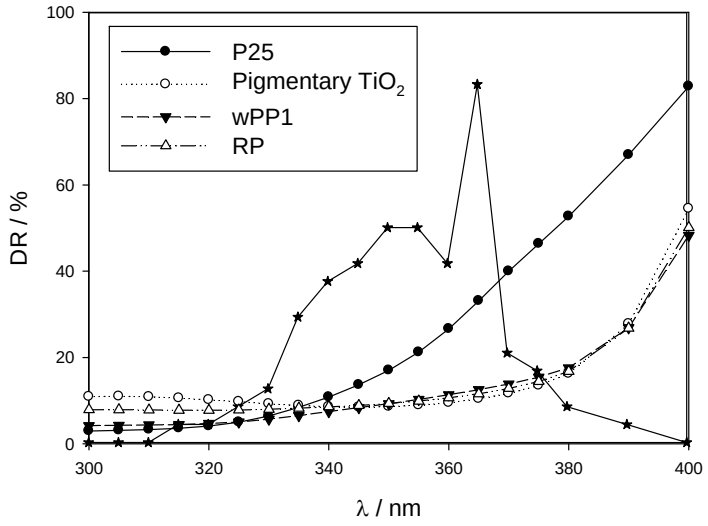

Figure 4.9 – Diffuse refectance (DR) spectra of P25, pigmentary TiO_2, wPP1 and RP (star points - lamp spectrum).

As stated above, pigmentary TiO_2 is the greatest UV light absorber in a paint film. Since the photoactivity is related to the amount of illuminated photocatalytic TiO_2, the optically activated photocatalyst among PsP1, PsP2 and RP films should be similar and they perform accordingly after the transient period.

Figure 4.10a shows the differential thermogravimetric (DTG) curves of fresh samples of PsP1, PsP2, BP and RP films. It is apparent a relationship between each DTG peak and a family of organic compounds, which in principle should allow following their specific photodegradation; from Figure 4.10b it is clearly visible the heterogeneous decrease on the size of the peaks of UV aged samples. If the peaks are related to different organic species in the paint matrix, UV aging does not uniformly degrade them. A preliminary study indicates that the resin and the dispersing agents are the components that suffer more photodegradation.

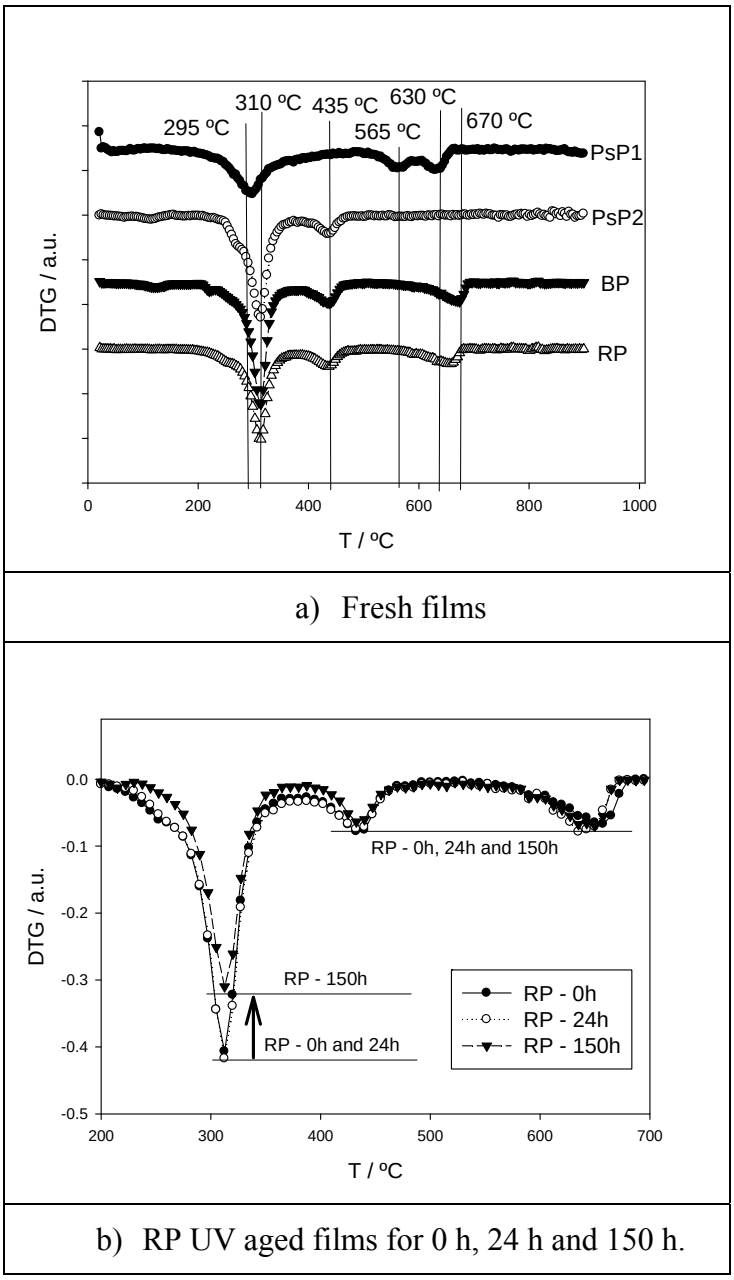

Figure 4.10 – DTG curves of (a) fresh samples of PsP1, PsP2, BP and RP films and (b) RP fresh and aged films for 24 h and 150 h.

4.4 Conclusions

The influence of the components of exterior water-based vinyl paint on the photoactivity of P25 was assessed. A special attention was given to the photodegradation of the organic phase during UV aging. Several films containing powder components and powder and organic components were prepared. The powder components are photocatalytic TiO_2, pigmentary

TiO_2 and extenders $CaCO_3$ and silicates. The powder films were obtained via dry and wet mixture protocols.

Concerning powder films obtained via dry mixture, it was observed that pigmentary TiO_2 impairs significantly the NO conversion and selectivity while silicates and $CaCO_3$ have a smaller impact in the photoactivity. Such conclusion on impair effect are similar for dry or wet production procedure, being however the impair effect of pigmentary TiO_2 much higher on the later one type of film.

The steady state of the $CaCO_3$-containing films, obtained via wet mixture, is attained after a correspondingly longer transient period of time, evidencing interference of the mixture process and/or of the carbonate.

P25 alone showed a greater photoactivity after wet mixing while, when mixed with pigmentary TiO_2 revealed much lower steady state NO conversion.

TG analysis to fresh and UV aged films revealed the strong photodegradation of the organic phase of the paint films prepared. After 150 h of UV aging, ca. 25 wt.% of the organic phase disappeared via photocatalytic oxidation, being the top layer of the film the most photoeroded. The degradation of the organic coating covering the photocatalytic TiO_2 particles was related to the transient photoactivity behavior of the PsP# and RP films. Moreover, it was concluded that RP film needs a stronger activation protocol for starting photocatalysing NO because of a synergetic effect between dispersants and binder coating photocatalytic TiO_2 particles.

Wet mixed powder film wPP4, containing all powder paint components as RP film, originated similar steady state photoactivity compared to RP. It was then concluded that the top layer of the 150 h UV aged RP film contains a similar amount of illuminated photocatalytic TiO_2 as the wPP4 film.

References

[1] United States Environmental Protection Agency, *How nitrogen oxides affect the way we live and breathe*, EPA-456/F-98-005, September 1998 (http://www.cleanairaction.org/pubs/pdfs/old_pubs/noxfldr.pdf - accessed February 2011).

[2] Leeuw, F.A.A.M., , *Environ Sci Policy* 2002; 5: 135–145.

[3] Agência Portuguesa do Ambiente, Online database on air quality (www.qualar.org, accessed on February 2011).

[4] Riga-Karandinos, A., Saitanis, C., *Chemosphere* 2005, 59, 1125.

[5] European Environment Agency, *NECD: Member State Country-Profiles*, 2007 (available at: http://www.eea.europa.eu/themes/air/nec-directive-member-state-country-profiles/nec-directive-member-state-country-profiles - accessed February 2011).

[6] Lim, T.H., Jeong, S.M., Kim, S.D., Gyenis, J., *J. Photochem. Photobiol. A: Chem.* 2000, 134, 209.

[7] Hashimoto, K., Wasada, K., Osaki, M., Shono, E., Adachi K., Toukai N., Kominami H., Kera, Y., *Appl. Catal. B: Environ.* 2001, 30, 429.

[8] Matsuda, S., Hatano, H., Tsutsumi, A., *Chem. Eng. J.* 2001, 82, 183.

[9] Allen, N.S., Edge, M., Verran, J., Stratton, J., Maltby J., Bygott C., *Polym Degrad Stab* 2008 93 1632.

[10] Diebold, U., *Surf. Sci. Rep.* 2003, 4, 53.

[11] Devahasdin, S., Fan Jr., C., Li, K., Chen, D.H., *J Photoch Photobio A* 2003, 156, 161.

[12] Benedix, R., Dehn, F., Quaas, J., Orgass, M., *Lacer* 2000, 5, 157.

[13] Kaneko M. and Okura I., (eds.), *Photocatalysis Science and Technology*, Tokyo, Kodansha Ltd., 2002.

[14] Herrmann, J.-M., *Top. Catal.* 2005, 34, 49.

[15] Braslavsky, S.E., *Pure Appl. Chem.* 2007, 79, 293.

[16] Osburn, L., *Proceedings 5th Post Graduate Conference on Construction Industry Development 2008*, 16-18 March, Bloemfontein, South Africa.

[17] Marley Eternit, Ecologic Roof Tiles – Breathing Life Into the Environment (available at: http://www.marleyeternit.co.uk/Roofing/Concrete-Tiles/EcoLogic-Ludlow-Major-Interlocking-Tile.aspx, accessed February 2011).

[18] Bygott, C.E., Maltby, J.E., Stratton, J.L., McIntyre, R., *Photocatalytic Coatings for the Construction Industry*, International RILEM Symposium on Photocatalysis, Environment and Construction Materials 8-9 October 2007, Florence, Italy, 251–258 [19] Águia C., Ângelo J., Madeira L.M., Mendes A., *Catal. Today* 2010, 151, 77.

[20] Koleske, J. V., *Paint and Coating Testing Manual*, 14th edition of the Gardner-Sward Handbook, Philadelphia, 1995.

[21] Águia C., Ângelo J., Madeira L.M., Mendes A., Photo-oxidation of NO using an Exterior Paint – Screening of Various Commercial Titania, *Journal of Environmental Management* (10.1016/j.jenvman.2011.02.010).

[22] – Yu, J, Yu, H, Cheng, B, Zhou, M, Zhao, X., *J. of Mol. Catal. A.* 2006, 253, 112.

[23] Murphy, A.B., *J. Phys. D: Appl. Phys.* 2006, 39, 3571.

Part IV – *The Photocatalyst*

Chapter 5 – Supported Photocatalytic TiO_2 Produced by Ion Exchange[4]

Abstract

In the present chapter, the performance of commercially available photocatalyst P25 (based on titanium dioxide), as well as synthesized new ones (TiO_2 supported in porous solid inorganic materials), is compared regarding photocatalytic oxidation of NO. Lower NO conversion achieved with the supported photocatalytic TiO_2 materials (TiO_2 content about 1 wt.%, except for zeolite Y with two exchange steps) than with the commercial ones, suggest the possible influence of intrinsic characteristics of the supported materials on the photoactivity. A strong synergetic effect between zeolite Y and P25, in mechanical mixtures, is observed; a film produced from mixture of P25 and zeolite Y, with only 15 wt.% in P25, originated approximately the same values of NO conversion (55 %) and selectivity (35 %) than a film with 100 wt.% of P25.

[4] *Águia, C., Xamena, F.X.L., Dominguez, E., García, H., Madeira, L. M., Mendes, A., 10th International Chemical and Biological Engineering Conference, 4-6 September 2008, Braga, Portugal, 117 (CD: pp. 277-282).*

5.1 Introduction

NOx are precursors for urban smog and troposphere ozone formation that are related with health damages [1]. Therefore, improvements in de-NOx technologies are needed.

Photocatalysis has been tested in the NOx abatement and photocatalytic construction materials, such as paints, have been pointed as a possible solution to help in the de-NOx of the environment [e.g. 2]. However, for successful application of this technology it is important to protect the matrix of these construction materials towards the photocatalytic process. In this line some studies have been performed and basically two strategies can be identified in the literature: i) decrease the amount of incorporated photocatalytic TiO_2 and select constituents with higher chemical stability [3]; and ii) use of supported TiO_2 particles on inorganic adsorbents [4]. Support TiO_2 particles on inorganic adsorbents shows attractive advantages, such as concentrate the target compounds to abate, over the product ones, by adsorption, increasing therefore the reaction rate [5].

In the work presented in this chapter, TiO_2 was supported on zeolites Y and USY (zeolyst) and montmorillonite K-10 (Sigma-Aldrich). The photoactivity of these composite materials was tested in powder pressed films and discussed taking into account some of their intrinsic characteristics. Comparison was made with the photoactivity of the P25.

5.2 Experimental

5.2.1 Supported photocatalysts, synthesis and characterization

The experiments described below aim at testing the photoactivity of supported TiO_2 on various adsorbent materials (hereafter named as supported photocatalytic TiO_2) and comparing their performance with that of commercial photocatalytic TiO_2. The supported photocatalytic materials were produced by ion exchange using $(Ti{=}O)K_2(C_2O_4)\cdot H_2O$ as TiO_2 precursor, as described by Cosa et al. [4]. The adsorbents used as support were

montmorillonite k-10 (mK-10) from Sigma-Aldrich, Zeolites Y (CBV100) and USY (CBV500) from Zeolyst. These materials were exchanged once or twice. The first exchange was performed with a 0.2 M solution in Ti and the second with a 0.6 M solution. The supported photocatalyic TiO_2 obtained by one or two ion exchanges were denoted as TiO_2@support and $(TiO_2)_2$@support, respectively, with "support" being USY, Y or mk-10. (P25+Y)_15 wt.% TiO_2 refers to the material produced from the mechanical mixture of zeolite Y and P25 TiO_2 (15 wt.% in P25).

Elemental analysis was performed by induced coupled plasma (ICP) using a Varian 715-ES instrument. The surface area and porosity of tha samples produced was studied by nitrogen adsorption at 77 K using a Micromeritics ASAP 2010.

5.2.2 Photocatalytic films

Powder pressed films were tested in the setup described below and in greater detail in chapter 2. Powder pressed films were produced by pressing the powder to the base of the reactor, made of amovible aluminum slabs, applying 5 bar for 7 min. Film size was 6 x 5 cm^2.

5.2.3 Experimental setup and photocatalytic tests

The operating conditions and construction of the setup were inspired on standard ISO 22197-1:2007(E). Basically it comprehends a thermostatic cabinet where the reactor and the feed system are assembled. In the rectangular base of the reactor, made of amovible aluminum slabs, is applied the photocatalytic film to be tested. A photoluminescent NO and NO_2 analyzer (Thermo Scientific 42C) is used to monitor the concentration of these species. The irradiance, relative humidity (RH), NO concentration at the inlet of the reactor (NO_{in}) and temperature were set to 7 $W \cdot m^{-2}$ (UV BLB lamp 365 nm – *Vilbert Lourmat*), 50 %, 1 ppm (in AirK), and 25 ºC, respectively. Total gas flow rate used was 0.7 $L_N \cdot min^{-1}$.

5.3 Results and discussion

Photocatalysis of NOx can proceed as reduction and/or as oxidation. However, photoreduction is not probable to occur in the presence of water and oxygen. Also, it is not referred the formation of N_2O in similar systems [6]. NO photocatalytic oxidation should then proceed to NO_2 and then to NO_2^- or NO_3^-. NO conversion (X_{NO}) and selectivity towards NO_2^- and NO_3^- were calculated using the following equations:

$$X_{NO} = \left(\frac{C_{NO}^{in} - C_{NO}^{out}}{C_{NO}^{in}} \right) \times 100 \quad (5.1)$$

$$S = \left(1 - \frac{C_{NO_2}^{out}}{C_{NO}^{in} - C_{NO}^{out}} \right) \times 100 \quad (5.2)$$

where C_{NO} and C_{NO_2} are the gas phase concentration of NO and NO_2, respectively, and the superscripts refer to the inlet and outlet streams of the photocatalytic reactor.

5.3.1 Physicochemical characterization

X-ray diffraction did not allow the identification of typical peaks of crystal structures of TiO_2. Such fact does not mean that a crystalline structure does not exist; actually, a photocatalytic activity was detected, as shown later on. The analysis of the diffractogram of zeolite Y with one and two exchanges (Figure 5.1) reveals complete loss of crystallinity, which must be a consequence of a structure loss due to TiO_2 incorporation.

Table 5.1 presents the weight fraction of Ti in each sample, and the BET surface area, obtained by ICP and nitrogen adsorption isotherms performed at 77 K, respectively. Results of $(TiO_2)_2$@Y show a very large amount of incorporated Ti, which can be one of the causes for crystalinity loss of zeolite Y, shown in Figure 5.1. Such loss produces a strong decrease in the BET surface area of zeolite Y from the first to the second ion exchange steps (Table 5.1

and Figure 5.1). A decrease was also noticed in the remain supported samples tested, however much less pronounced than with zeolite Y.

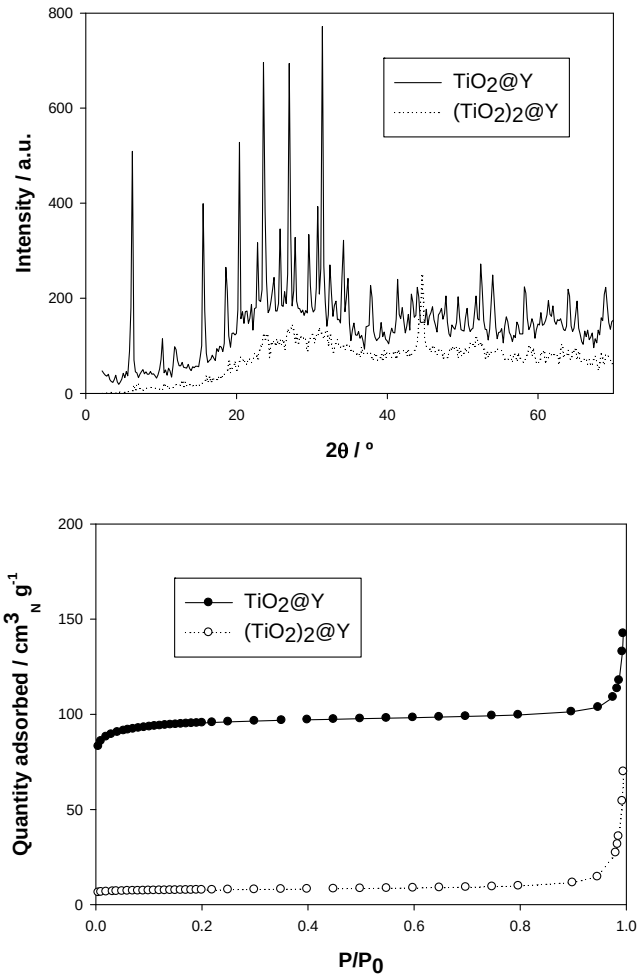

Figure 5.1 – X-ray diffraction patterns (top) and nitrogen adsorption isotherms performed at 77 K (bottom) for the supported photocatalysts into zeolite Y.

Table 5.1 – Results of elemental analysis performed by ICP, and BET surface areas obtained by nitrogen adsorption isotherms performed at 77 K.

	Y	**TiO_2@Y**	**$(TiO_2)_2$@Y**	**USY**	**$(TiO_2)_2$@USY**	**mK-10**	**TiO_2@mK-10**	**$(TiO_2)_2$@mK-10**
Ti (wt.%)	0.06	0.96	10.68	0.07	1.12	0.28	0.60	0.89
S_{BET} (m^2 g^{-1})	688	311	25	558	519	269	264	259

Diffuse reflectance was performed and has shown the light absorption characteristic of TiO_2. For zeolite Y, only after a second exchange step some activity is noticed (Figure 5.3), which can be ascribed to the particle diameter increase, leading to a red-shift and absorption of radiation in the wavelength range of the UV lamp used (Figure 5.2); TiO_2@Y has a bandgap of ca. 4.5 eV, which corresponds to ca. 275 nm. This wavelength is out of the range of the UV lamp used (315 nm < λ <390 nm). On the other hand, $(TiO_2)_2$@Y has a bandgap close to the one of anatase TiO_2 - 3.2 eV, which might indicate that TiO_2 particles are large enough. These values match with the destroyed structure presented in Figure 5.1; increase of the particles inside the pores of zeolite Y must led to the destruction zeolite structure.

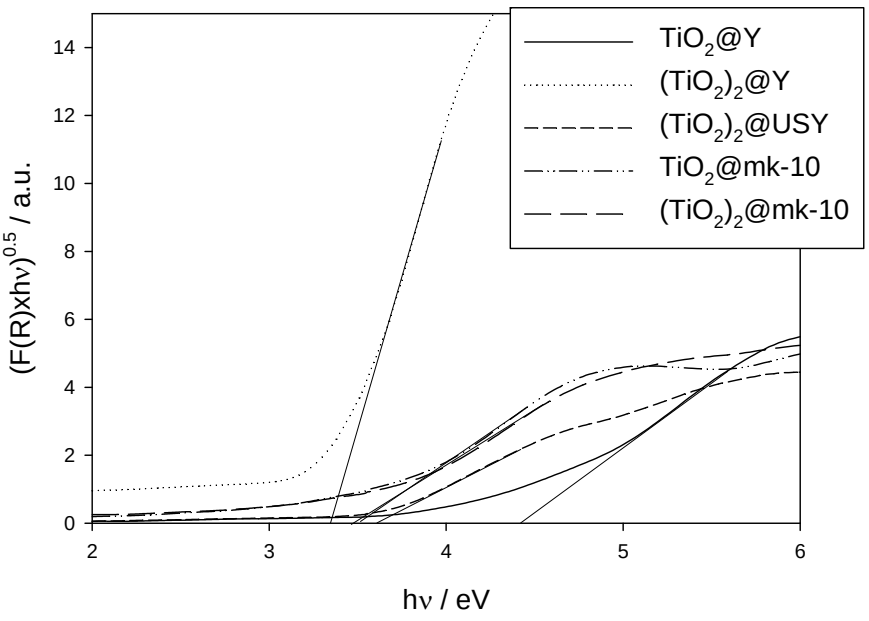

Figure 5.2 – Transformed Kubelka–Munk function vs. energy of the excitation source.

5.3.2 Photocatalytic tests

Table 5.2 presents the mass of each photocatalytic material used. The masses of TiO_2 employed in powder pressed films were obtained by direct weighting, in the case of

commercial photocatalysts, and were estimated, taking into account the amount of Ti exchanged and perfect TiO_2 molecular structure, in the case of the supported materials.

Figure 5.3 summarizes the NO conversions and selectivities (taken at steady state). From Table 5.2 one can see that there is a relatively large variation in the photocatalytic masses from experiment to experiment, due to the associated difficulties on its control. Figure 5.3 puts into evidence that commercial P25 provides, when used alone, NO conversions of ca. 50 %. It is thus worth noting that although the film area is the same as in the experiment where it is mechanically mixed with zeolite Y - "(P25 + Y)_15 wt.% TiO_2" (Table 5.2), the latter exhibits a similar NO conversion (Figure 5.3), despite of the much lower photocatalyst surface that is possibly exposed to radiation (as a consequence of a TiO_2 concentration of only 15 wt.%). This indicates that the adsorbent is playing a significant role on the photoactivity, an issue that needs however to be further investigated.

Regarding supported materials, it is possible to see that the increase in the number of ion exchange cycles leads to better performances (Figure 5.3). This is related to TiO_2 particles size (thus decreasing the so-called quantum size effect – blue shift) [5], for the case of zeolite Y, and Ti content for the case of mk-10 (Table 5.1); bandgap did not change from the first to the second ion exchange in this support (see Figure 5.2).

In general, conversions reached with the supported materials are low. Even so, it must be noticed the lower masses of TiO_2 per surface area of film when compared with the powder pressed films of commercial P25 (Table 5.2).

Table 5.2 – Photocatalytic materials and estimated TiO_2's mass in each experiment.

		Powder pressed films	
	Run#	**Mass of powder pressed (g)**	**$L_{photo\text{-}TiO2}$ (mg cm^{-2})**
Commercial TiO_2	P25	0.44	14.8
	(P25+Y)_15 wt.% TiO_2	1.00	5.0
Supported photocatalytic TiO_2	$(TiO_2)_2$@Y	1.60	9.7
	TiO_2@Y	1.61	1.0
	$(TiO_2)_2$@USY	1.32	1.1
	$(TiO_2)_2$@mK-10	1.23	0.8
	TiO_2@mK-10	1.78	0.7

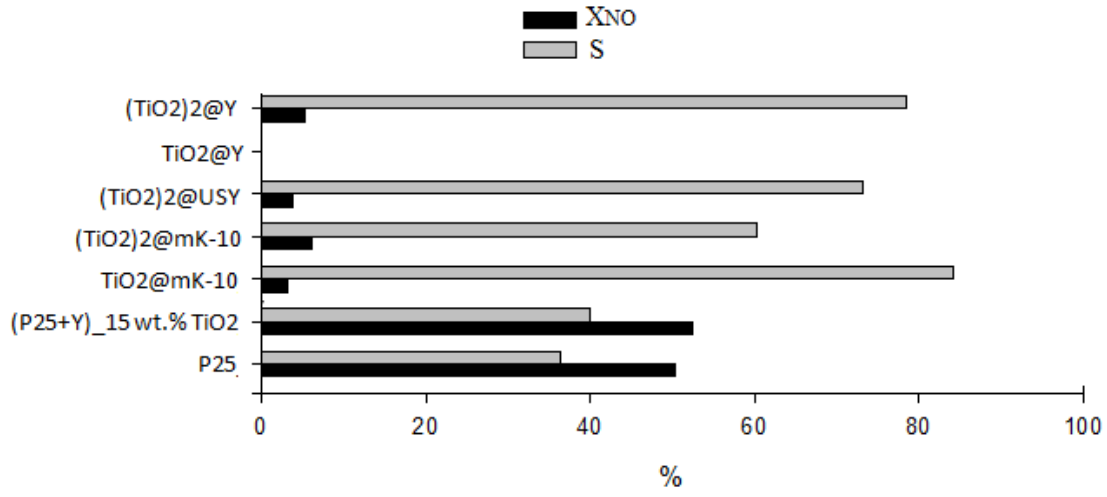

Figure 5.3 – NO conversion and selectivity at steady state for all tested films of Table 5.2.

5.4 Conclusions

Mixtures of commercial P25 with zeolite Y showed the same performance of a film with only P25, revealing the importance of the surroundings of the TiO_2 photocatalyst in its activity. The mass content of TiO_2 in adsorbents and absence of blue-shift, seem to play an important role on the photoactivity.

References

[1] US Environmental Protection Agency (1998). *NOx: How nitrogen oxides affect the way we live and breathe*, Office of Air Quality Planning and Standards Research Triangle Park, NC 27711.

[2] Strini, A., Cassese, S., Schiavi, L., *Applied Catalysis B: Environmental* 2005, 61, 90.

[3] Motohashi, K., Inukai, T., *Self-cleaning performance evaluation of commercial photocatalyst coting materials trough 5 years outdoor exposure*, International RILEM Symposium on Photocatalysis, Environment and Construction Materials 8-9 October 2007, Florence, Italy, pp. 80 - 86.

[4] Cosa, G., Galletero, M., Fernández, L., Márquez, F., García, H., Scaiano, J., *New J. Chem.* 2002, 26, 1448.

[5] Corma, A., García, H., *Chem. Commun*. 2004, 1443.

[6] Devahasdin, S., Fan Jr., C., Li, K., Chen, D.H., *J. Photochem. Photobiol. A* 2003, 156, 161.

Chapter 6 - Supported Photocatalytic TiO_2 Produced by Impregnation[5]

Abstract

The present chapter studies photocatalytic TiO_2 supported on zeolites, using an impregnation technique, and their performance for NOx abatement. Zeolites Y (Zeolyst CBV100 and CBV500), and β (Zeolyst CP811 HB20), were impregnated with TiO_2 to a concentration of ca. 3.3 wt.%. The composite and pristine zeolites were characterized for internal volume and surface area, NO adsorption isotherms, diffuse reflectance, SEM and X-ray diffraction. It was concluded that TiO_2 was mostly present on the external surface of the zeolite samples. The photocatalytic activity of powder pressed films made of these samples and of photocatalyst P25 (from Evonik) was assessed following approximately the standard ISO 22197-1:2007(E). TiO_2 supported on CBV100 originated the highest NO conversion (40 %), close to the one obtained with P25 (50 %). TiO_2 supported on CBV500 originated a NO conversion of 20 %, while TiO_2 on βCP811 did not show any photoactivity. TiO_2@CBV100 was incorporated in a paint film, ca. 9 wt.% of composite catalyst (this means ca. 0.3 wt.% of TiO_2), and its photocatalytic activity assessed. It was obtained a steady state conversion of NO of ca. 2.5 %, compared to 25 % conversion with a paint film incorporating 9 wt.% of P25; the specific photocatalytic activity of TiO_2 in both paint films was 0.16 $\mu g_{NO} \cdot g_{TiO2}^{-1} \cdot s^{-1}$ and 0.03 $\mu g_{NO} \cdot g_{TiO2}^{-1} \cdot s^{-1}$, for TiO_2@CBV100 and P25 paint films, respectively.

[5] *C. Águia, Francesc X. Llabrés i Xamena, E. Dominguez, H. García, L. M. Madeira, A. Mendes – under submission.*

6.1 Introduction

Photocatalysis makes use of photonic energy and a catalyst (photocatalyst) to promote chemical reactions [1]. The photonic energy is responsible for the excitation of valence electrons into the conduction band, creating the so-called electron-hole pair. These carriers move to the photocatalyst surface where they promote electrochemical reactions; the holes promote oxidations while the excited electrons promote reductions. The electrochemical potential of the band edges determine the possibility for a given reaction to occur while the charge carrier diffusivity and recombination time constant determine the efficiency of the photoelectrochemical process. An ideal photocatalyst should therefore exhibit the appropriate bandgap (which is directly related to the fraction of light spectrum absorbed) and band edges positions, have a larger recombination time constant compared to the diffusion time constant, be stable and cheap.

Nanoparticulated TiO_2 (photocatalytic TiO_2; herein also called photo-TiO_2) is the most used semiconductor in photocatalysis [2]. Anatase, the commonly used crystalline form of titanium dioxide, has a bandgap of 3.2 eV absorbing wavelengths shorter than ca. 387 nm. This semiconductor is very stable and the reduction potential of the valence band (2.7 V NHE at pH 7 [3]), when in contact with water molecules allows the production of highly oxidant hydroxyl radicals that can be used to oxidize hazardous chemical species. In this way, photocatalytic TiO_2 is able to oxidize hazardous chemical species both in gas [4, 5] and liquid phase [6, 7]. On the other hand, the reduction potential of the conduction band (-0.5 V NHE at pH 7 [3]) originates, in presence of O_2, the production of superoxide $O_2^{\cdot-}$, which can react with protons to produce hydrogen peroxide, also known as a powerful oxidation chemical specie [8].

Concerning air quality, NOx abatement is of great importance since they originate troposphere ozone and urban smog with consequent human health impacts [9]. Moreover,

despite recent and more restrictive regulation concerning maximum allowable NOx concentrations in atmosphere, there are still many places in the world where these limits are not respected, and namely in Lisbon [10].

Photocatalytic construction materials are being studied and developed to address the atmospheric pollution. Photocatalytic TiO_2 can be incorporated in concrete [11], roof tiles [12], pavement blocks [13] and coatings [14, 15]. Among all, paint coatings are of interest since a great fraction of surfaces is traditionally painted or can be painted. Moreover, paints have the exact thickness for being opaque avoiding excessive use of photocatalysts.

Nevertheless, as shown by the authors ([16] and chapter 4), the matrix of the paint films is eroded by the photocatalytic activity. Therefore, strategies must be implemented for paint protection. A possible approach is supporting the photocatalytic TiO_2 either occluded or wrapped by a solid resistant to the photocatalytic activity. When photocatalytic TiO_2 is grown inside the pore structure, the support works like a sieve, avoiding the direct contact of the paint matrix with photocatalytic TiO_2, but permitting NOx, water and oxygen to diffuse inside. It is also possible to make porous aggregates occluding the photocatalyst for obtaining the same effect. On the other hand, reducing the amount of photocatalyst added can produce an optimized balance between photoerosion of the paint and photoactivity. For reaching the same photoacatalytic activity, a reduction of the photocatalyst amount is viable if it would be possible to obtain a positive synergy between the photocatalytic TiO_2 and the support; Zeolites are being considered to support photocatalytic TiO_2 since it was observed a synergetic effect on the photoabatement of atmospheric NOx [17 - 22]. For instance, Ichiura et al. [18] evidenced the synergetic effect between zeolites A and Y with photocatalytic TiO_2, simply mechanically mixed, towards NO photoabatement. This synergy was reported to be related to the great adsorption ability of NO and NO_2 on zeolites, increasing the reaction rate and allowing a more complete oxidation of produced NO_2 towards nitrate.

In this chapter, the impregnation method was used to immobilize photocatalytic TiO_2 in two commercial grades of zeolite Y and one β zeolite. The performance of these composite photocatalytic materials towards NO oxidation was assessed following approximately ISO 22197-1:2007(E) standard. Performance was tested using the pure composite materials and inserted in paint. The results obtained indicate a significant synergy between the photocatalyst and the zeolite supports.

6.2 Experimental

6.2.1 Supported photocatalyst synthesis

Mesopore zeolites Y CBV100 (sodium form), CBV500 (ammonium form) and βCP811 - HB20 from Zeolyst, were used for supporting photocatalytic TiO_2. Zeolites (10 g) were previously treated under vacuum at 550 ºC overnight, in order to remove water and other adsorbed species. Zeolites were let to cool until room temperature under vacuum previously to their prompt impregnation with a TiO_2 precursor solution; 1.25 mL of titanium isopropoxide (Sigma-Aldich) in ca. 6 g of propan-2-ol (Sigma-Aldrich) was used, where propan-2-ol was employed to prevent prompt oxidation of titanium isopropoxide towards titanium hydroxide. Materials were then heated overnight at 500 ºC for TiO_2 formation. A concentration of 2 wt.% of titanium element was therefore introduced in each zeolite sample. Samples were denoted by "TiO_2@support", where "support" refers to CBV500, CBV100 and βCP811, accordingly.

6.2.2 Physicochemical characterization

Surface area and porosity of the samples were studied by nitrogen adsorption at 77 K using a Micromeritics ASAP 2010 equipment. Scanning electron microscopy (SEM) analysis was performed in ultra-high resolution field emission gun equipment (NOVA 200 Nano SEM).

Energy dispersive spectroscopy (EDS) was used for semi-quantitative chemical analysis using an EDAX Si(Li) detector. X-ray analyses were performed on a Bruker AXS D8 Discover x-ray diffractometer (XRD) equipped with a Göbel mirror with Cu Kα radiation in locked couple mode. UV/Vis diffuse reflectance (DR) was performed in optically thick films of the materials, in a Perkin Elmer 720 spectrometer equipped with a 60 mm integrating sphere, using Spectralon^{TM} as reference. Infrared (IR) spectra were recorded with a resolution of 4 cm^{-1} at 295 K using a Bomem MB-154S spectrometer (ca. 1.5 wt.% of sample mixed in KBr) and samples compressed into thin disk-shaped pellets. The NO adsorption isotherms on the photocatalytic composite materials were obtained at 25 °C using an in-house assembled volumetric method [23]. Samples were previously evacuated at room temperature down to 2 mbar.

6.2.3 Photocatalytic tests

A schematic representation of the photocatalytic reactor used is given in Figure 6.1.

Photocatalytic films (6 cm length and 5 cm width) were applied over aluminum slabs; the composite materials were tested in powder pressed films and the most photoactive of all was also tested when inserted in paint film loaded with 9 wt.% (wet base). An exterior vinyl type, water-based paint, with a pigment volume concentration (PVC) [24] above the critical value (CPVC) was used for receiving the composite materials. The powder films were obtained pouring the catalysts over the aluminum slab and pressing it up to 5 bar; the resulting films were ca. 0.5 mm thick. The paint film was obtained pulling a draw-down bar with a gap of 200 μm over the aluminum slab. After drying, the paint film obtained was ca. 60 μm thick. Both type of films were optically thick.

The aluminum slab was then inserted in the photoreactor which is described in greater detail in chapter 2 and elsewhere [25]. Briefly, the reaction chamber has 5 cm width, 25 cm length

and 0.5 cm height. The top part of the reaction chamber is made of a borosilicate glass window (Präzisions Glass & Optik GmbH) allowing UV light (Vilbert Lourmat - BLB 365 nm, 2 x 6 W), exterior to the chamber, to irradiate the photocatalytic film delivering an average UV irradiance of 7 $W \cdot m^{-2}$. The relative humidity (RH), feed flow rate, NO concentration and temperature used were 50 %, 0.7 $L_N \cdot min^{-1}$, 1 ppm and 25 ºC, respectively. Atmospheric pressure was used. NO and NO_2 analyses were performed using a chemiluminescence analyzer (Thermo Scientific 42C). The steady state was considered to be achieved whenever NO conversion and selectivity did not vary more than ±2.5 percentage points for 5 h. NO conversion (eq. 6.1) and selectivity towards the formation of the ionic species NO_2^- and NO_3^- (eq. 6.2) were used for assessing the photoactivity performance of the films:

$$X_{NO} = \left(\frac{C_{NO}^{in} - C_{NO}^{out}}{C_{NO}^{in}} \right) \times 100 \qquad (6.1)$$

$$S = \left(1 - \frac{C_{NO_2}^{out}}{C_{NO}^{in} - C_{NO}^{out}} \right) \times 100 \qquad (6.2)$$

where C_{NO} and C_{NO_2} stand for the concentration of NO and NO_2, respectively, and the superscripts (*in* and *out*) refer to the reactor's inlet and outlet streams.

The ability of the photocatalytic films to adsorb NO was evaluated, prior to the begining of the photocatalytic tests; with the UV light turned off, a negligible decrease in the exiting NO concentration was observed for all composite photocatalysts, P25 and photocatalytic paints produced, indicating no significant NO adsorption as compared to the photocatalytic activity. No photoactivity was observed for either pure zeolites or paint films without photocatalytic TiO_2.

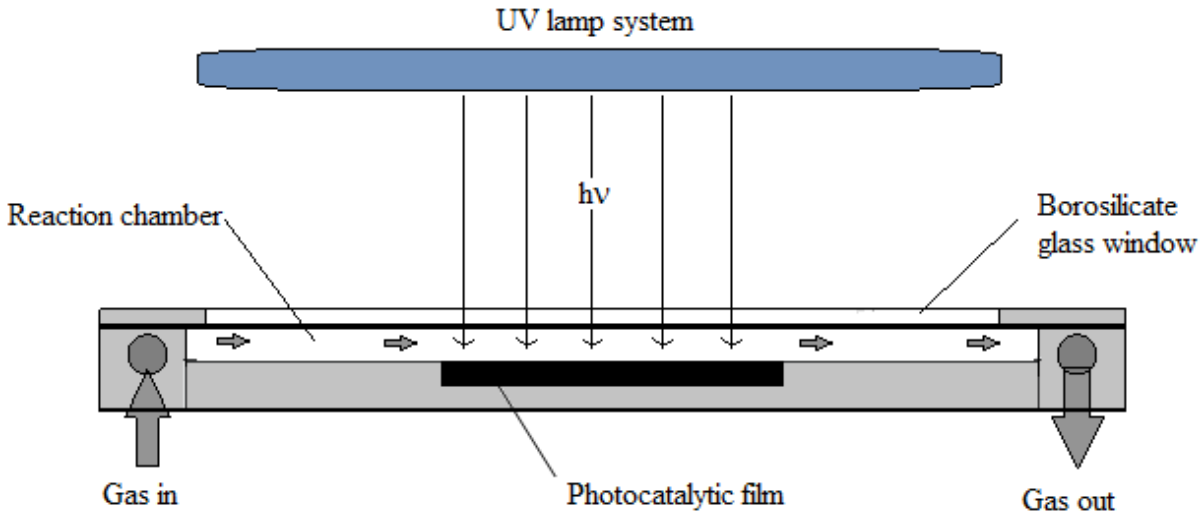

Figure 6.1 – Schematic representation of the photocatalytic reactor.

6.3 Results and discussion

6.3.1 Physicochemical characterization

The zeolite supports as well as the composite materials were characterized for BET surface area, pore volume and average pore size. The results are shown in Table 6.1. The differences in internal surface area, pore volume and average pore size of the materials with and without TiO_2 are not conclusive. This prevents any conclusion concerning the influence of TiO_2 presence on zeolite properties.

Table 6.1 – Pristine and composite zeolite surface area (SBET), pore volume (Vp) and average pore size (□P) of the prepared samples.

	Only Support			**TiO_2@support**		
Zeolite	S_{BET} ($m^2 \cdot g^{-1}$)	V_p ($cm^3 \cdot g^{-1}$)	□$_P$ (Å)	S_{BET} ($m^2 \cdot g^{-1}$)	V_p ($cm^3 \cdot g^{-1}$)	□$_P$ (Å)
βCP811	581.8	0.367	62.4	540.1	0.331	62.4
CBV100	688.4	0.027	33.8	665.7	0.033	37.2
CBV500	558.2	0.106	52.5	563.5	0.097	50.3

During the impregnation process TiO_2-zeolite composite materials were treated at a maximum of 550 °C. This high temperature may damage the crystalline structure of zeolites. XRD analyses were therefore performed showing no crystalline defects in any of the zeolites prepared (Figure 6.2). XRD analyses indicate no incorporation of TiO_2 into the zeolite matrixes; a small shift to higher diffraction angles observed in CBV100 and CBV500 samples is noticed after TiO_2 incorporation, which is reported to be related to a slight shrunken of the zeolites structure [26]. Typical anatase and rutile peaks are not observed in Figure 6.2. Independent works by Chatti et al. and Anandan and Yoon [27, 28] reported the same behavior; indeed, XRD can hardly detect TiO_2 if present in small concentrations like in the present case.

SEM images and EDS results, Figures 6.3 – 6.5 and Table 6.2, respectively, show the presence of titanium on the surface of the zeolite particles, indicating that probably most of TiO_2 did not crystallized inside the zeolite matrix. Figure 6.4b (concerning TiO_2@CBV100) and Figure 6.5b (concerning TiO_2@CBV500), along with the corresponding EDS analyses, show a non-homogeneous deposition of TiO_2. Zeolite βCP811 is organized in big agglomerates, Figure 6.3.

Figure 6.6 shows diffuse reflectance (DR) spectra of the pure zeolites and composite samples. For wavelengths smaller than ca. 390 nm it is noted a significant absorption of radiation for composite samples in opposition to pure zeolites. This is a behavior typically displayed by crystaline TiO_2, evidencing its presence.

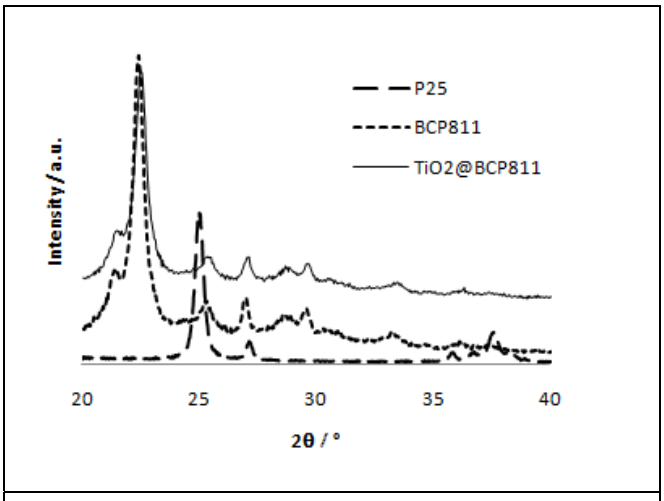

a) βCP811

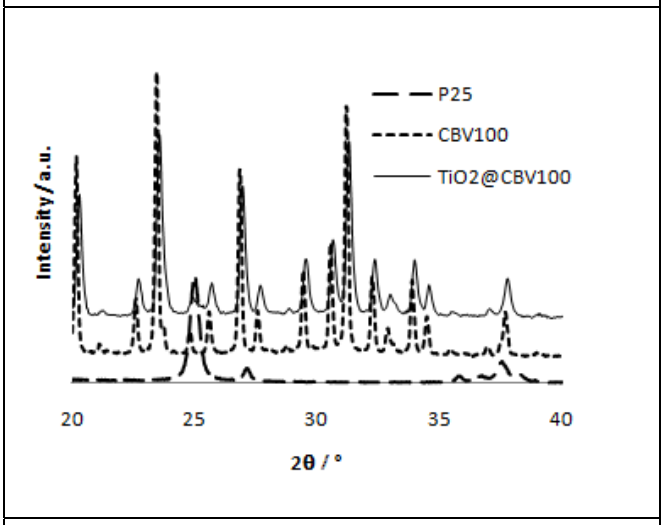

b) CBV100

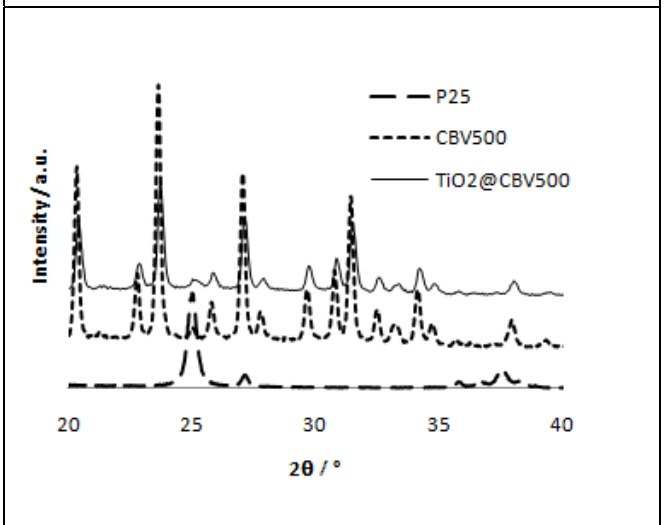

c) CBV500

Figure 6.2 – XRD patterns of supports and respective composite materials (P25 used for reference).

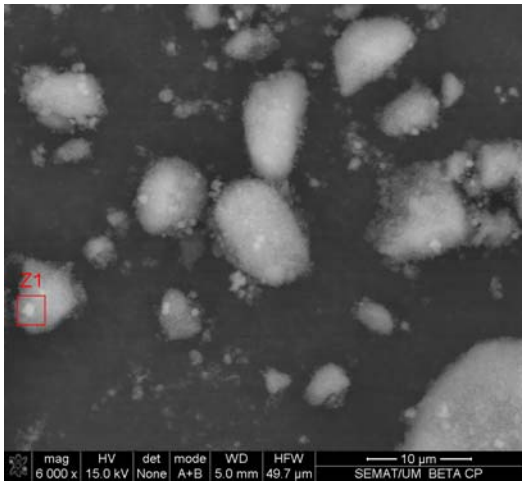

a) βCP811 zeolite

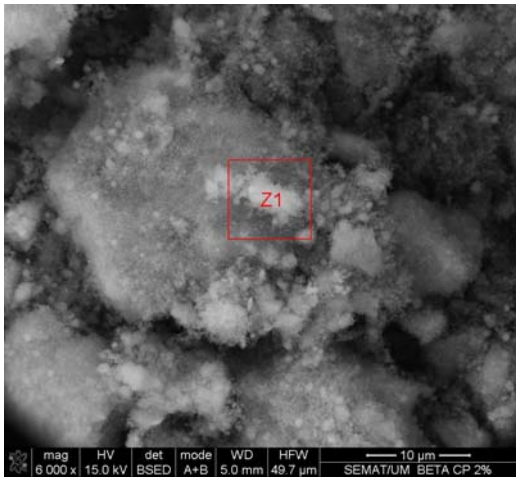

b) TiO_2@βCP811

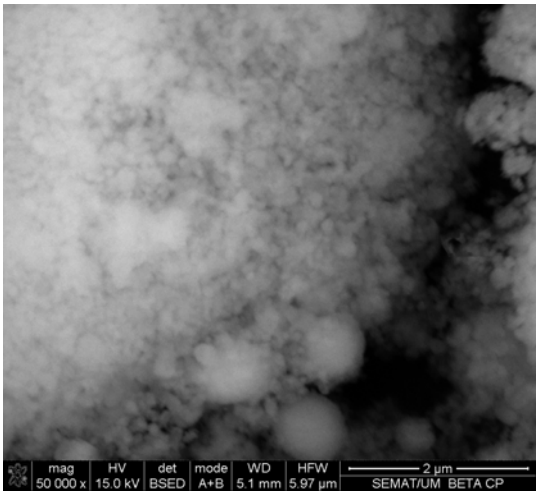

c) βCP811 zeolite

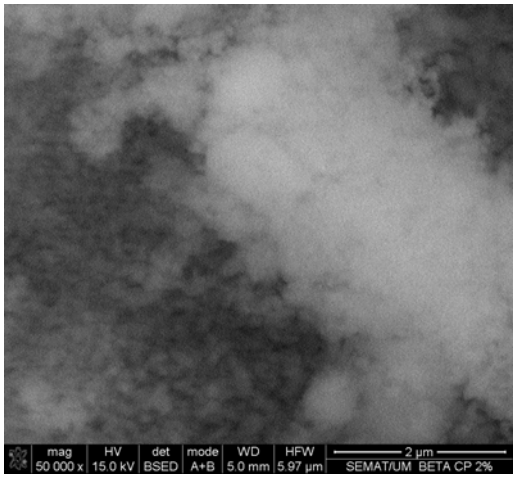

d) TiO_2@βCP811

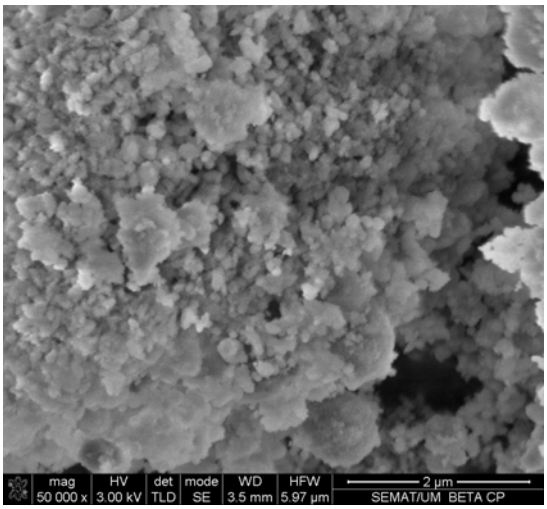

e) Zoom in of image a) at Z1

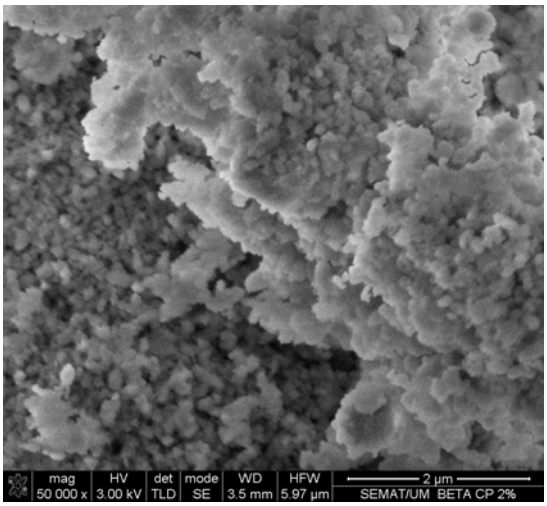

f) Zoom in of image b) at Z1

Figure 6.3 – SEM images of βCP811 (left side images) and TiO_2@βCP811 (right side images).

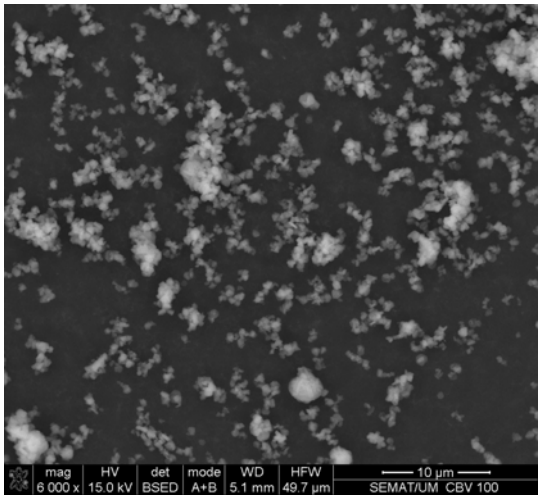

a) CBV100 zeolite

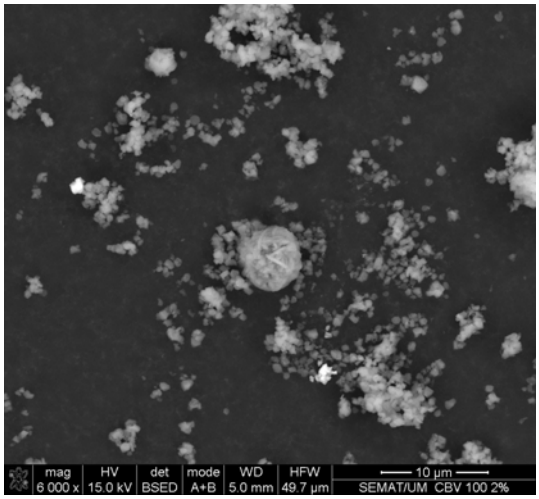

b) TiO_2@CBV100

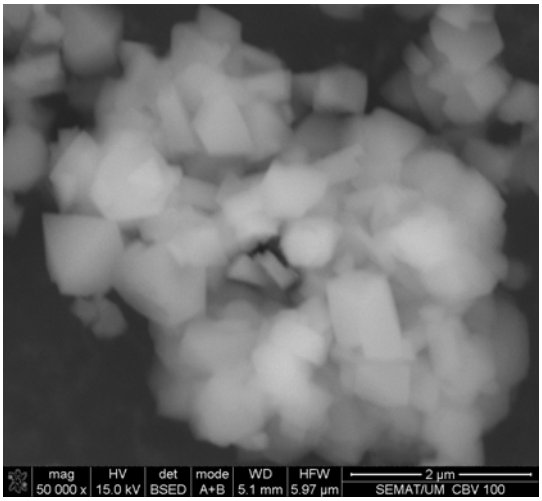

c) CBV100 zeolite

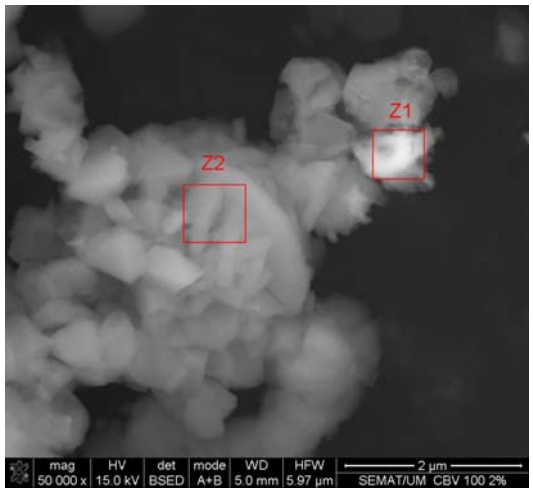

d) TiO_2@CBV100

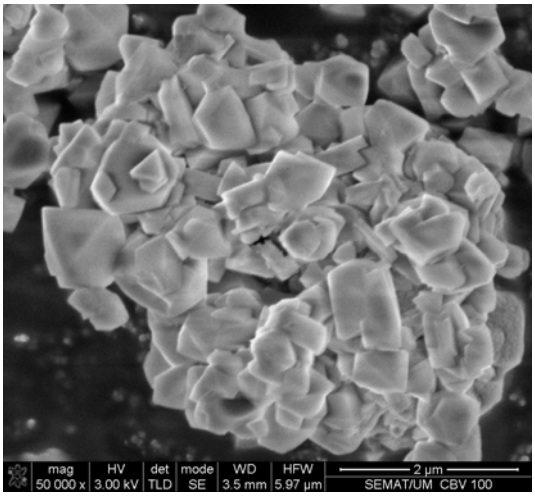

e) TLD detection mode of image c)

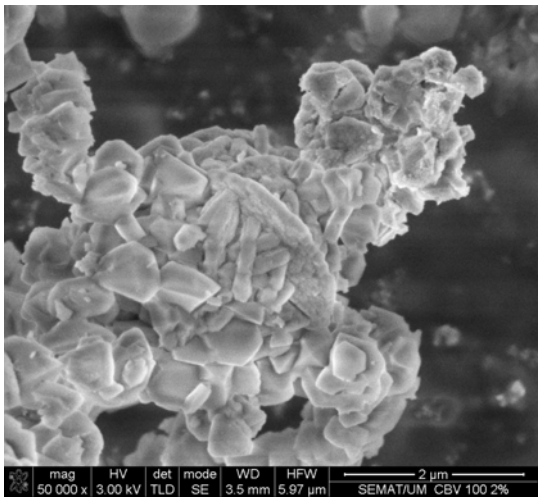

f) TLD detection mode of image d)

Figure 6.4 – SEM images of CBV100 (left side images) and TiO_2@CBV100 (right side images).

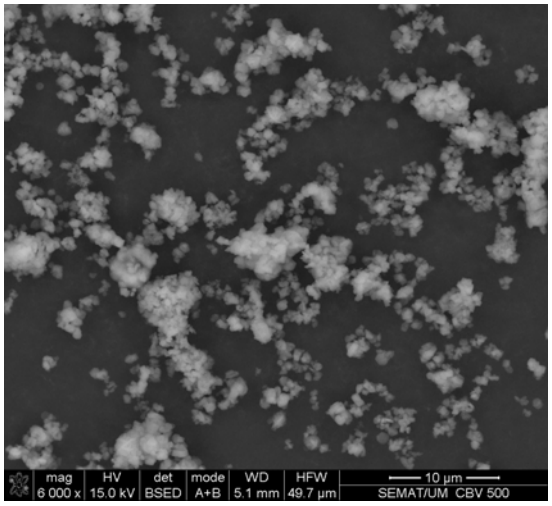

a) CBV500 zeolite

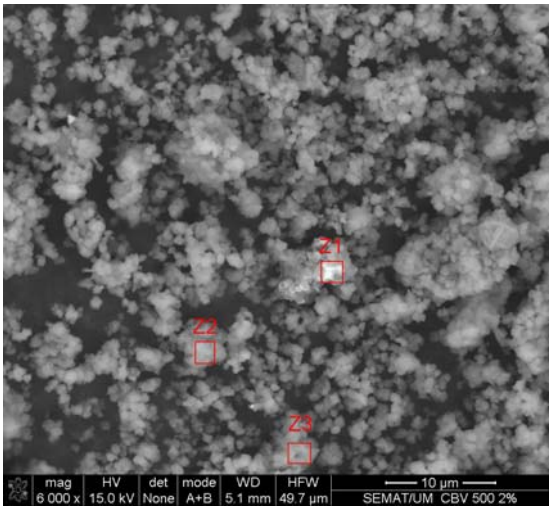

b) TiO_2@CBV500

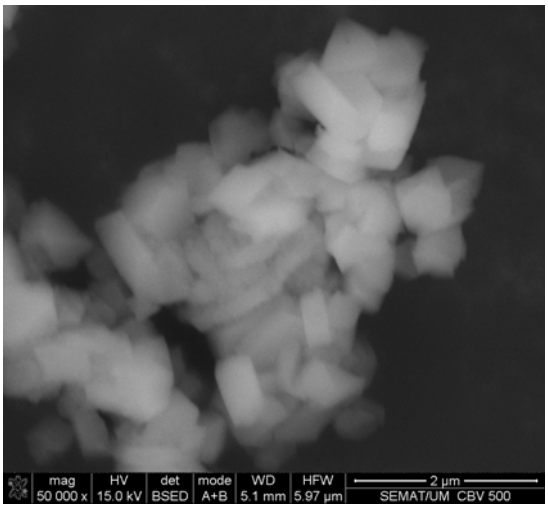

c) CBV500 zeolite

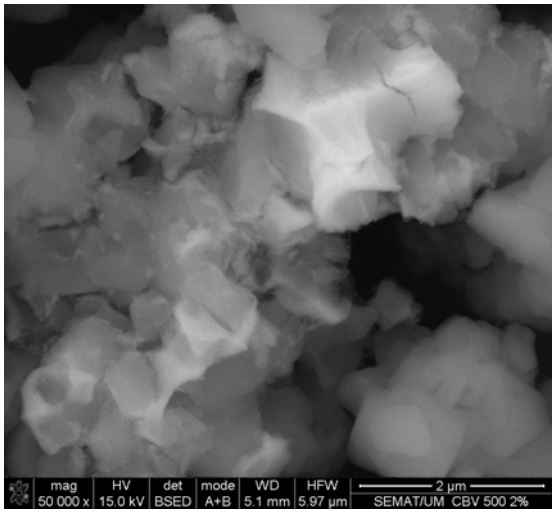

d) TiO_2@CBV500

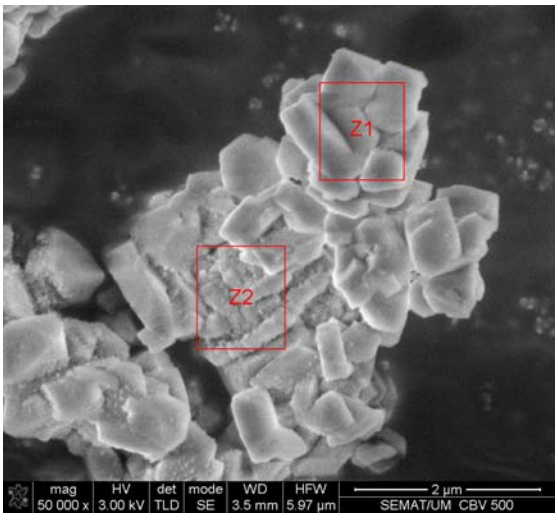

e) TLD detection mode of image c)

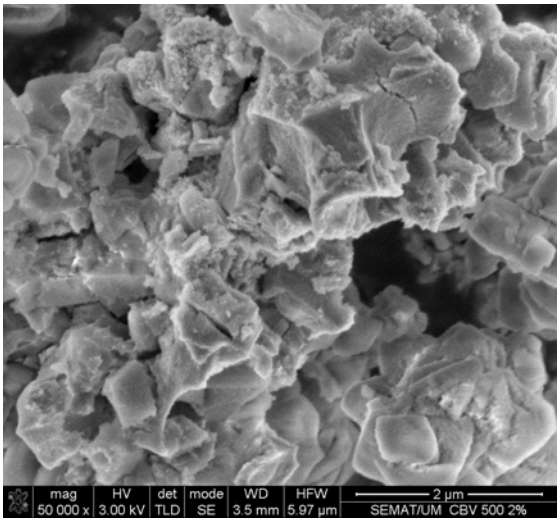

f) TLD detection mode of image d)

Figure 6.5 – SEM images of CBV500 (left side images) and TiO_2@CBV500 (right side images).

Table 6.2 – EDS analyses, corresponding to the zones indicated in Figures 6.3, 6.4 and 6.5.

			Wt. %						
	βCP811	**TiO_2@βCP811**	**TiO_2@CBV100**		**CBV500**		**TiO_2@CBV500**		
Element	**Z1**	**Z1**	**Z1**	**Z2**	**Z1**	**Z2**	**Z1**	**Z2**	**Z3**
O K	54.49	33.09	44.45	61.44	44.45	43.46	65.39	67.69	67.05
Si K	14.54	55.08	3.48	15.21	6.30	11.06	10.78	20.63	22.52
Al K	1.06	4.55	1.36	5.97	2.21	4.14	4.28	7.28	8.48
Ti K	0.00	7.28	8.21	0.00	0.00	0.00	15.37	0.00	0.00

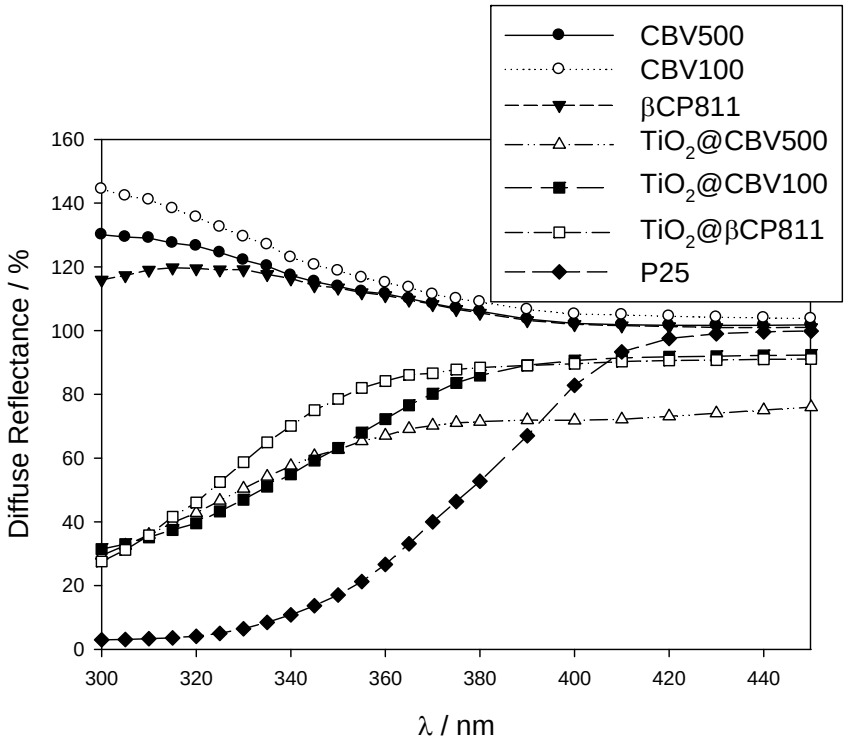

Figure 6.6 – Diffuse reflectance (DR) spectra of the zeolite in pure form and with TiO_2.

Absorption on the UV region of the composite photocatalytic materials is generally lower than for P25 (Figure 6.6), which should be related to the lower TiO_2 content. TiO_2@CBV500 has a high absorption towards the visible light spectrum. Infrared spectroscopy (Figure 6.7) made to this material and to corresponding zeolite before TiO_2 impregnation, show the

elimination of the peak centered at ca. 1400 cm^{-1}. Peaks in the wavenumber range between 1400 cm^{-1} to 1600 cm^{-1} are usually related to nitrogen components adsorbed on the Bronsted and Lewis sites of zeolite Y. Accordingly to the producer, CBV500 is a NH_4^+ exchanged zeolite, and then these peaks should be related to the presence of this ion. After TiO_2 impregnation in the CBV500 support, the composite material is calcinated and ammonium should be released, justifying the nitrogen peak disappearance. However, during the high temperature treatment ammonium evolution occurs, which can originate nitrogen doped TiO_2 crystals, supporting the ability for the visible light absorption displayed.

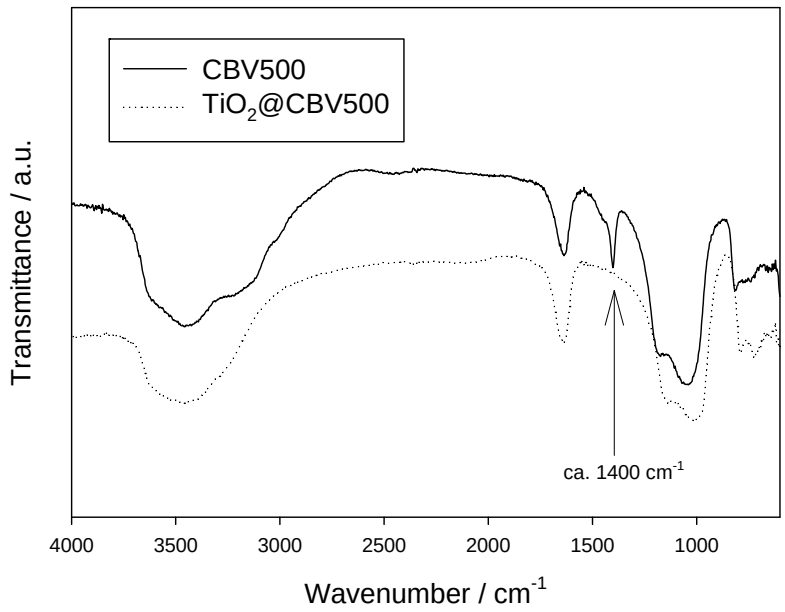

Figure 6.7 – Infrared results to CBV500 zeolite and respective photocatalytic material TiO_2@CBV500.

Near the absorption threshold of an indirect semiconductor, as it is the case of TiO_2, a direct relation exists between the energy of the exciting photon and the square-root of the product between the Kubelka-Munk function and the energy [29]. Bandgap can be determined by extrapolation of the linear part to the x-axis (Figure 6.8). These analyses show a quantization effect for all photocatalytic materials prepared, being particularly important for

TiO_2@βCP811 (0.35 eV compared to photocatalytic TiO_2 P25) – see Table 6.3.

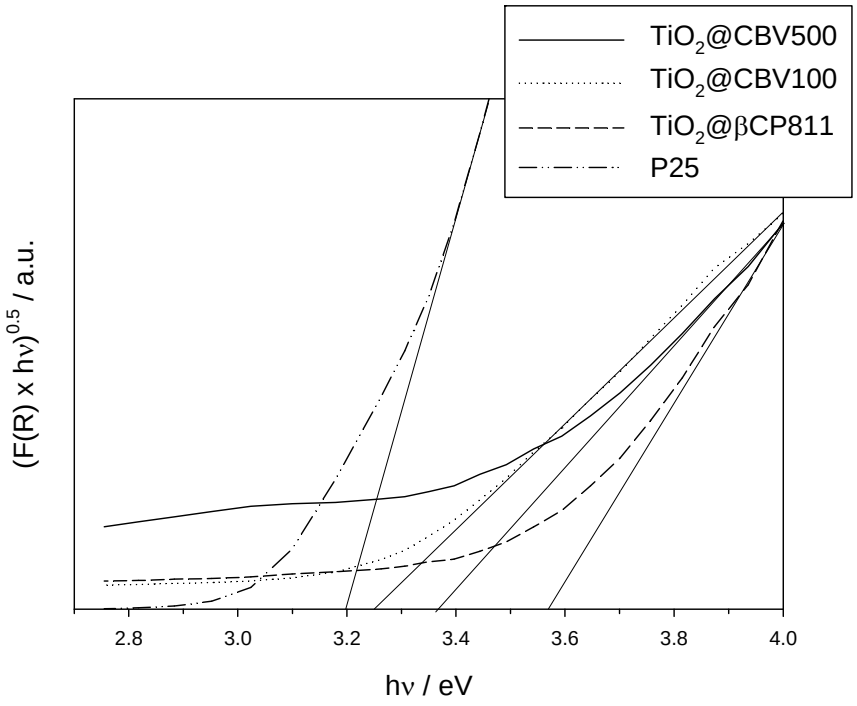

Figure 6.8 – Transformed Kubelka–Munk function vs. energy of the excitation source.

Table 6.3 – Photocatalyst bandgap (ΔE), bandgap shift related to P25 and corresponding wavelength for absorption threshold.

Material	**ΔE (eV)**	**Bandgap shift (eV)**	**λ (nm)**
P25	3.20	-	387
TiO_2@CBV100	3.25	0.05	380
TiO_2@CBV500	3.35	0.15	370
TiO_2@βCP811	3.55	0.35	350

Korman et al. [30] prepared TiO_2 particles with an average diameter of 2.4 nm and observed a bandgap shift of 0.15 eV. This indicates that TiO_2 crystals on TiO_2@CBV500 should have a similar size and on TiO_2@βCP811 TiO_2 crystals should be even smaller.

Photoluminescence analyses indicated that TiO_2 is agglomerated in all the composite material

with an octahedral coordination, as it can be usually found in bulk TiO_2 samples [31]; differences on photoactivity can not be therefore related to tretrahedral vs. octahedral arrangements of TiO_2 particles, as shown by Anpo and co-workers [31].

6.3.2 Photocatalytic tests

Table 6.4 presents the mass of each photocatalytic sample used in each photocatalytic test. TiO_2 mass was estimated assuming that samples contain 2 wt.% of titanium (3.3 wt.% of TiO_2).

Table 6.4 – Mass of composite photocatalyst used and P25, corresponding photo-TiO_2 mass and load (photo-TiO_2 mass normalized by the film area; 6 x 5 cm2).

Material	**Mass (g)**	**Photo-TiO_2 mass (g)**	**$L_{Photo\text{-}TiO2}$ ($mg \cdot cm^{-2}$)**
P25	0.444	0.444	14.8
TiO_2@βCP811	1.980	0.065	2.2
TiO_2@CBV100	3.125	0.103	3.5
TiO_2@CBV500	2.531	0.083	2.7

Powder films were made by pressing the photocatalytic materials for 5 min at 7 bar. This application method justifies the mass differences between samples (Table 6.4). TiO_2@βCP811 did not show photoactivity, which should be related to the large bandgap of this photocatalyst, 3.55 eV (Table 6.3). The UV lamp used has a light spectrum between 315 nm to 390 nm. Table 6.5 shows the maximum fraction of this spectrum energy that can be absorbed by the prepared photocatalysts. TiO_2@βCP811 can only absorb ca. 25 % of the UV light, which is a very small amount of energy.

Table 6.5 – Fraction of UV light absorption of the lamp spectrum by each photocatalytic material.

Material	UV light absorbed (%)
TiO_2@CBV100	95
TiO_2@CBV500	90
TiO_2@βCP811	25

Figure 6.9 shows the history of NO conversion and selectivity for P25 and composite photocatalysts TiO_2@CBV100 and TiO_2@CBV500.

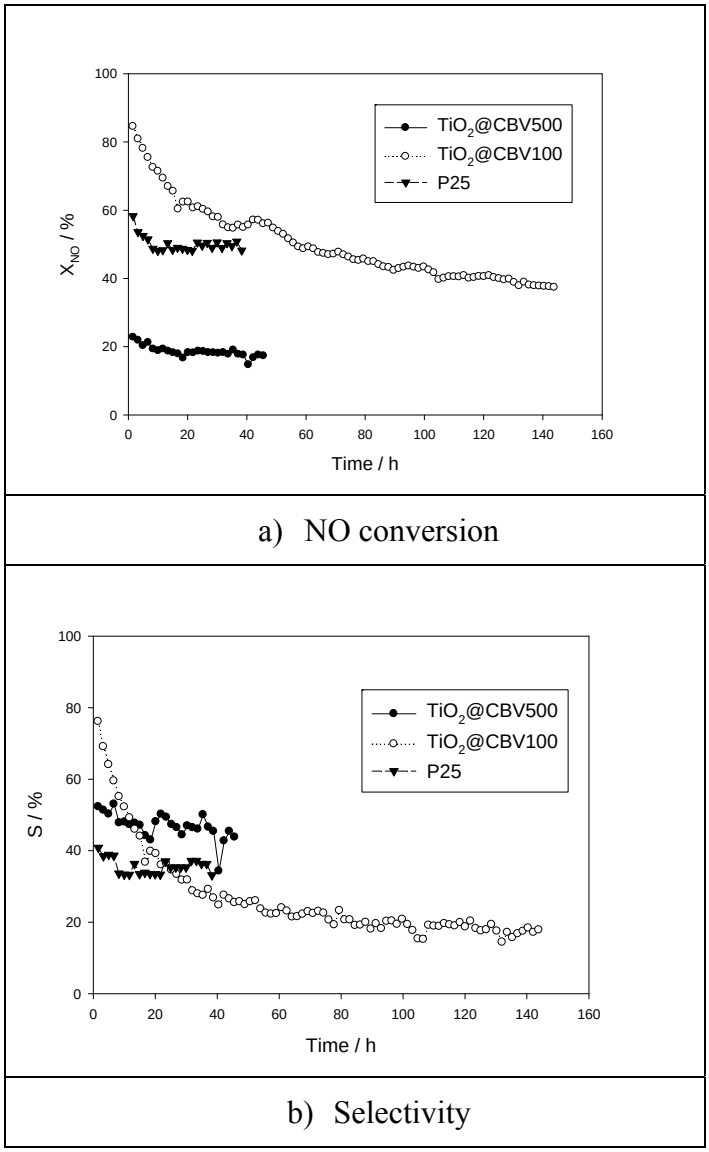

Figure 6.9 – History of NO conversion (a) and selectivity (b) for P25, CBV500 and CBV100.

Despite the small TiO_2 load, photocatalyst TiO_2@CBV100 performed close to P25; at steady state, the NO conversion was 40 % and 50 % and the selectivity 20 % and 40 %, respectively. The initial NO conversion was even higher for this composite material than for P25.

The longer transient period shown for TiO_2@CBV100 indicates that zeolite influences the photocatalytic process. In fact, this transient period is longer than the one observed for all pure powder pressed films of commercial photocatalytic TiO_2 reported in chapter 2 and elsewhere [25]. The greater NO adsorption capacity of TiO_2@CBV100 compared to TiO_2@CBV500 must play a role in the photoactivity of these materials. The NO Henry constant on TiO_2@CBV100 is ca. two times larger than on TiO_2@CBV500 - Figure 6.10.

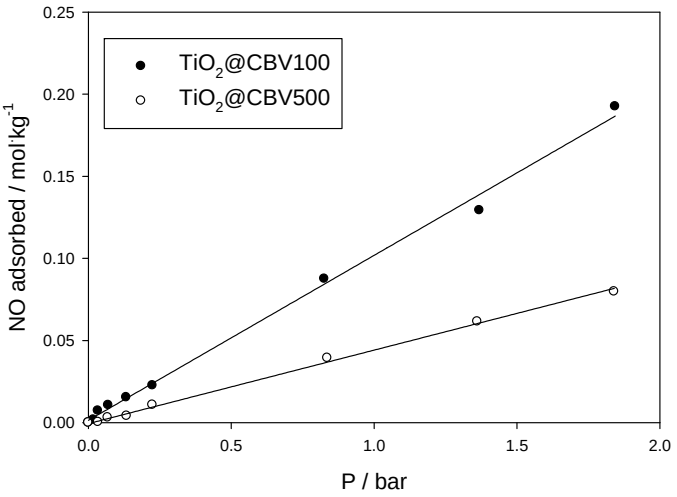

Figure 6.10 – NO adsorption isotherm on composite photocatalysts TiO_2@CBV100 and TiO_2@CBV500 at 25 °C.

Table 6.6 – Mass of composite photocatalyst and P25 in dry paint film, corresponding TiO_2 mass and load.

Material	**Mass (g)**	**Photo-TiO_2 mass (g)**	**$L_{Photo\text{-}TiO2}$ (mg·cm^{-2})**
P25	0.115	0.115	2.30
TiO_2@CBV100	0.070	0.0023	0.077

The NO conversion and selectivity for TiO_2@CBV100 (the best performing composite sample) and P25 incorporated in a water-based paint is shown in Figure 6.11. The steady state conversion is ca. 2.5 % and 25 %, respectively for TiO_2@CBV100 and P25, while selectivity is ca. 100 % and 25 %. High TiO_2@CBV100 selectivity should be related to the ability of the photocatalyst support to adsorb NO_2. Paint film incorporating TiO_2@CBV100 contained ca. 0.077 $mg \cdot cm^{-2}$ of TiO_2 while the paint film incorporating P25 contained ca. 2.3 $mg \cdot cm^{-2}$ of TiO_2 (Table 6.6). The steady state specific NO photooxidation rate of paint films is 0.16 $\mu g_{NO} \cdot g_{TiO2}^{-1} \cdot s^{-1}$ and 0.03 $\mu g_{NO} \cdot g_{TiO2}^{-1} \cdot s^{-1}$, respectively for TiO_2@CBV100 and P25 containing samples, putting into evidence the importance of the zeolite in the composite material when in paint films. Moreover, no paint chalking was noticed on the TiO_2@CBV100 based paint even after harsher activation.

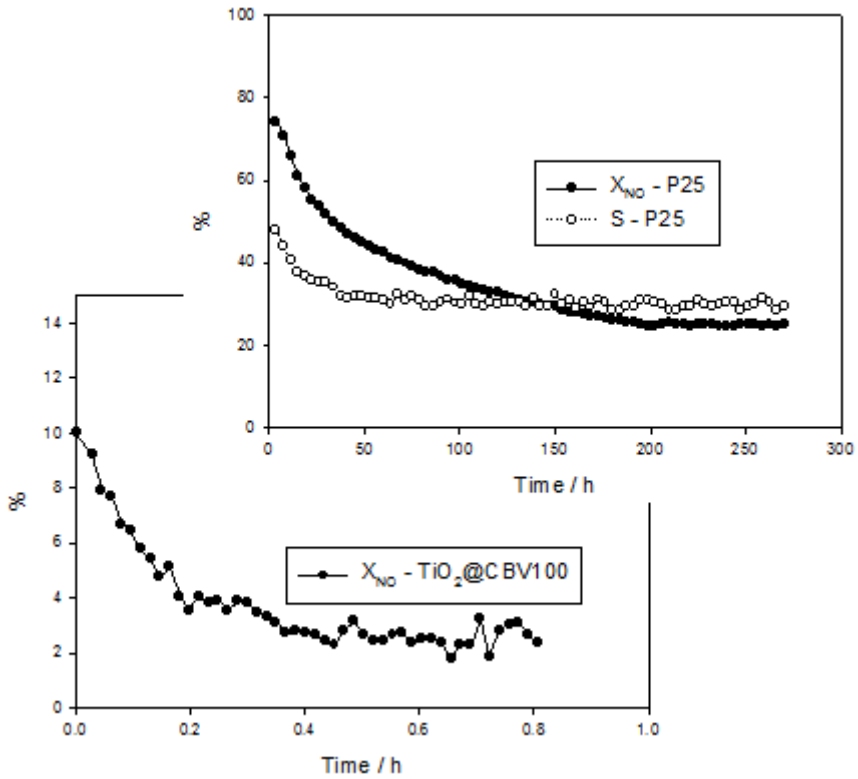

Figure 6.11 – NO conversion for photocatalytic paint containing 9 wt.% of P25 (open symbols) and 9 wt.% of TiO_2@CBV100 (ca. 0.3 wt.% of TiO_2).

6.4 Conclusions

In the present study ca. 3.3 wt.% of TiO_2 was incorporated into three different zeolites, CBV100, CBV500 and βCP811. It was concluded that Ti containing particles was mostly present on the external surface of the zeolites. The semiconducting nature of these particles was confirmed by diffuse reflectance, which allowed estimating the bandgap of the composite photocatalysts; it was observed a blue shift for all the composite samples here produced, but much larger for the TiO_2@βCP811 that showed no photocatalytic activity.

NO photooxidation experiments with powder films of TiO_2@CBV100, TiO_2@CBV500 and P25 demonstrated that supported photocatalysts have a high photoactivity; the steady state NO conversion for these samples was respectively 40 %, 20 % and 50 %. The composite photocatalysts exhibited a linear adsorption isotherm of NO at 25 °C and the Henry's coefficients are 0.10 and 0.044 for photocatalysts TiO_2@CBV100 and TiO_2@CBV500, respectively, which might contribute for the better photoacatalytic abatement of NO of the previous.

TiO_2@CBV100 incorporated in an exterior water-based paint (9 wt.% of photocatalytic material in wet base) exhibited a steady state NO conversion of ca. 2.5 %, reached after 1 hour of irradiation, compared to ca. 25 % for P25 after around 200 h. However, specific activity was much higher in the TiO_2@CBV100 sample.

References

[1] IUPAC Recommendations 2006, *Pure Appl. Chem.* 2007, 79 (3), 293.

[2] Robichaud, C., Uyar, A., Darby, M., Zucker, L., Wiesner, M., *Environ. Sci. Techno.* 2009, 43, 4227.

[3] Krol, R., Liang, Y., Schoonman, J., *J. Mater. Chem.* 2008, 18, 2311.

[4] Anpo, M., in: Tundo, P., Anastas, P., (Eds.), *Green Chemistry*, Oxford University Press,

2000, 1.

[5] Anpo, M., in: Corma, A., Melo, F.V., Mendioroz, S., Fierro, J.L.G., (Eds.), *Proceedings of the 12th International Congress on Catalysts*, Granada, *Studies in Surface Science and Catalysis* 2000, 130, 157.

[6] Ollis, D.F., AlEkabi, H., (Eds.), *Photocatalytic Purification and Treatment of Water and Air*, Elsevier, Amsterdam, 1993.

[7] Pelizzetti, E., Schiavello, M., (Eds.), *Photochemical Conversion and Storage of Solar Energy*, Kluwer Academic Publishers, Dordrecht, 1991.

[8] Devahasdin, S., Fan Jr., C., Li, K., Chen, D.H., *J. Photochem. Photobiol. A* 2003, 156, 161.

[9] United States Environmental Protection Agency, *How nitrogen oxides affect the way we live and breathe*, EPA-456/F-98-005, September 1998 (available at: http://www.cleanairaction.org/pubs/pdfs/old_pubs/noxfldr.pdf - accessed February 2011).

[10] Agência Portuguesa do Ambiente – online database on air quality (www.qualar.org, accessed February 2011).

[11] Guerrini, G.L., Peccati, E., *White Cement and Photocatalysis – Part 1: Fundamentals*, International RILEM Symposium on Photocatalysis, Environment and Construction Materials, 8-9 October 2007, Florence, Italy, 179-186.

[12] Marley Eternit, Ecologic Roof Tiles – Breathing Life Into the Environment (available at: http://www.marleyeternit.co.uk/Roofing/Concrete-Tiles/EcoLogic-Ludlow-Major-Interlocking-Tile.aspx, accessed February 2011).

[13] Beeldens, A., *Air purification by road materials: results of the test project in Antwerp*, International RILEM Symposium on Photocatalysis, Environment and Construction Materials, 8-9 October 2007, Florence, Italy, 187 - 194.

[14] Bygott, C.E., Maltby, J.E., Stratton, J.L., McIntyre, R., Photocatalytic Coatings for the

Construction Industry, International RILEM Symposium on Photocatalysis, Environment and Construction Materials 8-9 October 2007, Florence, Italy, 251–258.

[15] Paint company Sto – website for photocatalytic product Climasan (www.stoclimasan.com - accessed February 2011).

[16] Águia, C., Ângelo, J., Madeira, L., Mendes, A., Polymer Degradation and Stability (10.1016/j.polymdegradstab.2011.01.032).

[17] Zhang, S., Fujii, N., Nosaka, Y., *Journal of Molecular Catalysis A: Chemical* 1998, 129, 219,

[18] Ichiura, H., Kitaoka, T., Tanaka, H., *Journal of Materials Science* 2003, 38, 1611.

[19] Kaneko, M., Okura, I., (eds.), *Photocatalysis Science and Technology*, Tokyo, Kodansha Ltd., 2002, 123.

[20] Anandan, S., Yoon, M., *Journal of Photochem and Photobiol C: Photochem Reviews* 2003, 4, 5.

[21] Yoon, M., Negi, D. P. S., *Photoinduced electron transfer in some photosensitive molecules-incorporated semiconductor/zeolites: New photocatalytic systems*, Proc. Indian Acad. Sci. (Chem. Sci.), Vol. 114, No. 6, December 2002, 593–602.

[22] Melanie, A., O'Neill, F., Cozens, L., Schepp, N. P., *J. Phys. Chem. B* 2001, *105,* 12746.

[23] Santos, J. C., Magalhães, F. D., Mendes, A., Ind. Eng. Chem. Res., 2008, 47 (16), 6197.

[24] Koleske, J. V., *Paint and Coating Testing Manual*, 14th edition of the Gardner-Sward Handbook, Philadelphia, 1995.

[25] Águia, C., Ângelo, J., Madeira, L., Mendes, A., Polymer Degradation and Stability (10.1016/j.jenvman.2011.02.010).

[26] Iwamoto, M. Abe, T. Tachibana, Y., *Journal of Molecular Catalysis A: Chemical* 2000, 155, 143.

[27] Chatti, R., Rayalu, S., Dubey, N., Labhsetwar, N., Devotta, S., *Solar Energy Materials &*

Solar Cells 2007, 91, 180.

[28] Anandan, S., Yoon, M., *J. Photochem and Photobiol. C: Photo Rev.* 2003, 4, 5.

[29] Lin, H., Huang, C.P., Li, W., Ni, C., Shah, S., Tseng, Y., *Applied Catalysis B: Environmental* 2006, 68, 1.

[30] Kormann, C., Bahnemann, D. W., Hoffmann, M. R., J. Phys. Chem. 1988, 92, 5196.

[31] Matsuoka, M., Anpo, M., *Journal of Photochemistry and Photobiology C: Photochemistry Reviews* 2003, 3, 225.

Part V – *Conclusions and future work*

Chapter 7 - Conclusions and future work

7.1 Main Conclusions

Ten commercial photocatalytic TiO_2 samples were tested for NO abatement, under pure powder pressed form and incorporated in a water-based high pigment volume concentration paint (which originates high porosity dry films). Powder films were produced pressing the photocatalytic TiO_2 powder into a stable layer and paint films were obtained using a draw-down bar; both films were optically thick and were applied over aluminum slabs. This aluminum slabs were then inserted into a photoreactor for photoactivity assessment. No clear relation was found between the photoactivity of the powder films and when incorporated in the paint matrix; the highest yields over powder films were obtained with pristine VLP7000 (ca. 0.70), VLP7101 and UVLP7500 (ca. 0.55), while paint films based on PC500, UV100 and PC105 originated the best performances (yields of ca. 0.15). Such fact reveals that the paint matrix influences the photocatalytic TiO_2 photoactivity differently. Steady state was attained in shorter period with powder pressed films that also showed reproducible photoactivity, both during transient and steady state periods. On the other hand, paint films transient photoactivity showed to depend on the activation protocol and production batch, exhibiting however mostly the same steady state performance.

Further tests were therefore performed to better understand the role of the paint matrix and its components on photocatalytic TiO_2 activity; P25 was used in these runs. A paint was prepared using inorganic, typically in the powder form, and organic paint components. Inorganic components are pigments (pigmentary TiO_2), extenders (such as $CaCO_3$, silicates and $BaSO_4$), and the photocatalyst. Organic components comprehend the binder and additives: dispersing agents, opaque polymeric particles and other minority additives. In this way, powder pressed and pseudo-paint films (containing all powder and selected organic paint components) were produced. Powder pressed films were prepared folowing two different mixing protocols, dry

and wet basis; P25 and powder paint components in dry form were mixed, shacking them in a can for few minutes (dry protocol). The same components were mixed with deionised water using a mechanical stirrer, dried overnight and milled (wet protocol). Pure P25 films were also produced using the dry and wet protocol. It was noticed the greater NO conversion when wet protocol was used in pure P25, which was seen to be related to a diferent film behavior towards UV light. On the contrary, a lower NO conversion is obtained when wet protocol is involved in film preparation of P25 mixed with powder paint components. Also, a significant longer transient behavior was observed. Such fact is the prove that chemical and physical interferences exist between P25 and powder paint components, which are more intense when slury mixture is used, as in typical industrial paint production. $CaCO_3$, $BaSO_4$ and silicates are reflective materials in the UV region and revealed no significant impairment onto P25 photoactivity. On the contrary, pigmentary TiO_2 works as UV light absorber, contributing for the greatest impairment to P25 photoactivity.

When all powder paint components are wet mixed with P25, the film revealed close steady state behavior to the one found with the photocatalytic paint containing a similar concentration of photocatalyst. Moreover, transient period is as longer as the one shown for paint films. Such facts points to a low interference of organic components on P25 photoactivity, in paint film, at steady state. Paint and pseudo-paint (incorporating only part of organic components) photocatalytic films revealed similar steady state NO photooxidation. TG analysis made ot these films after 150 h UV aging showed similar photocatalytic degradation of the organic components (25 wt.%). These results indicate that after the photoerosion of organic paint components within the opticaly active layer of paint film, the paint surface becomes performing as if it was a wet powder pressed film; long-term photoactivity is ruled by powder components.

Reduction of photoerosion was intended supporting TiO_2 on usual adsorbents. In this way, protection could occur either by avoiding or at least reducing direct contact of TiO_2 with the paint matrix, namely the binder. Interaction of the support with the TiO_2 particles is important in order to create a synergetic effect. From all the materials tested, the one showing higher photoactivity was TiO_2 supported on zeolite Y CBV100, which contained ca. 3.3 wt.% TiO_2. It was concluded that TiO_2 was mostly present on the external surface of the zeolites. The presence of TiO_2 on the zeolite samples was confirmed by diffuse radiance, which allowed estimating the bandgap of the composite photocatalysts, revealing a value typical for anatase (ca. 3.2 eV). The steady state NO conversion for the TiO_2@CBV100 sample was 40 %, which compares with 50 % obtained for pure P25, with a much higher TiO_2 load. However, incorporation of the composite material in an exterior water-based paint (9 wt.% of photocatalytic material in wet base) exhibited a steady state NO conversion of only 2.5 % (reached after 1 hour of irradiation), compared to ca. 25 % NO for P25. However, specific NO photocatalytic conversion obtained were 0.16 $\mu g_{NO} \cdot g_{TiO2}^{-1} \cdot s^{-1}$ and 0.03 $\mu g_{NO} \cdot g_{TiO2}^{-1} \cdot s^{-1}$, for TiO_2@CBV100 and P25 paint films, respectively, and no paint chalking was noticed on the TiO_2@CBV100 based paint even after harsher activation.

7.2 Future work

The UV lamp used showed heterogeneous irradiation over the illuminated surface due to typical lamp hetergeneous irradiance with length. A more homogeneous illumination system would originate more precise photoactivity analyses favouring future reaction kinetics determination. An improved illumination system should then be designed and implemented in future works. This may be accomplished reorienting the present lamps perpendicular to the flow direction of the photoreactor.

The present work was based on NO photocatalytic oxidation towards NO_2, nitrite and nitrate acids. The reaction mechanism of NOx photocatalytic oxidation over pure photocatalytic TiO_2 is quite well described in literature. On the other hand, the mechanism within a paint matrix was not yet studied. Therefore, more studies must be performed in order to develop knowledge regarding the influence (chemical and physical) of paint components and matrix on the photocatalyst photoactivity photoactivity and reaction mechanism. Some authors claim that photocatalytic paint may release VOCs and free-radicals while photooxidizing pollutants such as NOx. This should be clarified since it is an important issue concerning the safety of using photocatalytic paints. The paint matrix photodegradation is a tricky issue. On one hand, it should occur for an efficient photoactivity of the paint but, on the other hand, it originates the paint chalking that is not desirable if it originates the paint quick degradation. Deposition of photocatalytic TiO_2 on usual adsorbents is one promising methodology but the proposed approaches still originate unsatisfying results for commercial application. Therefore, higher amounts of TiO_2 must be supported on the adsorbents in order to obtain a better balance between photoactivity and paint degradation. Other approache would be to develop a suitable binder, UV transparent, stable against photodegradation, highly permeable to reactants and products and that allows the photoactivity over the catalyst surface. Silicone based polymers exhibit promising results and should be addressed. Despite the very preliminary study conducted concerning the poisoning of the photocatalytic paint films, this study must be continued.

Regarding the photocatalysts, one must not neglect the possible (eco)toxicity of nanoscale particles. Recent studies have been reporting nanomaterials (< 100 nm), and namely nanoscale TiO_2, as neurodegenerative, reactive oxidative species producers and protein aggregation promoters, with consequent health impacts. Therefore, connection of photocatalyst nanoparticles onto larger micron-sized support particles (or forcing irreversible

agglomeration of TiO_2 nanoparticles), seems to be a safe and reasonable approach. For example, it was patented recently the use of graphene platelets coated with small nanoparticles of photocatalytic TiO_2 [1]. The continuous study on the composite materials here tested might allow to ignore such a problem in the future.

7.3 A possible roadmap

The work proposed would allow the development of knowledge in three main areas: reactor design (engineering), photocataytic material and film (material science), and light-film interaction (physics) (Figure 7.1). Such knowledge areas, working together, will allow the development of new technological solutions for different markets in the future, namely for highly demanding car coatings and flue gas treatment (Figure 7.2).

Possible applications for the abatement of other atmospheric pollutant gases should be considered. For an appropriate selection, one must focus on: - last evolution on emission and air concentration of particular gases; - state of the art of competitive technology and respective bottleneck for abatement; - future gas concentration/emissions evolution due to side-technological development; - physical local of presence (are people and nature threatened? are paints possible to be applied?); - ability of photocatalysis to deal with the gas concentration levels; - life-time of compound (related to impact factors). Targeted pollutants are usually issued by organizations such as WHO, IPCC, EPA, EEA, UNEP, WMO, among others, which are often related to further legislation development. Examples are persistent organic pollutants, VOCs, freons, CFCs, greenhouse gases, among others.

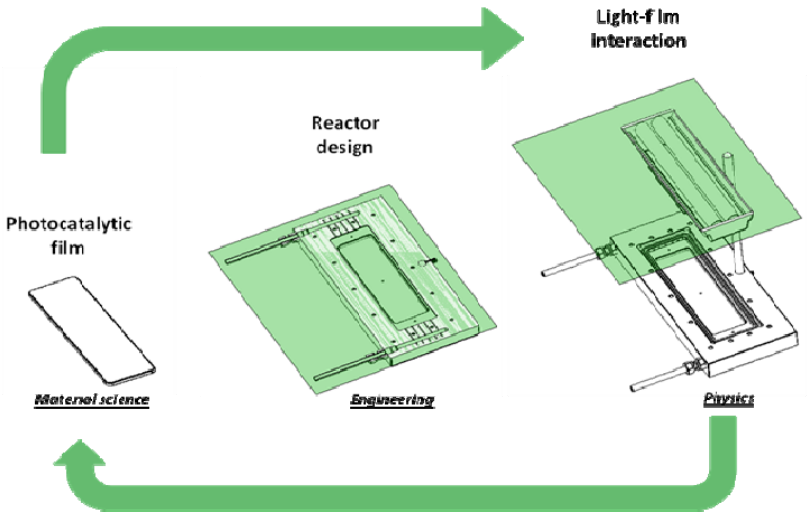

Figure 7.1 – A view of the photocatalytic technological solutions and its major areas of knowledge.

Figure 7.2 – An approach for chronological technological applications of photocatalytic paints.

References

[1] Tanaka, D., Mendes, A., "Composite grapheno-metal oxide platelet method of preparation and applications", PT 105064/10.

Appendix

Appendix A – Experimental setup – additional and brief overview

Two lab photoreactors were designed and builted by the author. A general overview of one of them is shown in Figure A.1.

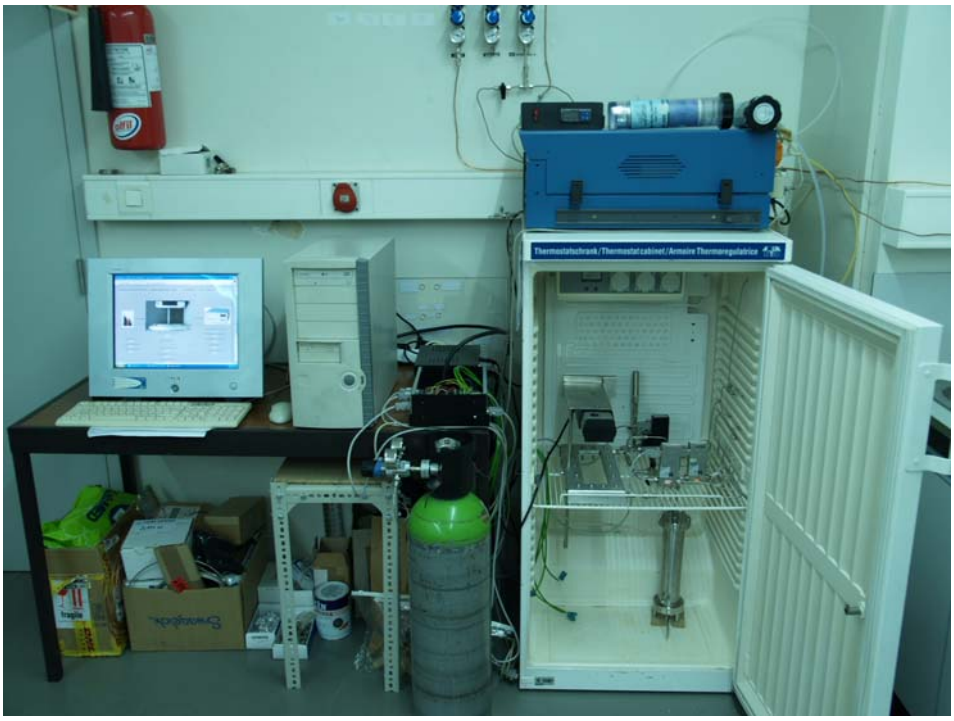

Figure A.1 – General overview of one of the lab photoreactors.

The feed system comprehends a cylinder containing 50 ppm of NO balanced with N_2 (Linde) and a drying air unit (Figure A.2). This last is made of a compressor (N145.1.2 AN.18, from KNF), two particulate filters (AFM30-F03 and AFD30-F03, from SMC), a membrane air dryier (IDG30L-F03-P, from SMC). The system is also made of a reservoir in order to obtain a constant and pressurized air flow supply.

Dry treated air and NO streams are continuously mixed to produce the desired NO concentrations for photocatalytic tests (1 ppm). To produce an air stream with the required humidity, a fraction of dry air flows through an humidifier (saturated air) mixing afterwards with the other fraction of dry air.

Figure A.2 – Detail of the thermostatic cabinet.

A detail of the thermostatic cabinet used for controlling the temperature, in the photoreactor, gas flow meters and controllers and humidifier can be seen in Figure A.2. The photoreactor is made of aluminum, with internal dimensions 0.05 m x 0.23 m x 0.005 m (width x length x height) and is equipped with a borosilicate glass window (Präzisions Glas & Optik GmbH) 0.005 m thick. The borosilicate window has an overall light transmittance of more than 90 % between 330 nm and 400 nm and no solarisation effect was observed. The gas entrance and exit of the reactor is made via two mixing chambers that connect with the internal reaction chamber through 5 holes with 1 mm diameter, allowing an homogeneous gas flow across the reactor width. Two thermocouples were inserted at the entrance and exit of the internal reaction chamber to better assess the temperature. Figure A.3 presents a photograph of the

designed photoreactor, with a paint film deposited in the down part of the reaction chamber (seen through the borosilicate window).

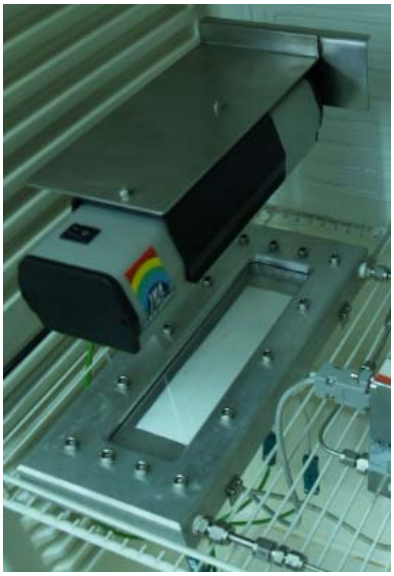

Figure A.3 – Detail of the photocatalytic reactor.

NOx analyses were made in-line by a NOx chemiluinescence analyzer (Thermo Scientific 42C – maximum 10 ppb uncertainty).

Flow rates, temperatures and NOx concentrations are monitorized/controlled by software specialy designed by the author, by means of labview 7.1 and a DAQ containing a NI USB-9211A and Advantech PCI 1710HG and PCLD 8710 boards.